AD-A216 285

EXPERIMENTAL INVESTIGATION TO
SUPPRESS FLOW-INDUCED PRESSURE
OSCILLATIONS IN OPEN CAVITIES

THESIS

Robert L. Sarno
Captain, USAF

AFIT/GAE/ENY/89D-32

DEPARTMENT OF THE AIR FORCE
AIR UNIVERSITY
AIR FORCE INSTITUTE OF TECHNOLOGY

Wright-Patterson Air Force Base, Ohio

90 01 02 115

EXPERIMENTAL INVESTIGATION TO
SUPPRESS FLOW-INDUCED PRESSURE
OSCILLATIONS IN OPEN CAVITIES

THESIS

Robert L. Sarno
Captain, USAF

AFIT/GAE/ENY/89D-32

EXPERIMENTAL INVESTIGATION TO SUPPRESS FLOW-INDUCED

PRESSURE OSCILLATIONS IN OPEN CAVITIES

THESIS

Presented to the Faculty of the School of Engineering

of the Air Force Institute of Technology

Air University

In Partial Fulfillment of the

Requirements for the Degree of

Master of Science in Aeronautical Engineering

Robert L. Sarno, B.S.

Captain, USAF

December 1989

Preface

High speed tangential flow over open cavities (e.g. aircraft weapon bays) can invoke large pressure oscillations within the cavity. These large oscillations can damage the cavity structure as well as items placed within the cavity. Previous experiments have investigated the effectiveness of several passive-type suppression methods with modest success. However, the effectiveness of a particular suppression device was usually Mach number dependent. The purpose of this experiment was to evaluate the effectiveness of using active-type suppression methods, and comparing with passive-type, in an attempt to find a design that was not Mach number dependent.

Table of Contents

List of Figures

List of Tables

List of Symbols

Symbol	Definition

Symbol   Definition

a Speed of Sound, ft/sec

D Cavity Depth, ft

f Frequency, Hz

K_v Vortex Velocity to Free Stream Velocity Ratio

l Length for Boundary Layer Growth

L Cavity Length, ft

M Mach Number, $\dfrac{U_\infty}{a}$

m Frequency Mode Number, Integer

N Number of Samples

P_{ref} Reference Pressure, "Threshold of Hearing"

$$P_{ref} = 2.9 \times 10^{-9} \text{ psi rms}$$

P_{rms} Measured Sound Pressure, psi rms

S Strouhal Number, $\dfrac{fL}{U_\infty} = \dfrac{m - \alpha}{M + \dfrac{1}{K_v}}$

S^* Modified Strouhal Number, $\dfrac{fL}{U_\infty} = \dfrac{m - \alpha}{\dfrac{M}{\left[1 + \dfrac{\gamma-1}{2} M^2\right]^{\frac{1}{2}}} + \dfrac{1}{K_v}}$

SPL Sound Pressure Level, dB $= 20 \log_{10} \dfrac{P_{rms}}{P_{ref}}$

U_∞ Free Stream Velocity, ft/sec

α Phase Delay Parameter

γ Ratio of Specific Heats

Symbol	Definition
δ	Boundary Layer Thickness, ft

Laminar Flow, $\delta = 5 \left[\dfrac{\nu l}{U_\infty} \right]^{1/2}$

Turbulent Flow, $\delta = 0.37\, l \left[\dfrac{U_\infty l}{\nu} \right]^{-1/5}$

Symbol	Definition
μ	Mach Angle, degrees
ν	Kinematic Viscosity, ft²/sec
σ	Sample Standard Deviation

AFIT/GAE/ENY/89D-32

Abstract Con+'d

Large pressure oscillations are generated by high speed
tangential flow over an open cavity. The purpose of this
experimental study was to determine the effectiveness of
suppressing pressure oscillations by manipulating the shear
layer over a two-dimensional cavity with a length-to-depth
ratio of two. Two methods, a frequency controllable control
surface (fence) and pulsating secondary airflow at the
cavity leading edge, were used to manipulate the shear
layer. The suppression effectiveness of the fence utilized
in both passive and active modes (zero to 120 Hz) was
evaluated at six airflow Mach numbers (0.62, 0.76, 0.90,
1.07, 1.28, 1.53). The effectiveness of pulsating secondary
airflow was evaluated at one airflow Mach number (1.28) and
two flow injection angles (parallel and 45 degrees to the
flow) at frequencies ranging from zero to 80 Hz. The effect
of steady flow injection was also evaluated at mass flow
rates per unit width ranging from 0.323 to 1.27
(lbm/sec/ft).

Pressure recordings from within the cavity were made
for each test. A narrow band Fourier analysis of these   Con+'d
recordings produced plots of the sound pressure level
amplitude versus frequency. Schlieren photographs of the

flow were also taken for each test to observe the shear and determine the cavity Mach number.

The effectiveness of a pulsating fence in suppressing the peak mode pressure oscillations proved to be less than that achievable with the fence static. However, due to mechanical restrictions of the model design, the maximum frequency was limited to only 120 Hz, an order of magnitude below cavity resonant frequencies.

The pulsed secondary flow injection technique was most effective when pulsed at a 45 degree angle to the external flow, but less effective than that achievable with steady 45 degree flow injection. However, the pulsed secondary flow suppression method was not effectively evaluated since substantial decrease in pulse amplitude occurred with small frequency increases. Recommend additional testing be accomplished to evaluate the effectiveness of both these methods at higher frequencies.

EXPERIMENTAL INVESTIGATION TO SUPPRESS FLOW-INDUCED PRESSURE OSCILLATIONS IN OPEN CAVITIES

I. Introduction

Background

The presence of a cavity in a surface exposed to high speed tangential airflow can create high level pressure oscillations within the cavity. These oscillations can be large enough to affect the structural integrity of the cavity and its surrounding structure due to sonic fatigue as well as adversely affecting the items carried within the cavity. If, for example, the cavity is an aircraft weapon bay, the oscillations could produce failure of store restraint and release mechanisms, as well as damage sensitive items within stores; in addition, these oscillations can also affect store separation from the aircraft (1:1).

There have been numerous experiments and analyses investigating different aspects of flow over a cavity. One of the earliest experiments was carried out by Karamcheti in 1955. Karamcheti noted that the intensities of the pressure oscillations were higher when the boundary layer upstream of the cavity was laminar rather than turbulent (2:5). Over the past 34 years, the amount of research done on cavities is far too numerous to adequately address in this thesis.

However, an excellent survey of flow over cavities was compiled by Komerath, Ahuja, and Chambers (3). The concepts covered in this survey include: Classification of flows over cavities, observed phenomena, prediction methods, suppression techniques, and current work as of 1986.

Objective

The purpose of this experimental investigation was to determine the effectiveness of suppressing pressure oscillations by manipulating the shear layer of a high speed tangential flow over a two-dimensional rectangular cavity. To manipulate the shear layer, two suppression techniques (a static/pulsating fence and steady/pulsating secondary flow injection at the cavity leading edge) were utilized.

Scope

The rectangular cavity considered in this investigation had a length-to-depth (L/D) ratio of two and is shown in Figure 1-1. The two suppression methods investigated included a static/pulsating fence and steady/pulsating secondary flow injection both at the cavity leading edge.

The pulsating fence was evaluated for a range of frequencies from zero to 120 Hz at six airflow Mach numbers. One convergent nozzle was used for subsonic flow conditions (M = 0.60, 0.75, and 0.90) and three converging-diverging nozzles were used for supersonic flow conditions (M = 1.10, 1.35, 1.70). In addition to dynamic testing with the fence,

1-2
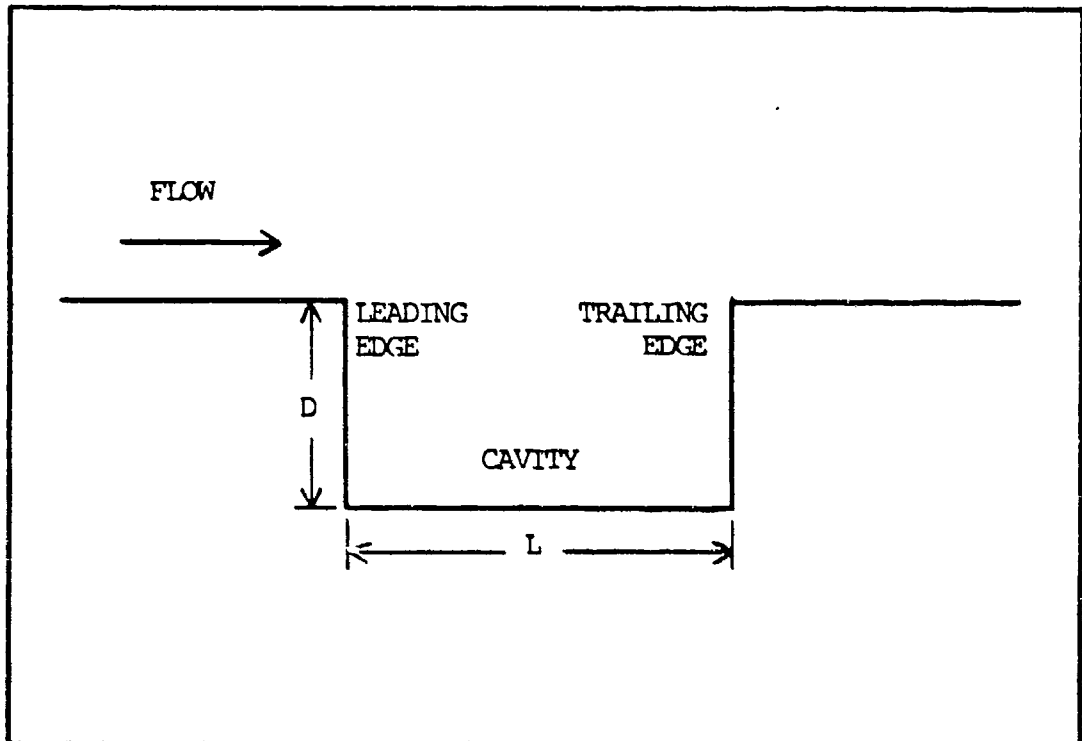
Figure 1-1. Cavity Geometry And Nomenclature

runs were also conducted using a variable height static
fence.

The pulsating secondary flow injection suppression
method was evaluated for a range of frequencies from zero to
80 Hz, at two flow injection angles (parallel and 45 degrees
to the flow), and at one airflow Mach number (M = 1.28).
Steady flow injection was also evaluated at M = 1.28 with
mass flow rates per unit width ranging from 0.323 to 1.420
lbm/sec/ft.

A schlieren photograph of the flow field in and above
the cavity was taken for each data point to observe and

document the behavior of the shear layer. In addition, for supersonic flow conditions the schlieren photograph was used to determine the flow Mach number at the cavity.

Dynamic pressure measurements of the cavity oscillations were recorded at discrete time intervals using dynamic pressure transducers mounted flush on the side walls of the cavity. This time dependent data was converted to the frequency domain using a Fourier transform routine. This provided plots of dynamic pressure amplitude as a function of cavity oscillation frequency.

II. Theory

Flow Dimension

Experimental studies by Covert (4:2) and Charwat (5:457) indicate that spanwise flow has no significant influence on cavity pressure oscillations. They found that the free-stream flow direction dominates the internal cavity flow so strongly that three-dimensional effects are restricted to small perturbations in the dominant flow direction. Therefore this study will address flow over a cavity as two-dimensional.

Classification of Flows

Cavity flows can be categorized as either open or closed types. Charwat, et al (5:458) referred to a flow as being "open" when the separated shear layer spans the cavity, Figure 2-1, and "closed" when the separated shear layer reattaches to the cavity floor, Figure 2-2. For supersonic speeds and for subsonic speeds with turbulent boundary layers, closed cavities are found to have a length-to-depth (L/D) ratio of 11 or greater (5:459). Sarohia (6) showed for subsonic speeds with a laminar boundary layer that closed cavities occurred when the L/D ratio was approximately seven or greater. The unsteadiness associated with closed cavity flow is predominantly random and does not exhibit periodic pressure oscillations. Therefore the focus of this test was on an open cavity configuration. .ls 1
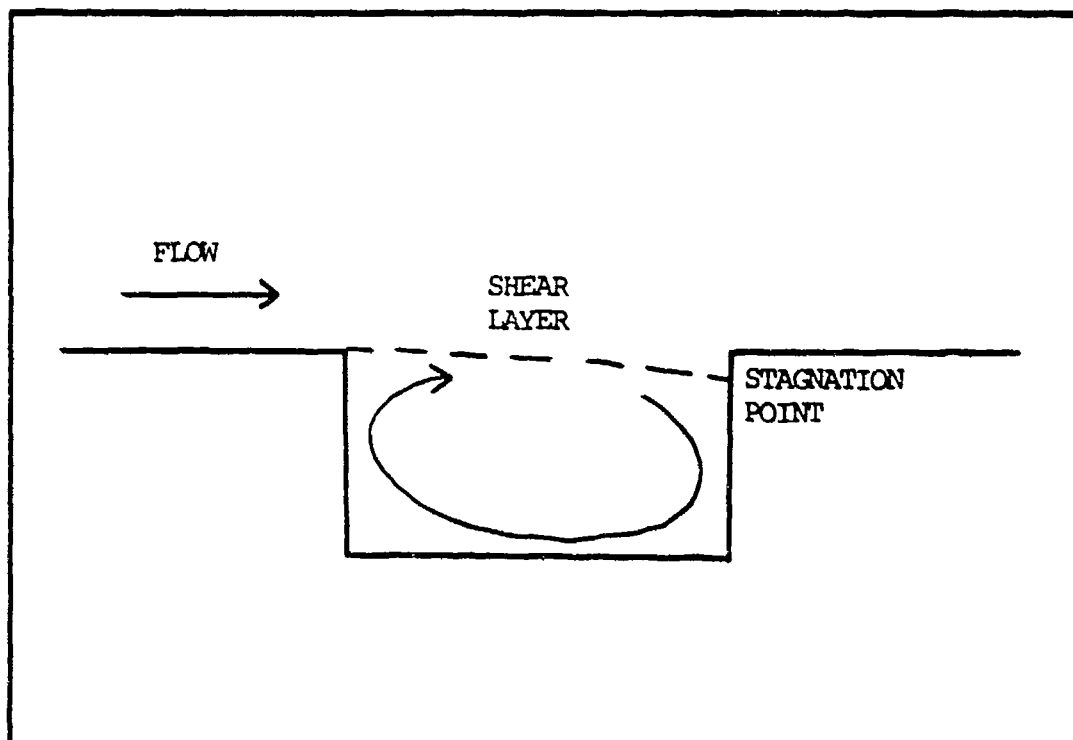
Figure 2-1.   Two-Dimensional Open Cavity Flow
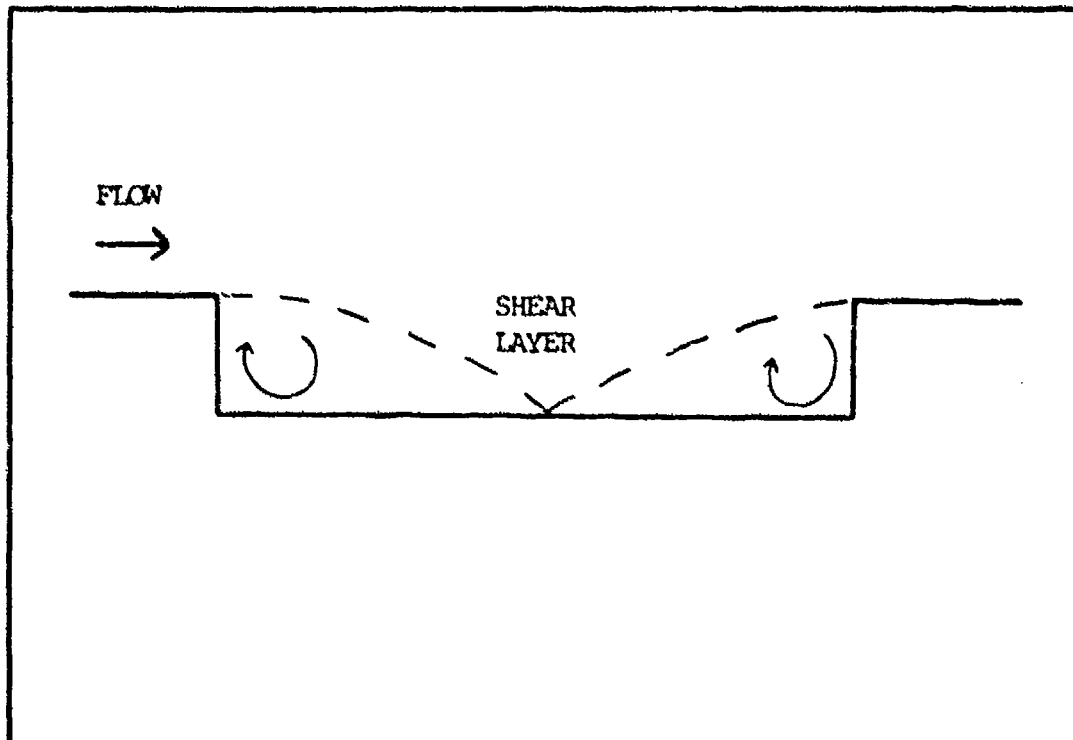
Figure 2-2.   Two-Dimensional Closed Cavity Flow

Classification of Cavities

Cavity geometry has been shown to be an important variable determining the type of response caused by flow over a cavity. A cavity may be considered "deep" if L/D < 1 and "shallow" if L/D > 1. A deep cavity will respond somewhat like an acoustic resonator driven in the depth direction with the oscillatory energy being supplied by the shear layer above the cavity. A shallow cavity, on the other hand, is driven in the length or streamwise direction (1:2). In this experiment, emphasis was only on a shallow cavity with L/D = 2.

Oscillation Process

Large pressure oscillations are generated by tangential flow over an open cavity. These flow-induced pressure oscillations are a result of the interaction of the free-stream shear layer and the medium within the cavity involving both acoustic and hydrodynamic mechanisms (7:2). As water table visualization techniques (7 - 9) indicate, the unsteady motion of the shear layer above the cavity results in mass addition and removal at the cavity trailing edge. In shallow cavities this mass addition and removal process is similar to that of a cavity whose rear bulk head acts like an oscillating piston (8:10). Heller and Bliss referred to this as the "pseudopiston" effect which is illustrated in Figure 2-3. A summary of their detailed discussion of the mechanisms involved follows (8:10-14).
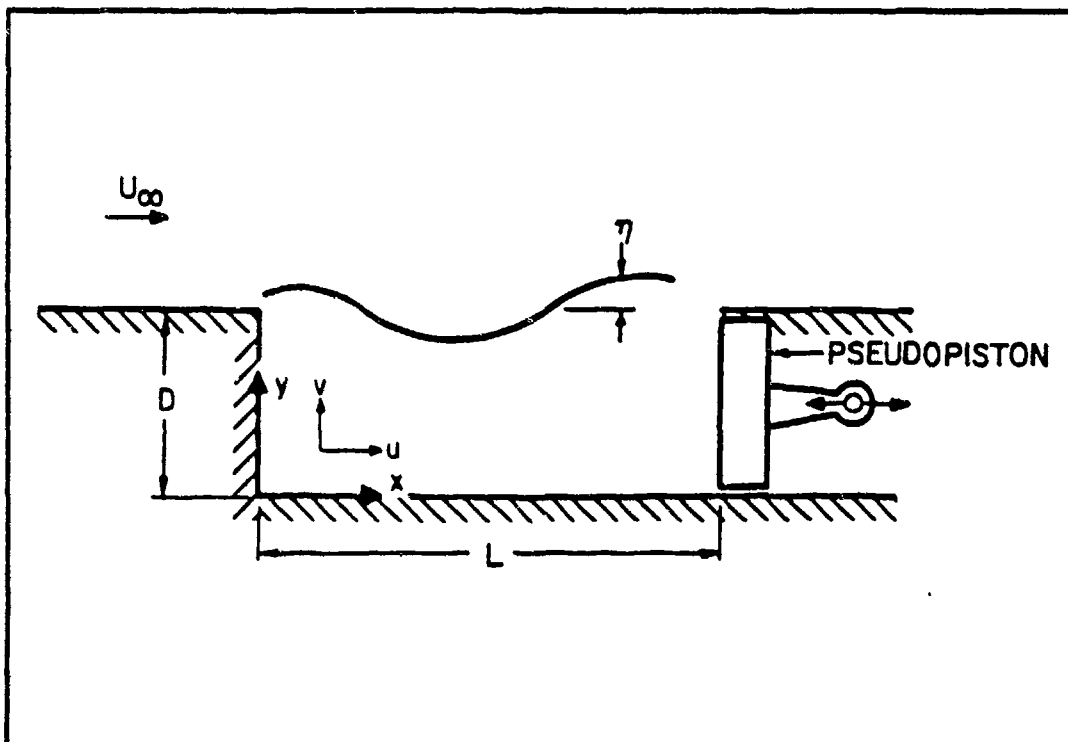
Figure 2-3. Simple Analytical Cavity Model (8:37)

The pseudopiston effect generates forward traveling waves in the cavity that are eventually reflected by the forward bulkhead and thus become rearward traveling waves. These traveling waves force the shear layer in an unsteady manner resulting in the mass addition/removal process that produces the cavity wave structure, thus closing the feedback loop. Energy to sustain this process is provided by the external flow (8:10). Figure 2-4, as illustrated by Heller and Bliss (8), depicts a typical oscillation cycle. Of the 18 sketches shown, six stages (by lettered row) are used to explain the cycle.
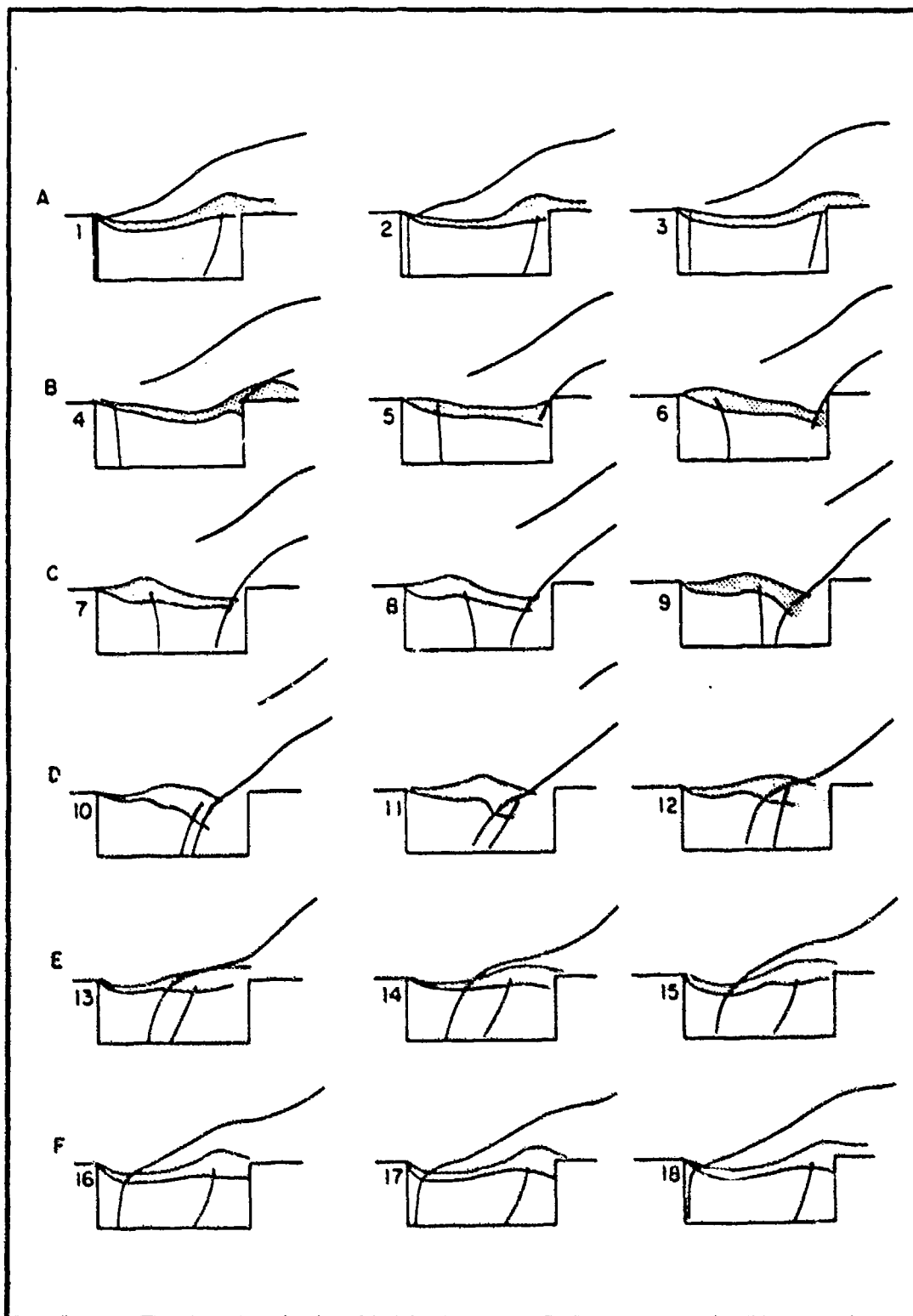
Figure 2-4. Typical Pressure Oscillation Cycle (8:12)

In the first stage of the cycle (A) a pressure wave from a previous disturbance is reflected off the forward bulkhead while the wave previous to it approaches the rear bulkhead causing the shear layer to bulge and expel fluid. As the shear layer waveform and forward reflected wave moves rearward (Stage B), the shear layer begins to interact with the cavity trailing edge and fluid is added back into the cavity initiating the next compression wave. While the forward wave continues rearward the shear layer dips lower into the cavity (Stage C), adding more fluid, and fully forming the rearward traveling compression wave. The rearward and forward traveling waves meet and interact near the cavity center (Stage D) and continue in their respective directions. The top part of the forward traveling wave enters the supersonic flow (Stage E), causing it to be tipped more than the external flow Mach angle while the rearward traveling wave, moving at subsonic relative speed, does not extend beyond the shear layer. As the rearward wave approaches the rear cavity bulkhead the shear layer once again begins to expel fluid (Stage F). The next stage of the process is the same as Stage A, and the oscillation cycle repeats (8:10-14).

This oscillation cycle applies to free-stream supersonic flows. However, the wave structure of the cycle for a subsonic flow is essentially the same. In fact, the forward

2-6

traveling wave will still be supersonic relative to the external flow (8:13).

Resonant Frequencies

Based on experiments, Rossiter (19) developed an acoustic feedback mechanism to model flow over a cavity based on the shedding of periodic vortices at the front lip of the cavity. These vortices are a result of the arrival of an acoustic wave radiated from an acoustic source near or at the rear lip of the cavity. The acoustic source, in turn, is a result of the vortices shed from the front lip (1:7). Based on this model Rossiter proposed the following semiempirical relationship for the non-dimensional cavity resonant frequency, Strouhal number:

$$S = \frac{fL}{U_\infty} = \frac{m - \alpha}{M + \frac{1}{K_v}} \tag{1}$$

where m is any positive integer and corresponds to the frequency mode number, α is an empirical constant that takes into account the phase difference between the upstream arrival of the acoustic wave and the subsequent shedding of a vortex, and K_v is also an empirical constant tied to a disturbance convection speed (1:34). Rossiter determined the value for $\alpha = 0.25$ and $K_v = 0.57$.

Rossiter's formula assumes that the speed of sound in the cavity is equal to the speed of sound of the free-stream. This is equivalent to assuming the cavity

temperature recovery factor is equal to zero. Heller, et al in their experiments determined the actual recovery factor to be equal to unity. Therefore, the speed of sound in the cavity is equal to the free-stream stagnation speed of sound. Consequently, Heller, et al proposed a modification to Rossiter's equation utilizing the stagnation speed of sound (1:34):

$$S^* = \frac{fL}{U_\infty} = \frac{m - \alpha}{\dfrac{M}{\left[1 + \dfrac{\gamma-1}{2} M^2\right]^{1/2}} + \dfrac{1}{K_v}} \tag{2}$$

Oscillation Suppression

Previous studies have shown that pressure oscillation amplitudes can be reduced if the shear layer can be stabilized so as to prevent the mass addition and removal process at the cavity trailing edge. Several experimentalists (9; 11; 12) have evaluated different passive-type methods of stabilizing the shear layer with modest results. However, the effectiveness of any particular suppression device was usually Mach number dependent. Since it has been shown that the cavity pressure oscillations tend towards resonance at discrete frequencies for a given flow condition, it was speculated that perhaps the shear layer could be forced at a frequency different from the resonant frequencies or at some sub-multiple of the resonant frequency with a phase change. Due to complexities

involved, the latter was not evaluated as part of this effort.

III. Experimental Equipment

Test Section Assembly

The test section, shown in Figure 3-1, consisted of a two-dimensional nozzle assembly attached to a flat surface with a rectangular cut-out (cavity) sandwiched between two pieces of 0.75 inch thick clear Plexiglas. The nozzle assembly and the surface containing the cavity were machined from 5/16 inch thick aluminum. Paper gasket material was applied to all aluminum assemblies to prevent leakage. The sandwiched assembly was bolted to a base plate and mounted on a calming chamber.

Four nozzle assemblies were designed to provide the desired flow conditions. One subsonic nozzle assembly incorporating a smooth converging curve was used for M = 0.60, 0.75, and 0.90 flow conditions. Three supersonic converging-diverging nozzle assemblies designed for M = 1.10, 1.35, and 1.70 flow conditions were developed using isentropic relations and an iterative scheme incorporating the method of characteristics. The exit area of each nozzle assembly was identical to allow interchangeability of the nozzles with the surface/cavity assembly. Since the geometry of the nozzles was designed to have fully expanded flow (i.e. $P_{exit} = P_{atm}$) when the desired flow condition was reached, each nozzle assembly was fitted with a static pressure port at the exit.
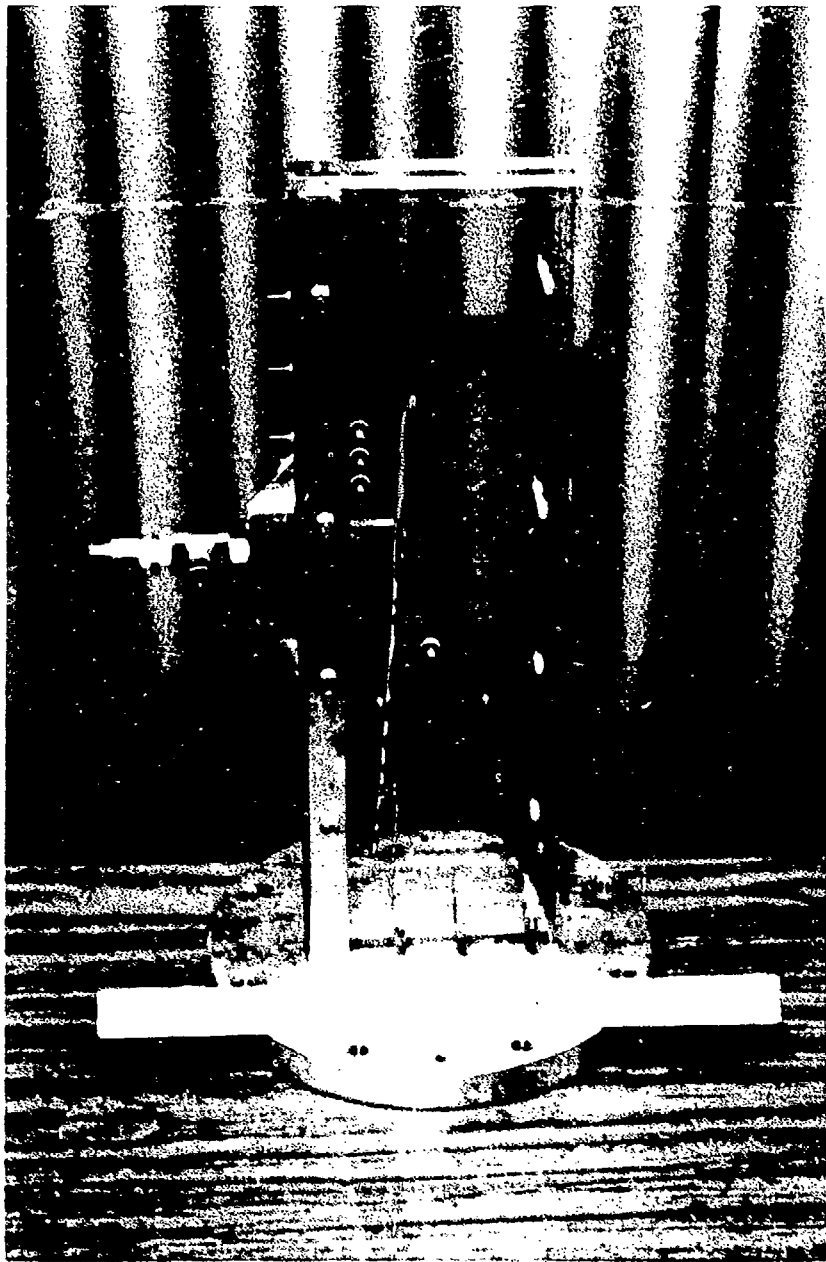
Figure 3-1.   Test Section Assembly

The nozzles accelerated and directed the flow tangent over a flat surface containing a rectangular cut-out, representing the cavity, positioned two inches downstream of the nozzle exit (Figure 3-2). The cavity depth was fixed at one inch while the length was adjusted by inserting or removing blocks that made up the rear bulkhead of the cavity. Cavity lengths of two, three, and 4¾ inches were possible. However, only a cavity with a length of two inches was evaluated. Four static pressure ports, equally spaced, were located along the cavity floor.
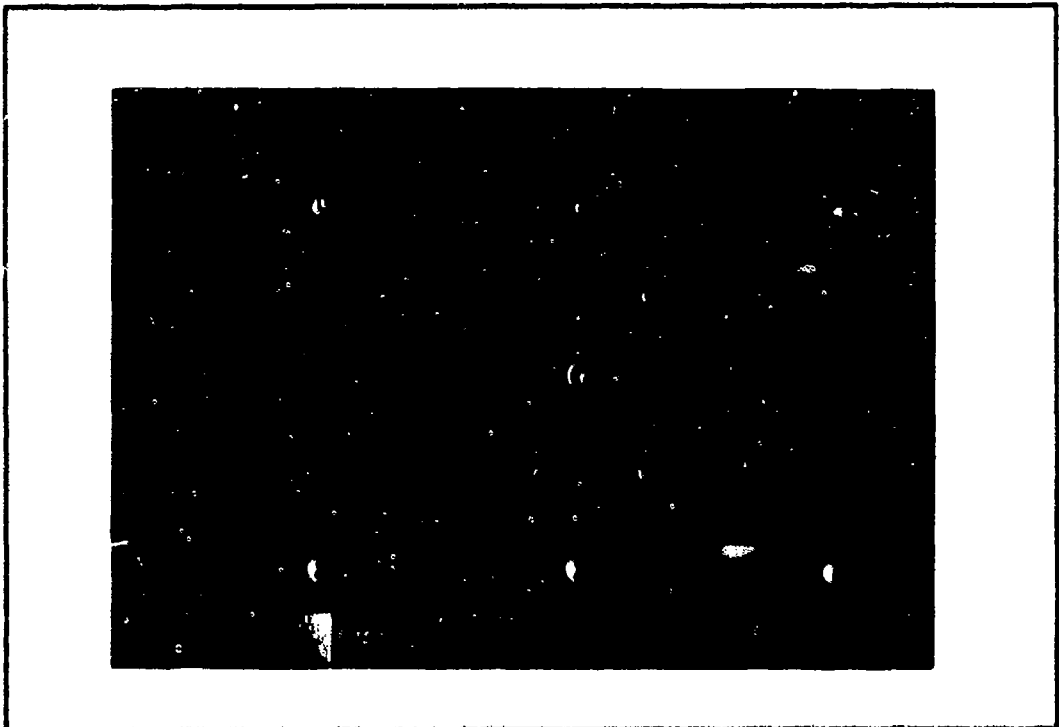
Figure 3-2.   Nozzle and Cavity Assembly

The flat surface from the nozzle exit to the cavity leading edge housed the suppression mechanisms. Figure 3-3 illustrates the design for the pulsing fence mechanism. As shown, the fence is a solid rectangular thin piece of metal attached to a spring loaded pin, driven by hexagonal cam. The cam was coupled to a rheostat controlled 24 volt D.C. motor with a belt as shown in Figure 3-4. To measure the frequency of the pulsation, holes were drilled at each peak of the cam and a light source directed light through the cam and on to a photoresistive cell connected to a frequency counter. The pulsing fence mechanism with the spring and cam removed was also used for the variable height static fence investigation.

Two designs were evaluated for the pulsed secondary flow injection suppression technique. The first design, Figure 3-5, allowed flow injection at an angle of 45 degrees to the external flow at the cavity leading edge. The second design, Figure 3-6, allowed flow injection parallel to the external flow and 0.020 inch below the cavity leading edge. Both nozzle designs were supplied secondary flow via a motor controlled valve. The valve, shown in Figure 3-7, was a ball type valve whose shaft was connected via a gear box to the D.C. motor described above. A grease fitting was also added to the valve for lubrication.

The clear Plexiglas side panels not only allowed for flow visualization, but were also used to position the
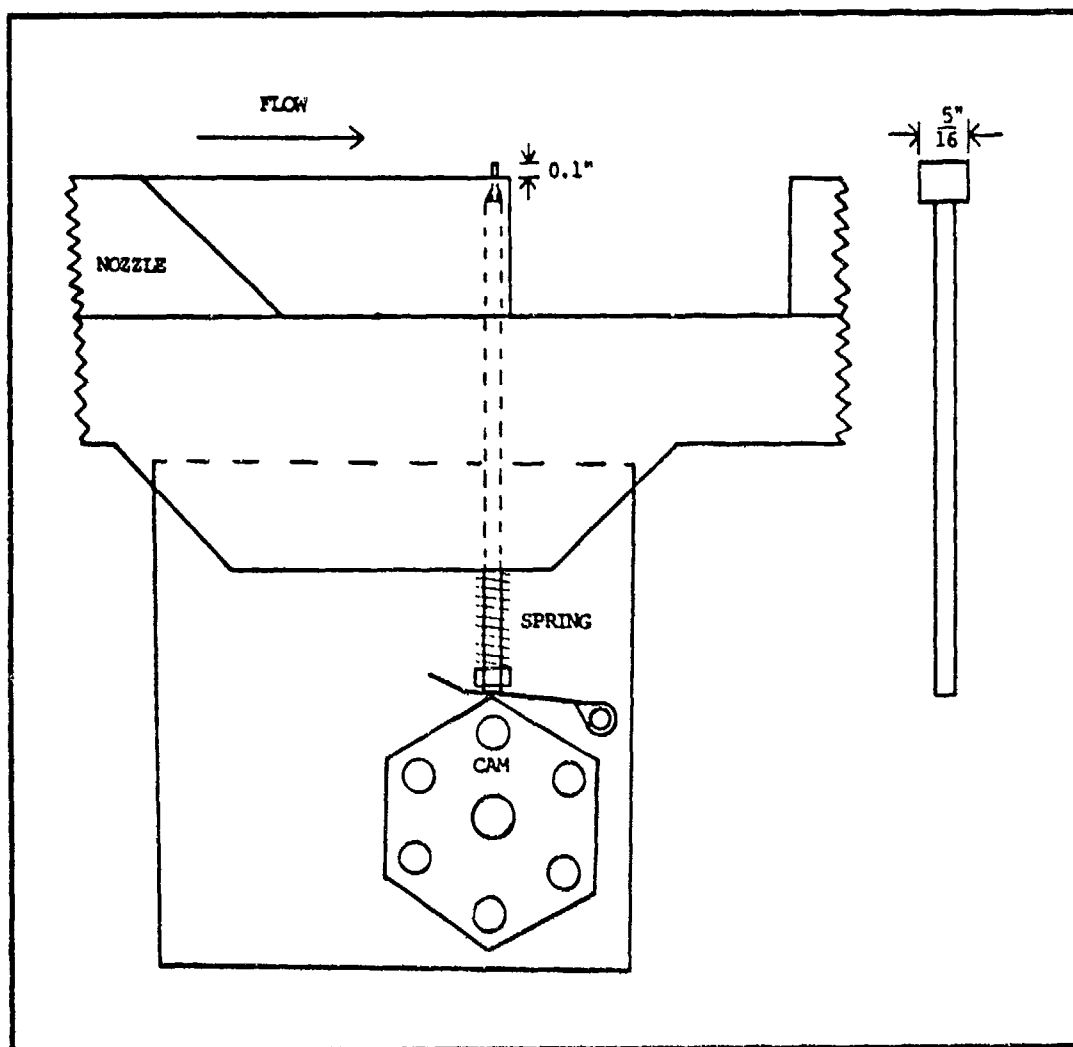
Figure 3-3. Pulsing Fence Mechanism

dynamic pressure transducers flush on the side wall of the

cavity. Figure 3-8 shows the relation of those positions

relative to the cavity. In addition, pins extending through

the aluminum assemblies into the Plexiglas were used to

ensure precise alignment of components.
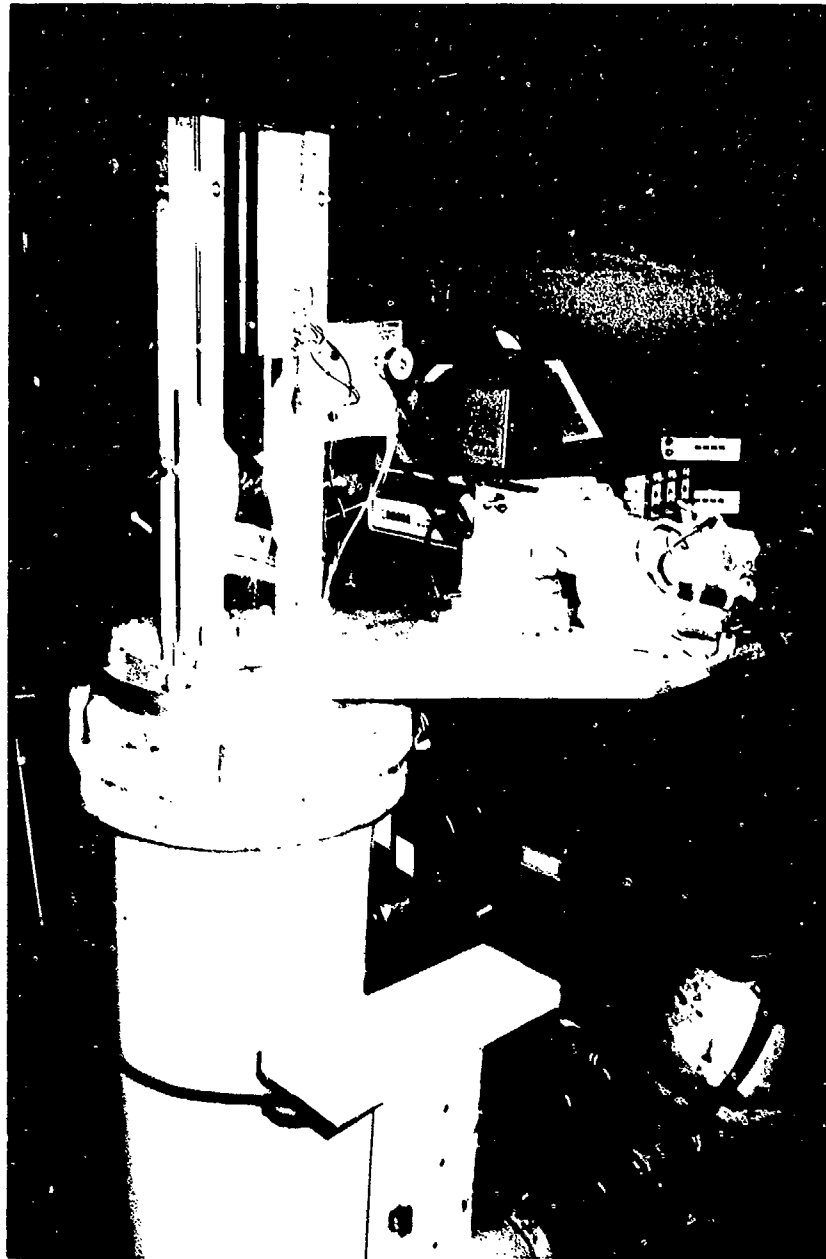
Figure 3-4. Photograph of Pulsing Fence Mechanism
With Belt Driven Motor
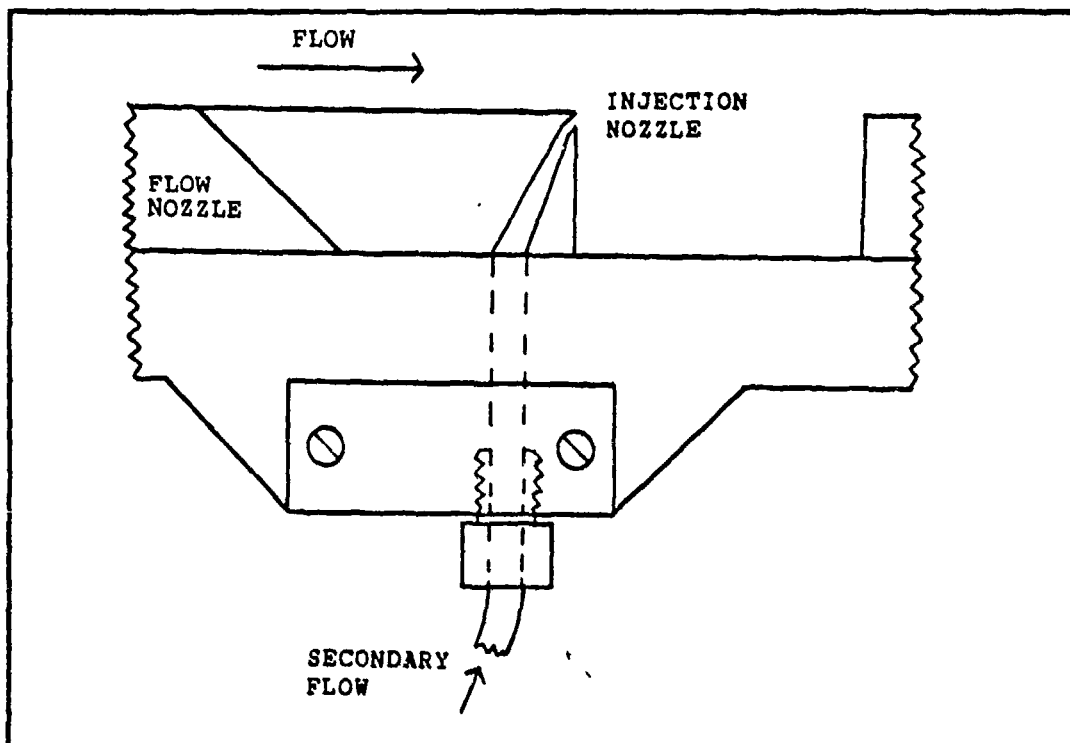
Figure 3-5.   45 Degree Flow Injection Assembly
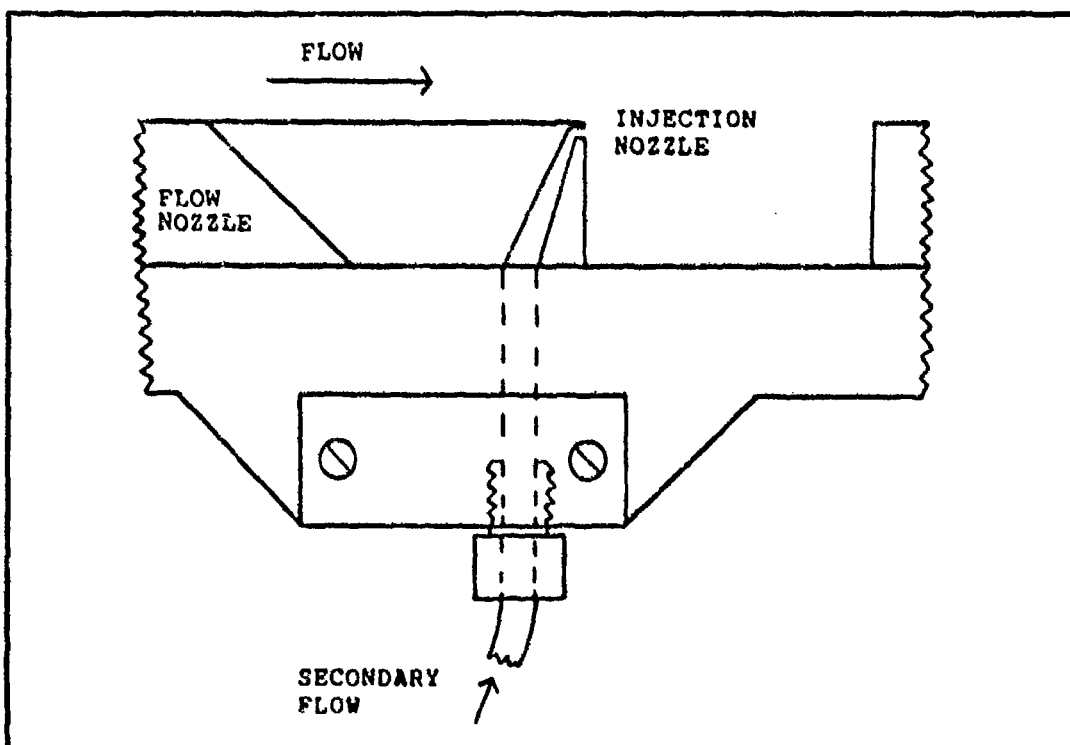
Figure 3-6.   Parallel Flow Injection Assembly
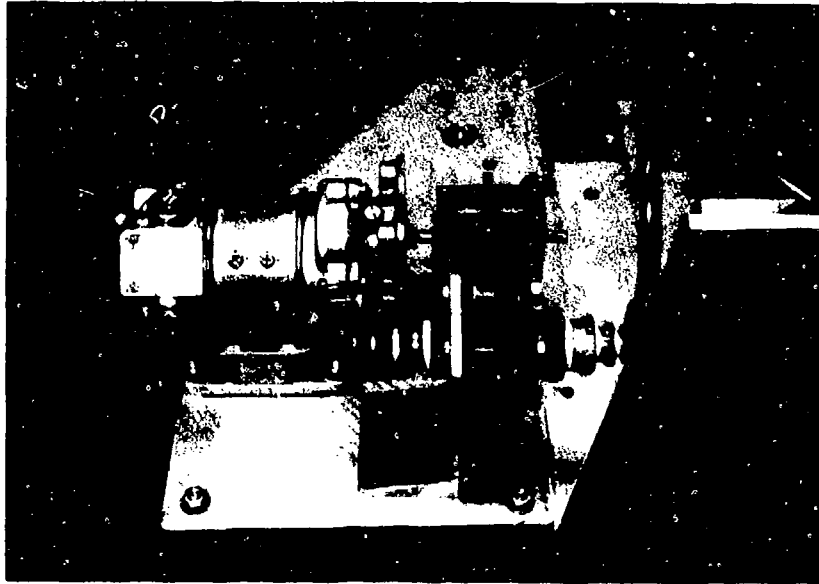
Figure 3-7. Photograph of Ball Valve with Motor
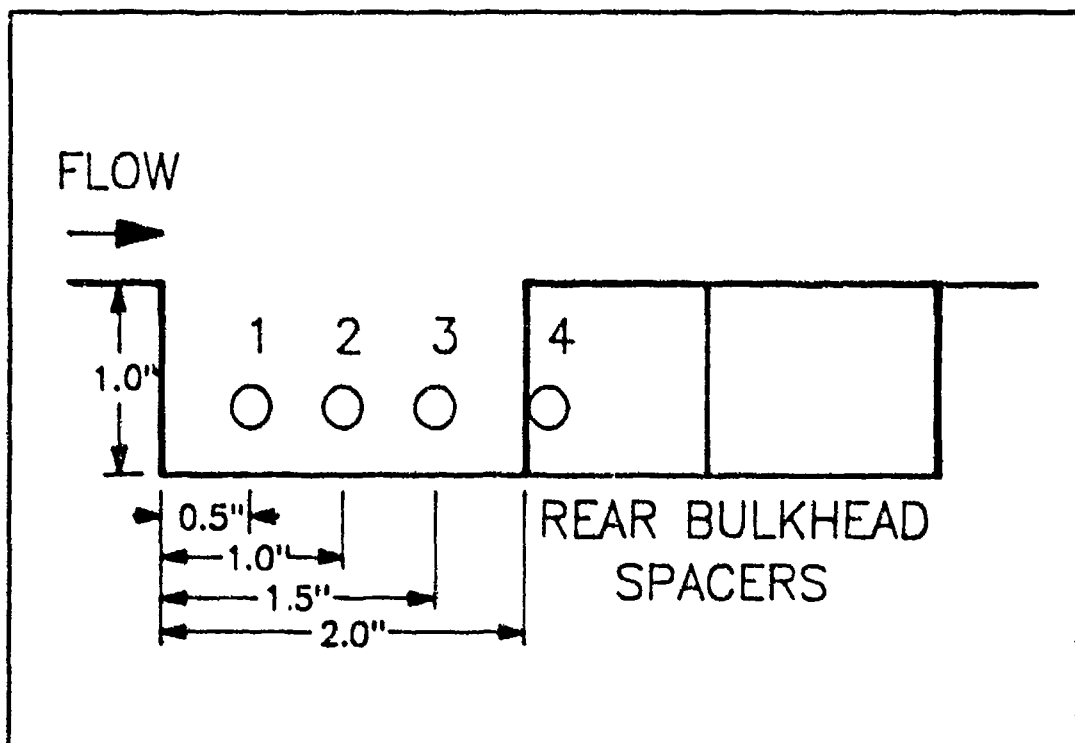
Figure 3-8. Pressure Transducer Cavity Positions

Air Supply System

Compressed air was supplied from two compressors each capable of supplying 0.50 lbm/sec of air at approximately 90 psig. The compressed air was first run through a drier to remove any moisture and then through a filter to remove any particles that could have scratched the Plexiglas. After the filter, the air was routed through a three-inch, high-pressure hose to a straight pipe assembly containing a thermocouple and flange where an orifice was inserted. Upstream static pressure and differential pressure across the orifice were recorded for each run to calculate mass flow rate. From the orifice, the air was piped to a dome valve that was used to regulate the supply pressure. The air was then run into the calming chamber where static pressure (assumed to be the stagnation pressure) was measured. Inside the calming chamber a second filter was in place to trap any remaining particles prior to entering the test section assembly. Figure 3-9 contains a photograph of the test section assembly mounted on the calming chamber.

Instrumentation

Pressure Measurement. Figure 3-10 contains a schematic of the instrumentation. Sound pressure measurements within the cavity were taken with three Endevco Model 8506 piezoresistive dynamic pressure transducers. Signal conditioning and amplification was accomplished with three Endevco Model 4423 signal conditioners powered by a single

3-9
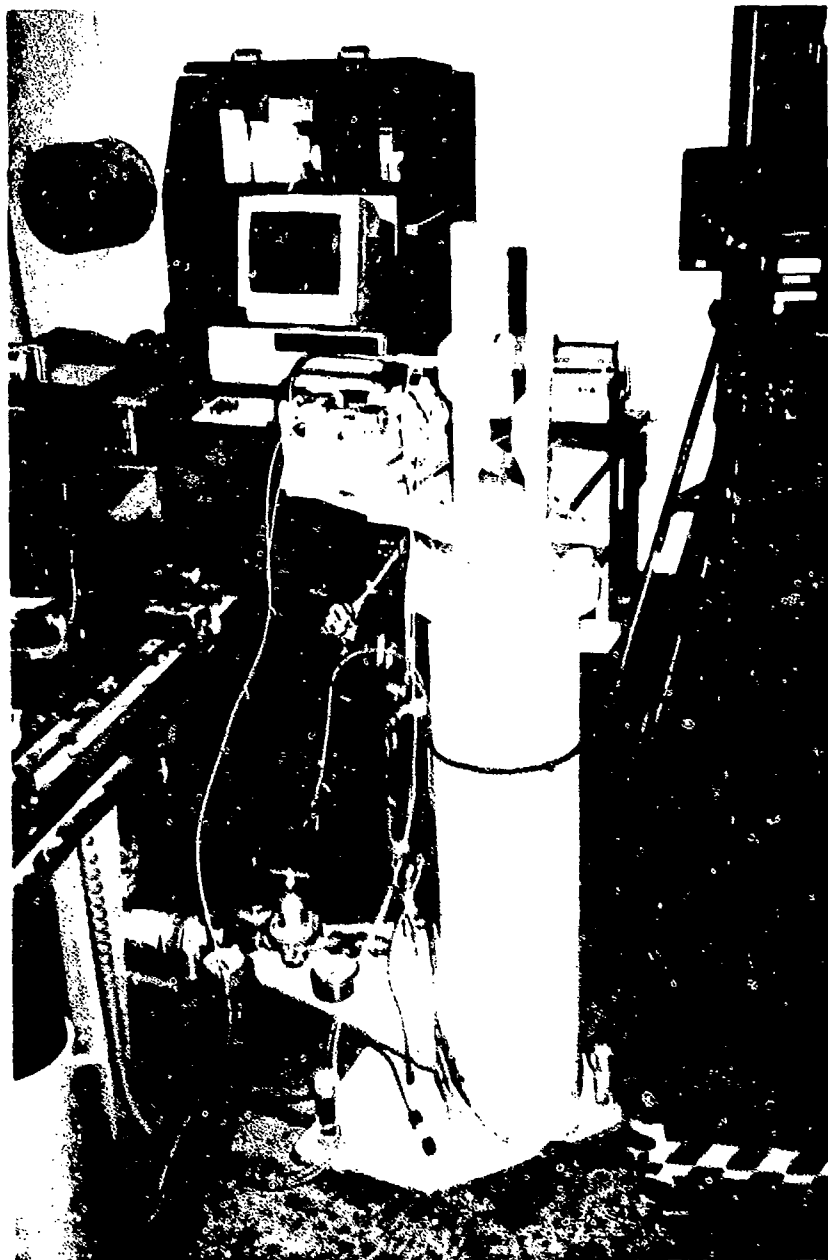
Figure 3-9.   Photograph of Test Section
Mounted on Calming Chamber
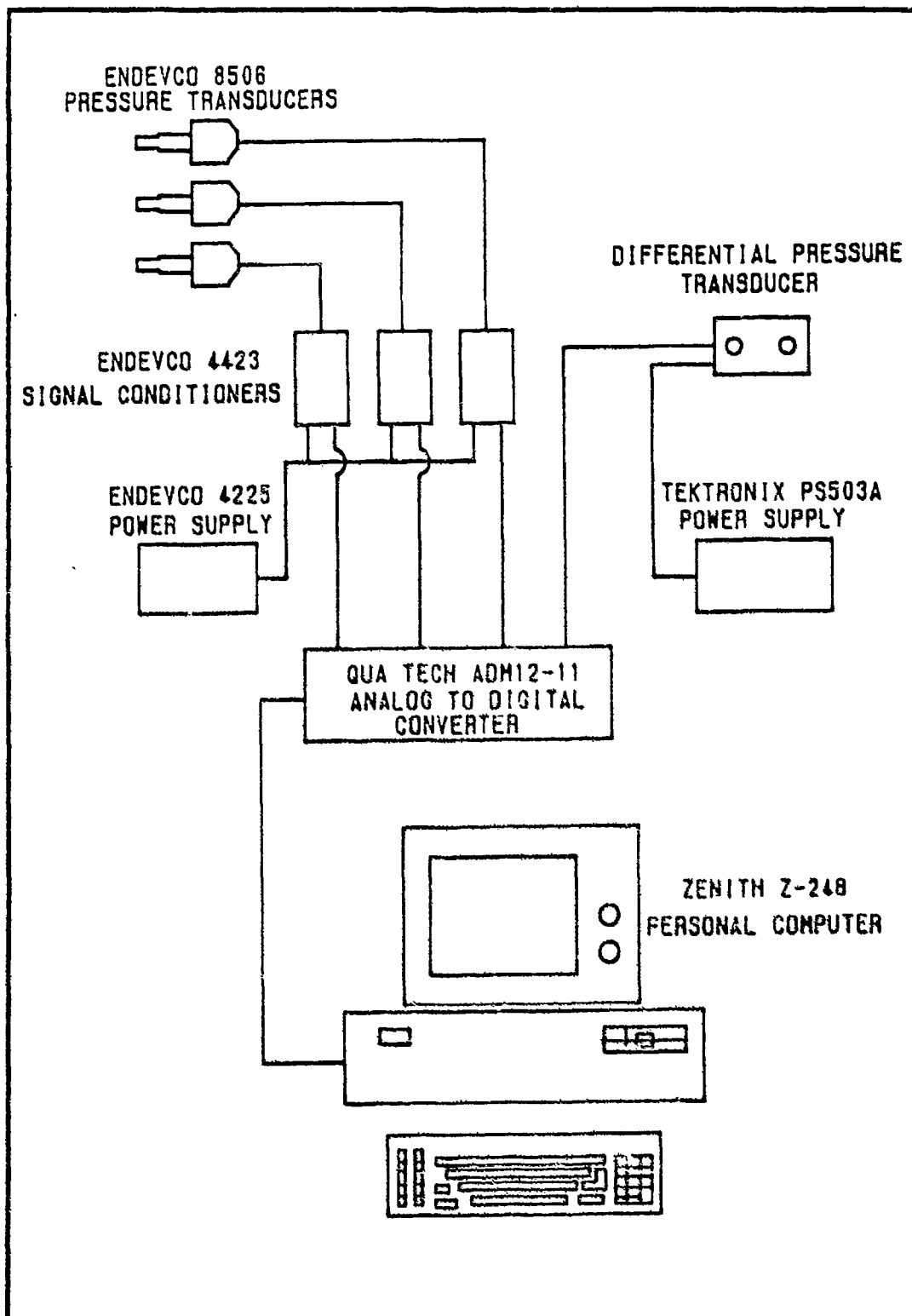
Figure 3-10. Schematic of the Instrumentation

Endevco Model 4225 Power Supply. The three conditioned and amplified signals were interfaced with a Zenith Model Z-248 personal computer through a Qua Tech Model ADM12-11 twelve bit analog to digital converter module and stored in integer data files.

Static pressure within the calming chamber was measured with an Endevco Model 8530 piezoresistive pressure transducer powered by a Tektronix Model PS503A D.C. Power Supply and read on a Hewlett Packard Model 3466A Digital Multimeter. Static pressures at the nozzle exit and cavity floor were measured with a bank of U-tube mercury manometers with one side open to the atmosphere.

Flow Visualization. A schlieren optical system was set up as shown in Figure 3-11. This system used a spark lamp with a spark duration of approximately 1/6 microsecond, enabling a photograph to be taken showing the shear layer, Mach lines, and shock waves for each cavity run.
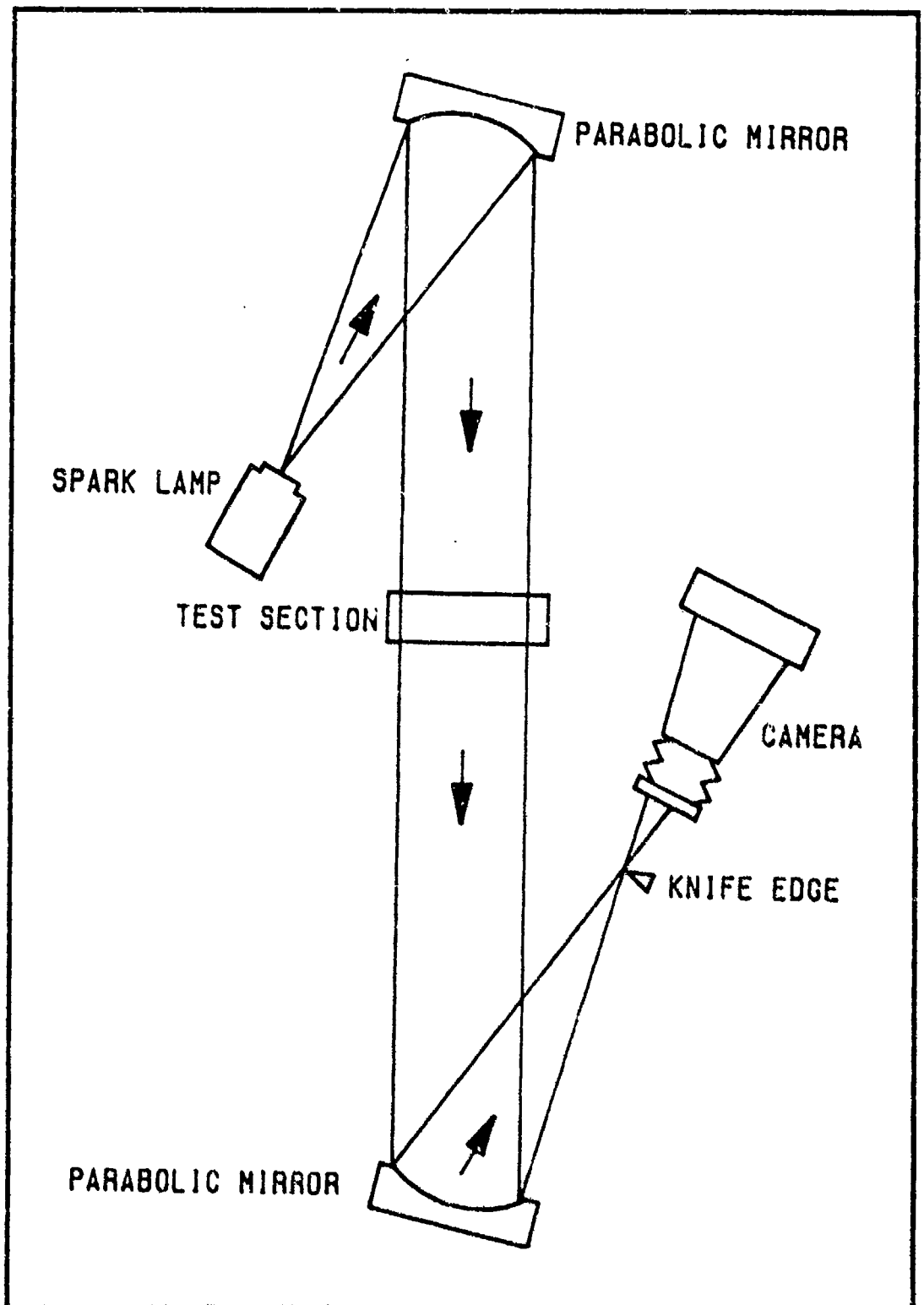
Figure 3-11. Schematic of the Schlieren Setup

3-13

IV. Experimental Procedures

Calibration

All pressure transducers were calibrated statically using a dead weight calibrator. This provided an overall sensitivity value (mV/psi), incorporating transducer and amplifier as a system, for each channel. The particular transducers used to measure sound pressure level were also tested dynamically to verify applicability of static calibration for dynamic measurements using a Larson-Davis Model CA250 Precision Calibrator. This calibrator produced a 114.0 dB 250 Hz level output signal. This dynamic test was also used to verify operation of the data collection equipment as well as post processing algorithms.

Flow Condition Determination

To determine the required pressure for a desired flow Mach number, the air flow supply valve was opened and the delivery pressure was modulated with a dome valve (pressure regulator) until the nozzle exit pressure stabilized to atmospheric pressure. Measurement of the Mach angle from a schlieren photograph of this flow condition showed a consistently lower nozzle exit Mach number than the nozzle design condition. This was mainly attributed to boundary layer growth that was not accounted for during nozzle design. Therefore, the supply pressure was increased to improve the flow over the cavity. This supply pressure was

then used for all subsequent runs at that flow condition. For subsonic runs, mass flow rate, as calculated from differential pressure measured across a known orifice area (13:197-210), was used to determine the pressure required for a desired flow test condition.

Data Acquisition

After adjusting to the required supply pressure for a given flow condition, the reading obtained from a pressure transducer in the calming chamber was monitored to ensure steady state repeatable flow conditions. Upon achieving the desired pressure, data sampling was initiated. Data from the cavity pressure transducers were sampled at a rate of 29,917 Hz and stored as an integer data file. Due to computer array size limitations, only 2,049 data points, per channel, could be sampled. In addition to recording sound pressure levels, a fourth channel was used to measure either differential pressure across the orifice meter or dynamic pressure amplitude at the entrance of the secondary flow injection nozzle. While the four channels of data were being written to a data file, flow temperature, calming chamber pressure, nozzle exit pressure, and cavity floor static pressures were recorded. For flow visualization, a schlieren photograph was also taken.

Data Reduction

Since the raw data file was a discretely sampled, integer valued, digitized representation of an analog signal, the digitized data had to be first converted from an integer bit value to a voltage. The voltage was then converted to pressure amplitude by dividing by the applicable sensitivity value determined during calibration. This resulted in discretely sampled pressure data. This pressure data was then processed using a Fast Fourier Transform (FFT) algorithm (14:381-396). This provided data of pressure amplitude (psi) versus discrete frequency (Hz). The pressure amplitude values were then converted to decibels (dB) using the following equation:

$$\text{Sound Pressure Level (SPL)} = 20 \log_{10} \frac{P_{rms}}{P_{ref}} \text{ dB} \qquad (3)$$

where $P_{ref} = 2.9 \times 10^{-9}$ psi rms is the statistical "threshold of hearing" for the human ear. This SPL versus frequency data was plotted using a graphics program written by Golden Software, Inc., called Grapher. A representative plot is shown in Figure 4-1. As indicated in this plot, the first three modes corresponding to the modified Rossiter's equation (2) are clearly evident.

Data Analysis and Comparison

To determine the suppression effectiveness for a given run configuration, a baseline (to be used for comparison)

was established for each configuration and flow condition tested. The baseline data sets were generated by averaging the SPL amplitude (dB), for each discrete frequency, of at least five runs at identical flow conditions without the suppression device. A sample plot of the averaged data for the same flow condition and configuration used in Figure 4-1, is shown in Figure 4-2. As a comparison between these figures indicate, the averaged data had much less variation between discrete frequencies except at specific modes.

Averaging the amplitudes for the baseline data set worked well, but the variation between sample data points was unknown. Therefore, a sample standard deviation (σ) was computed for each discrete frequency using the following equation:

$$\sigma = \left[\frac{\sum_{i=1}^{N} (SPL_i - \overline{SPL})^2}{N - 1} \right]^{1/2} \tag{4}$$

where N is the number of samples used to compute a particular baseline data set. If a normal distribution is assumed for the variation of the data points, then 68 percent of the data points will be within $\pm 1 \sigma$ of the sample average and 95 percent of the data points will be within $\pm 2 \sigma$ of the sample average. Due to the significantly higher percentage, $\pm 2 \sigma$ was used to estimate the variation of the data. To facilitate visualization of this
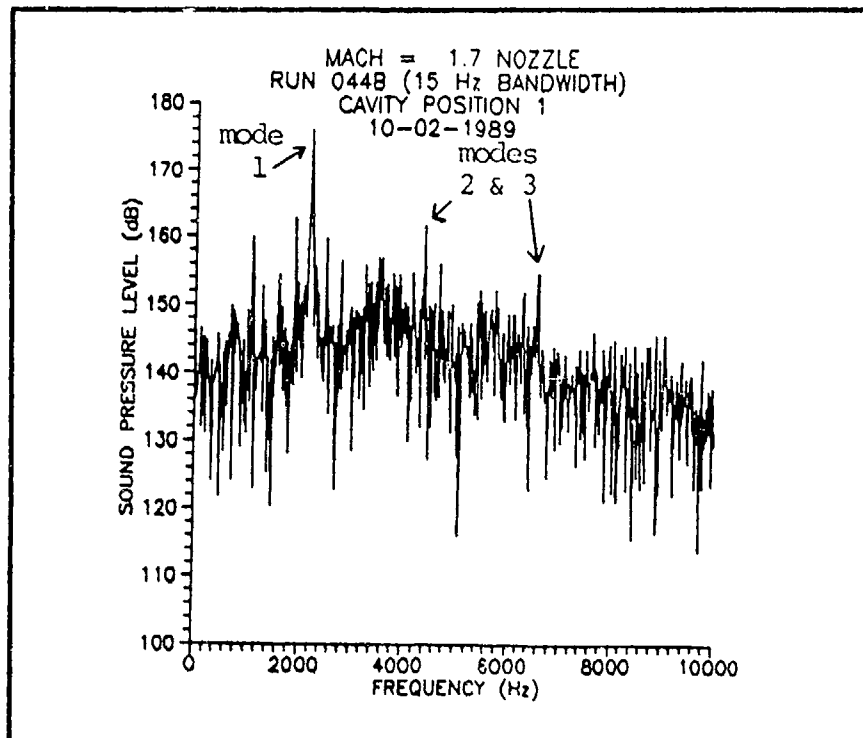
Figure 4-1. Sample Pressure Oscillation Plot
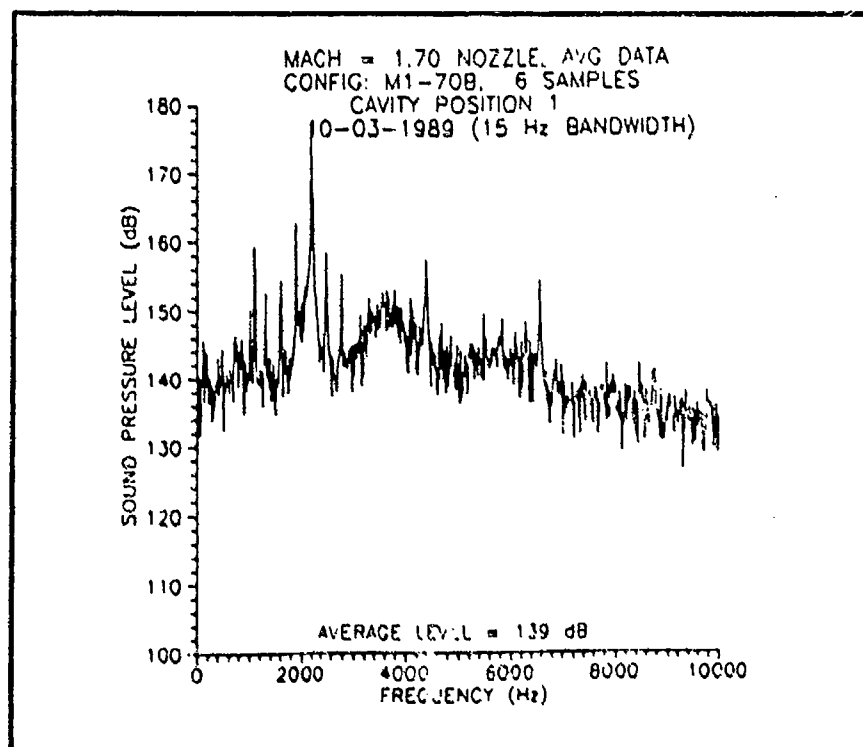
Figure 4-2. Sample Average Baseline Data Plot

variation, plots of the average data ± 2 σ were also generated for each of the baseline data sets. Samples of these are shown in Figures 4-3 and 4-4.

These baseline plots (average data, and average ± 2 σ) provided a qualitative method to compare the effectiveness of a particular suppression device. But with a large number of runs, a quantitative type method was required to provide the experimenter with a quick estimate of the suppression effectiveness of a particular run. Therefore, an algorithm was developed that compared by frequency the 25 peak amplitudes of the baseline data set with the corresponding amplitudes of the current run. However, since quite often the suppression device caused a frequency shift of a mode to the next discrete frequency interval, this comparison alone was somewhat misleading. Consequently, the 25 peak amplitudes of the current run and the corresponding baseline data set amplitudes were added to the comparison. A sample printout of the resulting comparison (25 peak amplitudes of the baseline data set and 25 peak amplitudes of the current run) is provided in Table 4-I.

The 25 peak amplitude comparison was very useful for evaluating, over a large spectrum of pressure oscillation frequencies, the suppression effectiveness of a particular configuration. However, since one mode usually had a much higher amplitude than any other mode, and keeping in mind the logarithmic scale for decibels, reduction of this peak

4-6

Figure 4-3.   Sample Average + 2 σ Baseline Data Plot

Figure 4-4.   Sample Average – 2 σ Baseline Data Plot

Table 4-I.   Sample 25 Peak Amplitude Comparison Printout

```
                    MACH  =   1.7   NOZZLE
                  RUN  044B    10-03-1989
          COMPARISON  WITH  M1-70B  ( 6 SAMPLES)
                      (15 Hz BANDWIDTH)
```

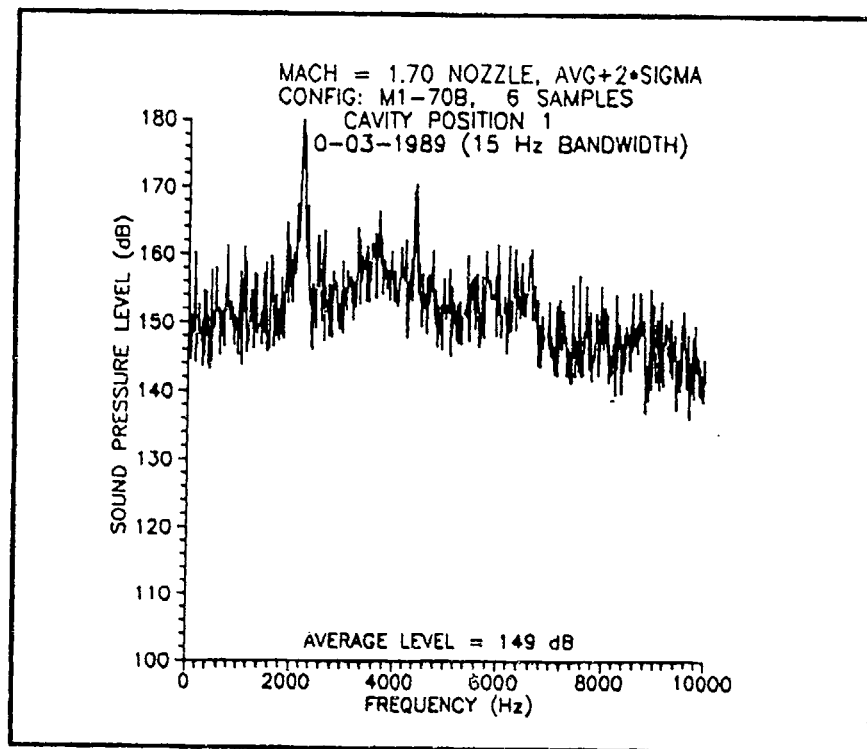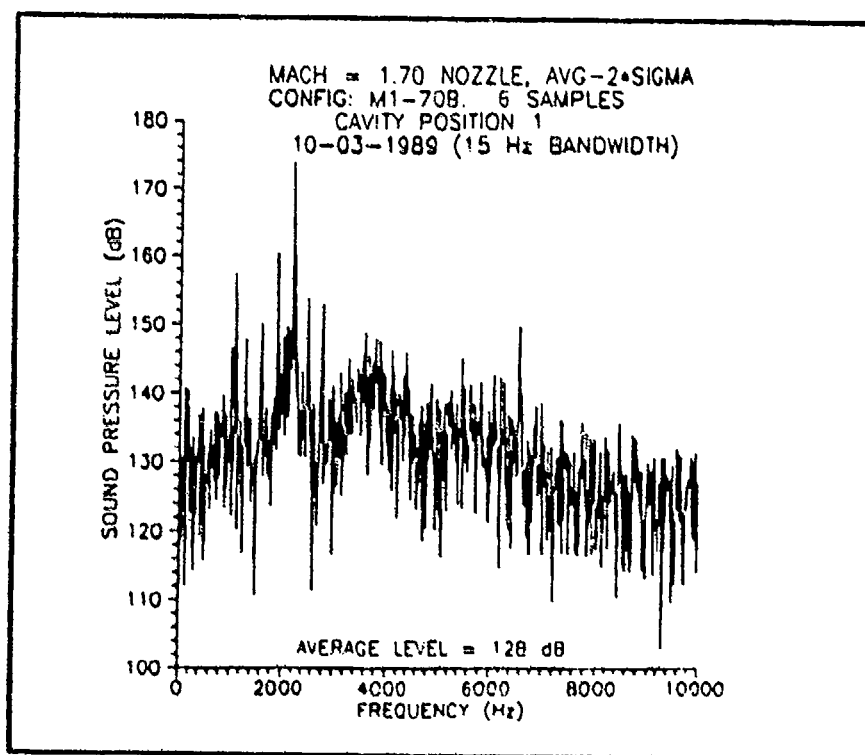| MAX AMPL MODE FREQ	SAMPLE DATA AVG SPL dB CAVITY POS			STD DEV.SIG CAVITY POS			AVG-2*SIGMA CAVITY POS			RUN DATA ACT SPL dB CAVITY POS			DIF W\AVG CAVITY POS			DIF W\-2SIG CAVITY POS		
	1	2	3	1	2	3	1	2	3	1	2	3	1	2	3	1	2	3
2191	177	163	178	1	1	1	174	161	175	176	163	177	-1	-0	-1	2	2	2
2220	166	153	167	3	2	3	160	149	161	162	153	164	-4	-1	-3	2	4	3
1899	162	148	163	1	2	1	160	143	162	163	152	163	0	3	-1	2	8	1
1096	159	154	160	1	2	1	157	151	158	160	153	158	1	-1	-2	2	2	0
2162	159	147	160	7	6	8	144	135	144	164	151	165	6	4	5	20	16	21
2498	158	145	159	2	3	3	154	139	153	160	145	161	2	0	2	6	5	8
4382	157	163	158	6	5	6	146	154	147	147	154	147	-10	-9	-10	1	1	1
2250	157	146	158	6	3	4	146	139	150	158	148	159	2	2	1	13	9	9
2133	156	137	155	3	8	4	149	121	146	158	145	159	3	8	4	9	24	13
2790	155	144	156	1	2	1	153	140	154	157	141	156	1	-3	-1	4	1	3
1607	154	143	154	2	3	3	150	138	149	155	143	154	0	0	-1	4	6	3
6574	154	155	154	2	2	5	150	151	144	155	154	156	1	-1	3	5	3	13
2074	153	136	154	2	11	2	150	114	149	153	116	154	-1	-20	0	3	1	5
3798	153	151	146	2	1	3	148	150	140	155	152	150	2	1	4	6	3	9
3652	153	141	135	5	4	3	143	132	128	145	142	134	-8	1	-1	3	10	6
1300	152	136	158	2	9	1	148	118	150	153	137	152	0	0	-1	5	18	
3564	152	136	138	3	3	4	146	130	131	151	131	142	-1	-4	3	5	1	11
2279	152	140	153	4	3	4	145	134	144	156	138	157	4	-1	4	11	5	13
2104	152	142	154	8	2	8	137	137	137	150	140	153	-2	-2	-1	13	3	16
3681	152	140	148	3	4	2	145	131	144	152	140	145	1	-2	-3	7	9	1
3287	152	155	144	3	3	6	145	150	132	150	153	138	-1	-2	-5	5	3	7
4090	152	158	153	3	3	2	146	154	148	147	157	152	-4	-1	-1	1	3	4
4353	152	158	153	5	5	2	142	151	149	150	156	151	-2	-1	-2	8	5	2
4412	151	158	153	6	4	4	140	150	146	141	154	148	-10	-3	-6	1	1	1
3608	151	140	136	1	6	4	149	128	128	151	138	132	0	-1	-4	2	10	5
2191	177	163	178	1	1	1	174	161	175	176	163	177	-1	-0	-1	2	2	2
2162	159	147	160	7	6	8	144	135	144	164	151	165	6	4	5	20	16	21
1899	162	148	163	1	2	1	160	143	162	163	152	163	0	3	-1	2	8	1
2220	166	153	167	3	2	3	160	149	161	162	153	164	-4	-1	-3	2	4	1
4397	156	163	157	7	7	7	142	148	145	162	167	163	6	6	6	20	19	18
1096	159	154	160	1	2	1	157	151	158	160	153	158	1	-1	-2	2	2	0
2498	158	145	159	2	3	3	154	139	153	160	145	161	2	0	2	6	5	8
2250	157	146	158	6	3	4	146	139	150	158	148	159	2	2	1	13	9	9
2133	156	137	155	3	8	4	149	121	146	158	145	159	3	8	4	9	24	13
3521	148	143	132	7	7	5	134	136	123	157	143	137	9	-0	5	23	6	13
3594	150	143	135	6	5	5	138	134	127	157	142	132	6	-1	-3	19	9	
2790	155	144	156	1	2	1	153	140	154	157	141	156	1	-3	-1	4	1	
4689	148	152	146	5	2	4	138	148	138	156	153	152	8	2	6	18	5	
3258	147	141	139	5	4	4	137	133	131	156	145	135	9	4	-4	19	12	
2279	152	140	153	4	3	4	145	134	144	156	138	157	4	-1	4	11	5	13
6574	154	155	154	2	2	5	150	151	144	155	154	156	1	-1	3	5	3	
4163	148	146	145	4	5	4	140	136	136	155	141	146	7	-6	1	15	5	10
3798	153	151	146	2	1	3	148	150	140	155	153	150	2	1	4	6	3	
1607	154	143	154	2	3	3	150	138	149	155	143	154	0	0	-1	4	6	
3915	150	140	137	4	3	3	143	134	131	155	143	139	4	3	2	11	9	
4368	151	159	155	9	7	5	134	150	145	162	158	158	3	-3	4	21	12	14
10664	146	145	150	7	9	6	132	127	138	154	149	157	8	3	8	22	9	
2300	149	142	151	7	9	4	131	134	143	154	138	155	5	-4	4	23	4	
3374	143	142	144	4	5	2	140	132	140	153	140	144	5	-1	0	13	8	
3550	150	137	135	5	5	7	141	127	121	153	129	131	3	-8	-4	13	2	

| PEAK MODE AVG | 155 | 147 | 153 | 4 | 4 | 4 | 147 | 140 | 145 | 156 | 147 | 153 | 1 | -0 | 1 | 9 | 7 | 2 |
| ALL MODE AVG | 139 | 143 | 140 | 5 | 5 | 5 | 129 | 133 | 129 | 139 | 143 | 139 | -0 | -0 | -1 | 10 | 10 | 10 |

mode was most crucial. Therefore, a peak mode summary was also generated from the run data. It compares the largest peak amplitude of the current run with the average level of the largest peak amplitudes of the baseline data set. This comparison was done independently of the actual frequencies (i.e. 2,000 Hz amplitude compared with a 500 Hz amplitude). Once again a sample standard deviation was calculated for the single peak amplitude of the baseline data set and the sample average minus 2 σ was used for the comparison. A sample of this printout is shown in Table 4-II.

Resonant Frequency Comparison

The modified Rossiter equation for resonant frequency discussed in Chapter III was used to estimate the resonant frequencies. The modified Strouhal number equation is repeated below for convenience:

$$S^* = \frac{fL}{U_\infty} = \frac{m - \alpha}{\dfrac{M}{\left[1 + \dfrac{\gamma-1}{2} M'\right]^{\frac{1}{2}}} + \dfrac{1}{K_v}} \tag{2}$$

where f is the resonant frequency for the m'th mode. To solve this equation, cavity Mach number is required. But Mach number determination was not a straight forward task. The nozzle design condition and nozzle pressure ratio (P_{exit}/P_o), often yielded different estimates of flow Mach number.

Table 4-II.   Sample Peak Mode Summary Printout

```
              PEAK  MODE  SUMMARY

COMPARISON  WITH  M1-70B  ( 7 SAMPLES)

              10-06-1989


SAMPLE DATA: AVERAGE LEVEL (dB)   176.9   163.3   177.9
             STANDARD DEVIATION     1.4     1.0     1.3
             AVERAGE FREQUENCY   2191.2
```

RUN NUMBER	MODE FREQ	MAX AMPLITUDE, 1st MODE CAVITY POSITION			DIF W/(AVG-2*SIGMA) CAVITY POSITION		
		1	2	3	1	2	3
041B	2191	178	165	179	4.0	3.3	3.8
042B	2191	175	162	177	1.4	0.7	1.4
043B	2191	175	163	176	1.0	1.3	1.0
044B	2191	176	163	177	1.9	1.5	1.9
045B	2191	178	165	178	3.6	3.3	3.3
046B	2220	169	160	168	-5.3	-0.8	-7.5
047B	3959	158	127	137	-16.4	-34.4	-37.7
048B	4163	160	128	137	-14.3	-33.7	-38.5
049B	2191	177	163	178	2.8	1.5	2.4
050B	2191	178	164	179	4.2	2.9	4.2
051B	2206	173	161	173	-1.1	-0.4	-2.6
052B	44	172	171	171	-2.4	10.1	-4.9
053B	50	171	171	170	-3.0	9.4	-5.2
054B	88	171	170	170	-3.0	8.6	-5.6
055B	102	173	172	171	-1.3	10.6	-3.8
056B	131	171	169	168	-3.4	7.8	-6.9
057B	2849	159	134	152	-15.6	-27.2	-22.8
058B	2863	166	146	160	-8.0	-15.5	-15.2
059B	2191	178	164	179	4.4	3.2	4.1
060B	2250	170	161	169	-3.9	-0.3	-6.6
061B	5054	168	158	166	-5.8	-1.4	-8.8
062B	5186	164	160	163	-10.2	-1.5	-12.2
063B	2965	163	158	168	-10.7	-3.3	-7.6
064B	5682	157	161	154	-17.5	-0.6	-21.2
065B	5639	164	163	162	-10.6	2.2	-13.6
066B	5595	163	160	159	-11.4	-0.9	-15.7

4-10

Mach number could also be determined from the Mach angle (μ) measured in the schlieren photographs by the following relation:

$$M = \frac{1}{SIN\ \mu} \qquad (5)$$

However, measurement of the Mach angle from the schlieren photographs was not only difficult, but usually varied by several degrees from picture to picture for identical flow conditions. This was attributed to the very unsteady behavior of the flow induced by the cavity.

To improve Mach number estimation, two additional methods for calculating Mach number were incorporated. One method used an atmospheric pressure ratio. Since the nozzle exit pressure was usually slightly higher than atmospheric pressure (P_{atm}), it was assumed that the flow continued to expand to P_{atm} after exiting the nozzle and thus P_{atm}/P_0 was used to estimate the flow Mach number at the cavity.

Another estimate was obtained from the measured mass flow rate incorporating boundary layer growth in the nozzle. Since the distance between the Plexiglas side panels was relatively small (5/16 inch), small boundary layer growth on the Plexiglas could significantly reduce the nozzle exit area and thus affect Mach number computation. Therefore a laminar boundary layer was assumed in the nozzle and its height was calculated by (15:25):

$$\delta = 5 \left[\frac{\nu 1}{U_\infty} \right]^{1/2} \tag{6}$$

A sample printout showing the different calculated values of
Mach number and the resulting resonant frequencies for the
first three modes is shown in Table 4-III. As shown, each
of these resonant frequencies (first three modes) were
compared (percent difference or error) with the actual
frequencies for the first three modes indicated on the plot
of SPL versus frequency for that particular run.

Table 4-III. Sample Resonant Mode Frequency Summary

RESONANT MODE
FREQUENCY SUMMARY

RUN NUMBER	ACTUAL MODE FREQUENCY MODE 1	MODE 2	MODE 3	TYPE OF DATA USED FOR FREQUENCY CALCULATION	CALC MACH NUMBER	MODE 1 RESON FREQ	ERROR (%)	MODE 2 RESON FREQ	ERROR (%)	MODE 3 RESON FREQ	ERROR (%)
0418	2191	4382	6559	DESIGN CONDITION	1.70	2229	-1.7	5202	-15.8	8173	-19.8
				ISENTROPIC FLOW Pe/Po	1.57	2162	1.3	5046	-13.2	7929	-17.3
				ISENTROPIC FLOW Pa/Po	1.58	2169	1.8	5068	-13.4	7951	-17.5
				UPSTREAM MACH ANGLE	1.41	2075	5.6	4841	-9.5	7607	-13.8
0428	2191	4397	6574	DESIGN CONDITION	1.70	2230	-1.8	5204	-15.5	8178	-19.6
				ISENTROPIC FLOW Pe/Po	1.57	2163	1.3	5048	-12.9	7933	-17.1
				ISENTROPIC FLOW Pa/Po	1.58	2170	1.8	5062	-13.1	7955	-17.4
				UPSTREAM MACH ANGLE	1.41	2076	5.6	4843	-9.2	7610	-13.6
0438	2191	4397	6585	DESIGN CONDITION	1.70	2231	-1.8	5206	-15.5	8180	-19.5
				ISENTROPIC FLOW Pe/Po	1.57	2164	1.2	5050	-12.9	7936	-17.0
				ISENTROPIC FLOW Pa/Po	1.58	2170	0.9	5064	-13.2	7958	-17.2
				UPSTREAM MACH ANGLE	1.44	2092	4.7	4881	-9.3	7678	-14.1
0448	2191	4397	6574	DESIGN CONDITION	1.70	2230	-1.8	5204	-15.5	8178	-19.6
				ISENTROPIC FLOW Pe/Po	1.57	2164	1.3	5049	-12.9	7933	-17.1
				ISENTROPIC FLOW Pa/Po	1.58	2170	1.0	5063	-13.2	7955	-17.4
				UPSTREAM MACH ANGLE	1.44	2091	4.8	4879	-9.9	7668	-14.3
0458	2191	4368	6559	DESIGN CONDITION	1.70	2232	-1.8	5208	-16.1	8183	-19.8
				ISENTROPIC FLOW Pe/Po	1.57	2165	1.2	5052	-13.5	7939	-17.4
				ISENTROPIC FLOW Pa/Po	1.58	2171	0.9	5066	-13.8	7961	-17.6
				UPSTREAM MACH ANGLE	1.44	2093	4.7	4883	-10.5	7673	-14.5
0468	2220	5011	7400	DESIGN CONDITION	1.70	2232	-0.5	5208	-3.8	8184	-4.6
				ISENTROPIC FLOW Pe/Po	1.57	2165	2.5	5052	-4.8	7938	-6.8
				ISENTROPIC FLOW Pa/Po	1.58	2171	2.2	5066	-1.1	7961	-7.0
				UPSTREAM MACH ANGLE	1.41	2077	6.9	4847	3.4	7616	-2.8
0478	0	3959	6580	DESIGN CONDITION	1.70	2232	0.0	5209	-24.0	8185	-20.6
				ISENTROPIC FLOW Pe/Po	1.57	2165	0.0	5052	-21.6	7939	-18.1
				ISENTROPIC FLOW Pa/Po	1.58	2171	0.0	5067	-21.9	7962	-18.4
				UPSTREAM MACH ANGLE	1.49	2125	0.0	4959	-20.2	7793	-16.6
0488	0	4163	0	DESIGN CONDITION	1.70	2232	0.0	5209	-20.1	8185	0.0
				ISENTROPIC FLOW Pe/Po	1.57	2165	0.0	5052	-17.6	7939	0.0
				ISENTROPIC FLOW Pa/Po	1.58	2171	0.0	5067	-17.8	7962	0.0
				UPSTREAM MACH ANGLE	1.44	2093	0.0	4883	-14.8	7674	0.0

V. Results and Discussion

Two methods were evaluated for their effectiveness in reducing the amplitude of pressure oscillations invoked by high speed flow ($M = 0.62$ to 1.53) over an open cavity. The two suppression methods, which incorporated manipulation of the shear layer over the cavity, are; a pulsed and static fence (Figure 3-3), secondary flow injection 45 degree (Figure 3-5) and parallel (Figure 3-6) to the external flow.

Before presenting specific results, a discussion on Sound Pressure Level (SPL) units, decibel (dB), is essential to familiarize the reader with relative magnitude of a particular amplitude. As discussed in Chapter IV, dynamic sound pressure (psi rms) is related to SPL (dB) by:

$$\text{Sound Pressure Level (SPL)} = 20 \log_{10} \frac{P_{rms}}{P_{ref}} \text{ dB} \qquad (3)$$

where $P_{ref} = 2.9 \times 10^{-9}$ psi rms is the statistical "threshold of hearing" for the human ear. For comparison purposes, Table 5-I relates some commonly experienced sound pressures and their resulting SPL. As shown, an increase (or decrease) in SPL by 20 dB increases (or decreases) sound pressure (psi rms) by a factor of 10. A table of these relationships, for use during amplitude comparisons, are provided in Table 5-II. In addition a conversion table (SPL, dB, to sound pressure, psi rms) is provided in Table 5-III.

Table 5-I. Commonly Experienced Sound Pressures

Common Experience	Sound Pressure (psi rms)	Sound Pressure Level (dB)
Threshold of Hearing	2.9×10^{-9}	0
Electric Clock	2.9×10^{-8}	20
Inside a Library	2.9×10^{-7}	40
Conversation, 3 ft	2.9×10^{-6}	60
Inside an Office	2.9×10^{-5}	80
Lathe at 3 ft	2.9×10^{-4}	100
Threshold of Pain	2.9×10^{-3}	120
Jet Engine at 50 ft	2.9×10^{-2}	140

Table 5-II. Pressure (psi) Multiplication Factors
Corresponding to changes in Sound
Pressure Level (dB)

Delta SPL (dB) Increase (or decrease)	Resulting Multiplication (or division) Factor For psi rms
1	1.1
3	1.4
6	2.0
10	3.0
15	5.6
20	10.0
25	17.8
30	30.0

Table 5-III.   SPL Conversion Table

Sound Pressure Level (dB)	Sound Pressure (psi rms)
120.0	0.0029
125.0	0.0052
130.0	0.0092
135.0	0.0163
140.0	0.0290
145.0	0.0516
150.0	0.0917
155.0	0.1631
160.0	0.2900
165.0	0.5157
170.0	0.9171
175.0	1.6308
180.0	2.9000

Cavity Effect on Free-Stream Flow

Prior to evaluating a specific suppression device, the supply pressure to attain a desired flow condition was required. Besides using nozzle exit pressure ratio, Mach angle (measured off a schlieren photograph) was used to determine flow Mach number. However, the cavity often invoked very unsteady behavior in the external flow due to the pressure oscillations within. This made determination of the Mach number, using the Mach angle, for a given supply pressure extremely difficult. To illustrate this point, Figures 5-1 and 5-2 show two schlieren photographs of the flow field, at identical supply pressures (M = 1.35 nozzle), with and without the cavity. As the photograph with the cavity shows, several shocks are present and some are somewhat curved, whereas in the photograph without the
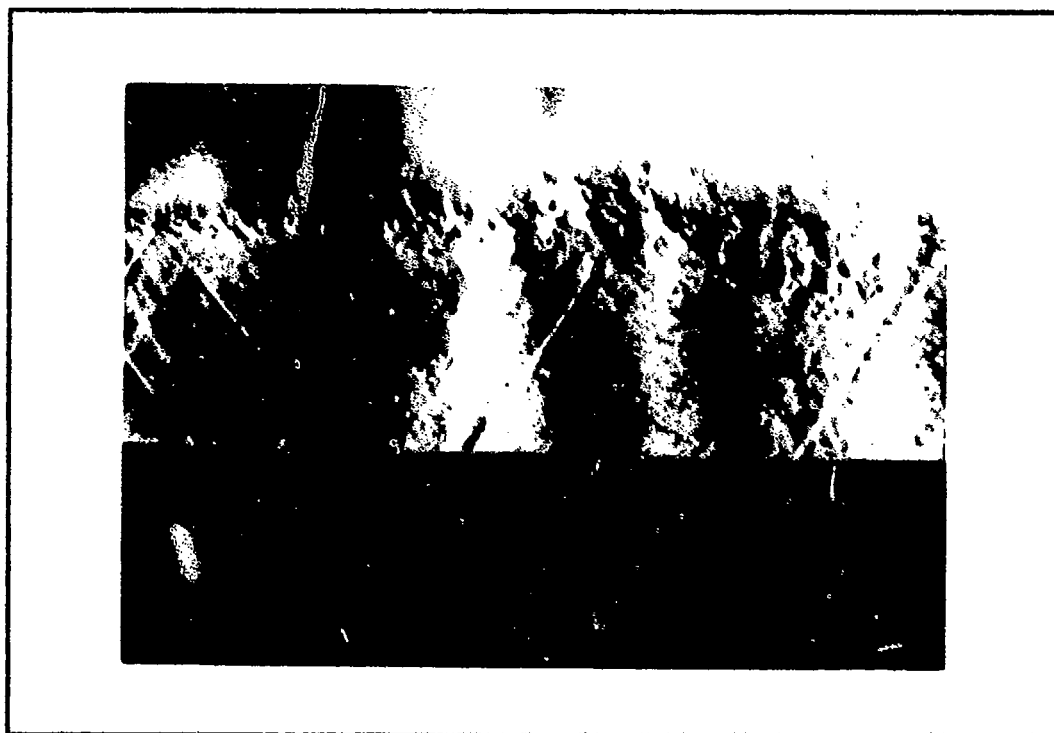
Figure 5-1.   Photograph of Flow With Cavity, M = 1.35

Figure 5-2.   Photograph of Flow Without Cavity, M = 1.35

cavity the shocks are all uniformly straight and parallel. Furthermore, due to the unsteady behavior with the cavity, different photographs, at identical supply pressures, often showed significantly varied flow Mach angle at the cavity. This was attributed to the oscillation of the shear layer above the cavity discussed in Chapter II. Consequently, the Mach angle from schlieren photographs without the cavity were primarily used to determine flow Mach number. The relation between nozzle design Mach number and measured Mach number along with the calculated Reynolds number is presented in Table 5-IV.

A representative subset of the data collected for the fence, 45 degree flow injection, and parallel flow injection configurations is contained in Appendices A, B, and C respectively. Due to the large quantity of data, only data from cavity position one (considered representative of the cavity) is provided. In addition, selected schlieren photographs are also included.

Resonant Frequency Prediction

The modified Rossiter equation for non-dimensional Strouhal number (S^*) was used to predict resonant frequencies within the cavity due to the external flow conditions. As Shown in Table 5-V, the predicted values when compared with the actual mode frequencies measured in the cavity varied from 1.3 to 21 percent. This variation is reasonable

5-5

Table 5-IV.   Experimental Mach and Reynolds Numbers

| | Nozzle Mach Numbers | | | Cavity Mach Numbers | |
Design	$\dfrac{P_{exit}}{P_o}$	Mass Flow Rate	Schlieren Mach Angle	$\dfrac{P_{atm}}{P_o}$	Reynolds Number
0.60	0.58	0.63	N/A	0.58	9.57×10^5
0.75	0.73	0.80	N/A	0.74	1.25×10^6
0.90	0.87	0.93	N/A	0.89	1.59×10^6
1.10	1.03	1.07	1.03	1.07	2.92×10^6
1.35	1.23	1.31	1.28	1.26	4.51×10^6
1.70	1.56	1.53	1.50	1.58	7.75×10^6

Table 5-V.   Resonant Frequency Comparison

| | First Mode | | | Second Mode | | |
Actual Mach No.	Frequency Actual (Hz)	Calc. (Hz)	Error (%)	Frequency Actual (Hz)	Calc. (Hz)	Error (%)
0.62	1600	1311	18.1	3400	3060	10.0
0.73	1700	1449	14.8	4100	3380	21.0
0.90	2000	1709	14.6	4200	3988	5.0
1.07	2177	1809	20.3	4500	4221	6.6
1.28	2147	1949	10.2	4309	4547	-5.2
1.56	2191	2163	1.3	4382	5048	-13.2

since Heller, et al estimate the error to be ± 10 percent

for cavities with L/D ≥ 4 and greater for cavities with

L/D < 4 (1:96).

Pulsating Fence Suppression Technique

The fence was deflected, transversely into the main flow, with an amplitude of 0.10 inch over a frequency range from zero to 120 Hz. Higher frequencies, 140 to 220 Hz, were also tested but, the fence deflection assembly became damaged due to excessive cyclic loading. Also, the data obtained at the single Mach number where these higher frequencies were attempted, showed no significant change in the peak amplitude levels. Therefore the pulsed fence evaluation was limited to 120 Hz. The data used to generate the graphs to be discussed next appears in Appendix A.

The suppression effectiveness of pulsing the fence at frequencies from 20 to 120 Hz was poor except at M = 1.53 flow condition. As Figure 5-3 shows, the effect of increasing the fence pulse frequency had no appreciable effect on the first mode Sound Pressure Level (SPL) for Mach numbers ranging from M = 0.62 to 1.28. Whereas at M = 1.53 a decrease of 22 dB (176 to 154 dB) occurred over the range of zero to 80 Hz. However, as a plot of the second mode shown in Figure 5-4 indicates, the SPL increased 9 dB (161 to 170 dB) over the range from zero to 120 for M = 1.53, while all other Mach numbers except M = 0.90 remained relatively constant. For M = 0.90 the amplitude of the second mode increased 11 db (149 to 160 dB) while the first mode decreased 14 dB (160 to 146 dB) from zero to 20 Hz and
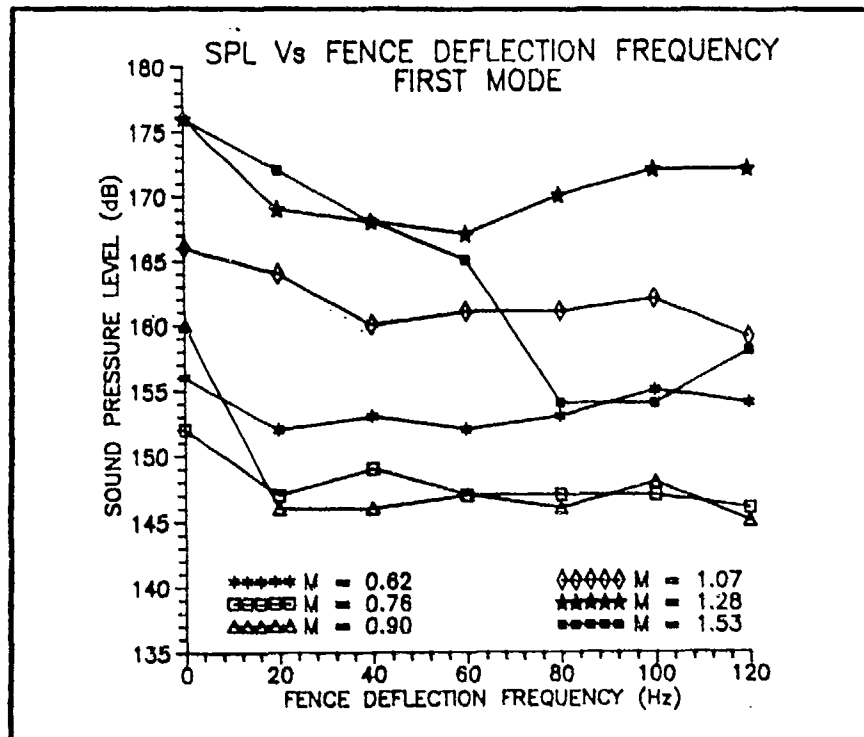
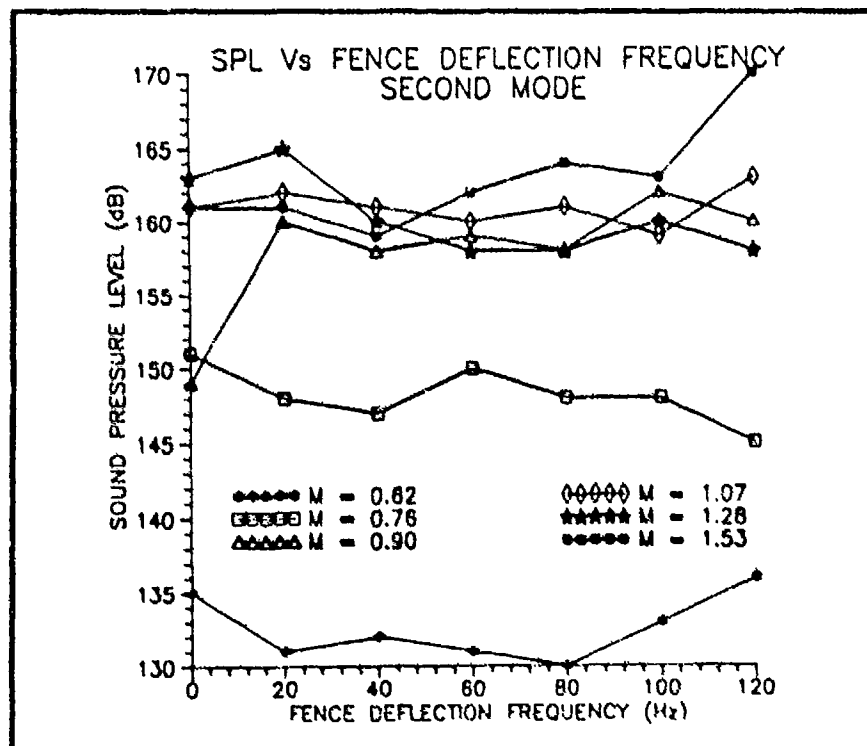**Figure 5-3. First Mode SPL Vs Fence Deflection Frequency**

Figure 5-4. Second Mode SPL Vs Fence Deflection Frequency

both modes remained at a relatively constant level from 20 to 120 Hz.

The purpose of pulsing the fence was to try to force the shear layer at a frequency different from the cavity/flow resonant frequency. The pulsing did force the shear layer since the frequency of the pulse was clearly evident in the SPL spectrum plots. However, it invoked pressure oscillations that were of the same magnitude and sometimes higher than the oscillations it was to suppress. Figure 5-5 shows an SPL versus frequency plot for the M = 1.53 flow condition with no fence. Figure 5-6 shows the SPL spectrum for the same conditions but with the fence being pulsed at 80 Hz. Comparing these two figures, the first mode was significantly reduced while the second mode increased slightly. Also shown in Figure 5-6 is the pressure oscillation (80 Hz) invoked by the pulsating fence which is larger than any other peak amplitude in the spectrum. Since the pulse amplitude of the fence was fixed, the effect of lower amplitudes was not investigated. However, runs to evaluate the effect of varying height of a static fence on suppression of pressure oscillations in the cavity were accomplished.

Static Variable Height Fence

Since the amplitude used in the pulsed fence evaluation generated such large pressure oscillations in the cavity, the relation between fence height and cavity response was
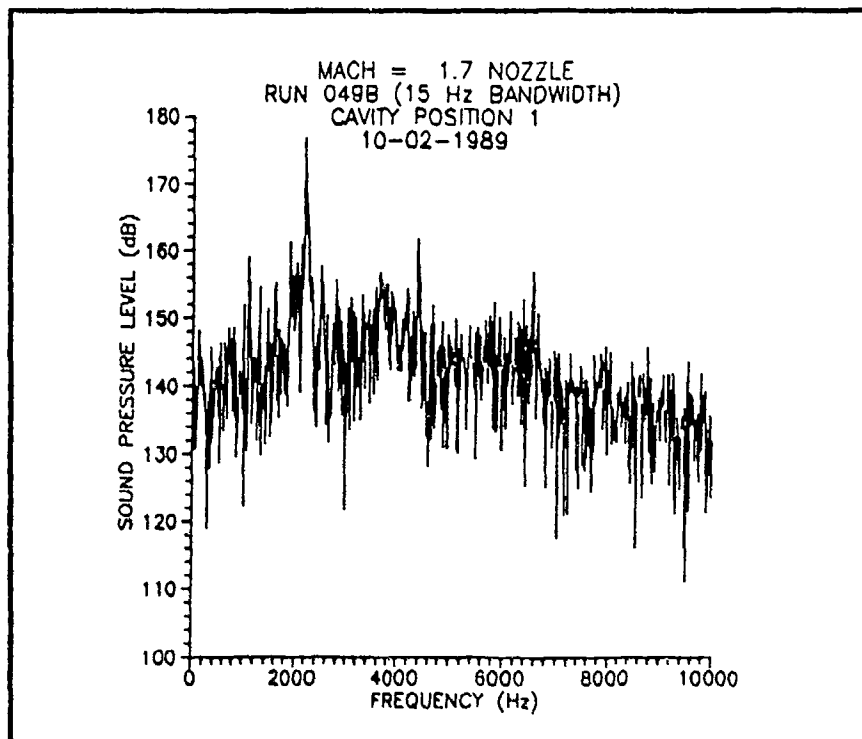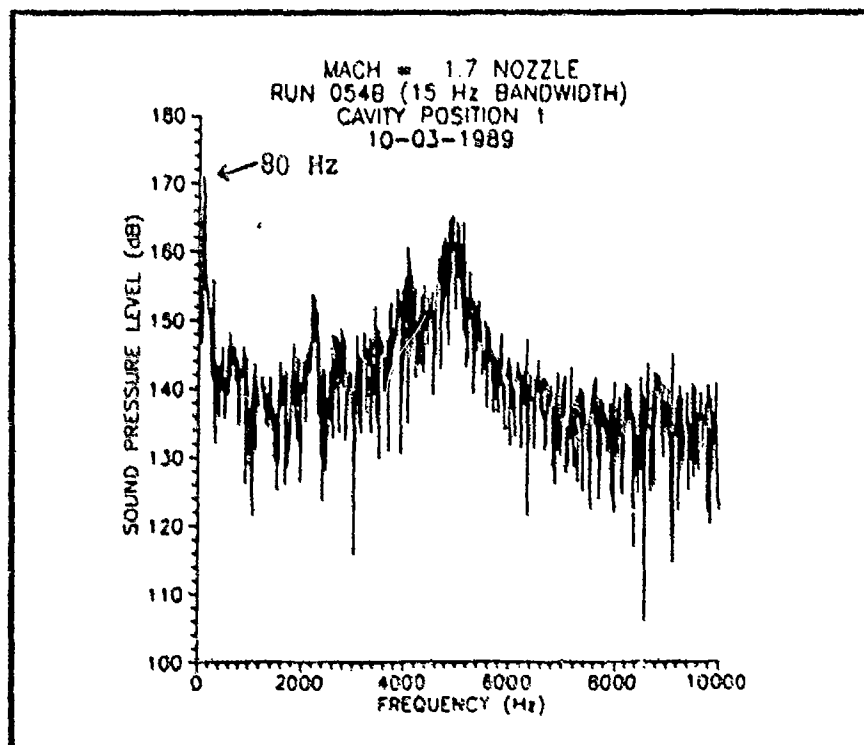
Figure 5-5.   Cavity Pressure Oscillations, No Fence

Figure 5-6.   Cavity Pressure Oscillations,
With Fence Pulsing at 80 Hz

5-10

evaluated. This test utilized the same fence used in
the pulse test, but it was modified so that the fence height
could be set manually. Fence heights of 1/64, 3/64, 5/64,
and 7/64 inch were tested at Mach numbers ranging from 0.63
to 1.53.

The results from this evaluation are summarized in
Figures 5-7 and 5-8 which contain plots of SPL versus fence
height, at various Mach numbers, for the first and second
modes respectively. The fence height is plotted as a
percentage of the boundary layer thickness. Since the
lowest Reynolds number for this test is higher than the
critical Reynolds number for transition from a laminar to a
turbulent boundary layer, the boundary layer thickness
equation for turbulent flow was used (15:38):

$$\delta = 0.37 \ 1 \left[\frac{U_\infty 1}{\nu} \right]^{-1/5} \tag{7}$$

As shown in Figure 5-7, the fence was relatively
ineffective in suppressing the first mode at M = 1.07 and
all three subsonic flow conditions. This result is
consistent with those observed by Malnquist (12:29) who
evaluated several fences at fixed heights. At M = 1.28
however, a 30 dB decrease (173 to 143 dB) in SPL for the
first mode occurred in a fence height range from 67 to 156
percent of the boundary layer thickness. At M = 1.53, a 34
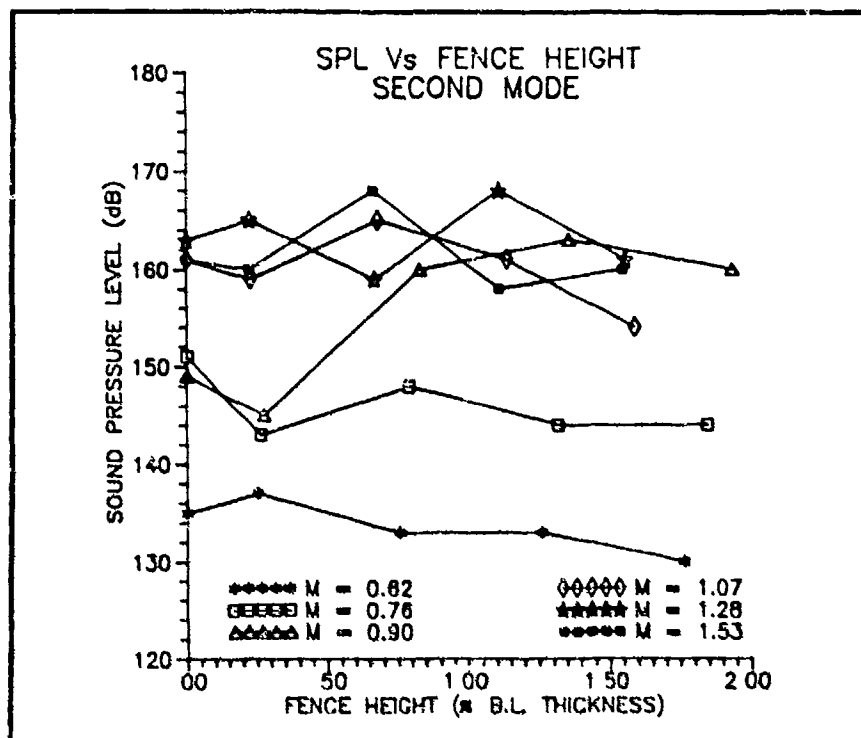dB decrease (178 to 144 dB) in SPL for the first mode

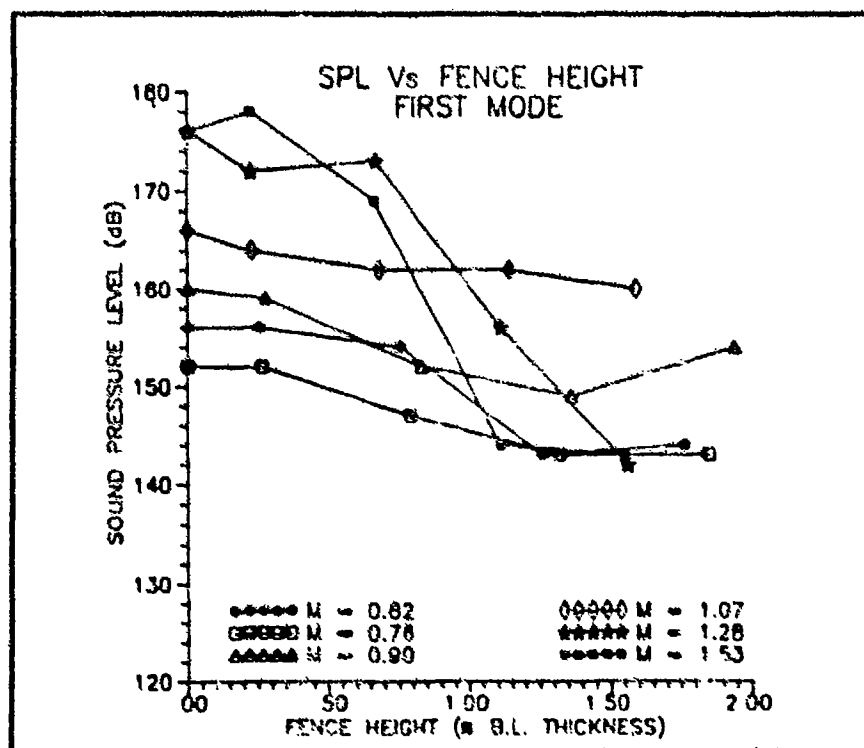Figure 5-7.   First Mode SPL Vs Fence Height

Figure 5-8.   Second Mode SPL Vs Fence Height

occurred in a fence height range from 22 to 111 percent of
the boundary layer thickness. The second mode, Figure 5-8,
was relatively unaffected by the fence at all heights tested
and at all Mach numbers except M = 0.90 where increasing
fence height resulted in 19 dB gain (149 to 163 dB) in SPL.
This gain was probably due to the flow accelerating as it
passed over the fence (i.e. the fence acted like a
converging/diverging nozzle). This is supported since these
higher second mode SPL amplitudes are in the same range as
those for the supersonic flow conditions.

To illustrate the effect of Mach number (for the data
used in Figures 5-7 and 5-8), Figures 5-9 and 5-10 show the
SPL for the first and second modes respectively plotted as a
function of Mach number for varying fence heights. As
Figure 5-9 illustrates for the first mode, the fence was
moderately effective (13 to 7 dB decrease in SPL) at all
fence heights in the subsonic range and significantly
effective (up to 32 db decrease in SPL) at fence heights of
5/64 inch and greater in the supersonic range. However, the
second mode as shown in Figure 5-10 was not as significantly
affected by fence height. In fact, at a given flow
condition the affect on SPL due to increasing fence height
is not as orderly as that found for the first mode (i.e. for
the first mode at M = 1.28, increasing fence height resulted
in a decreasing trend for SPL, but for the second mode the
trend for decreasing SPL correlated with fence heights of
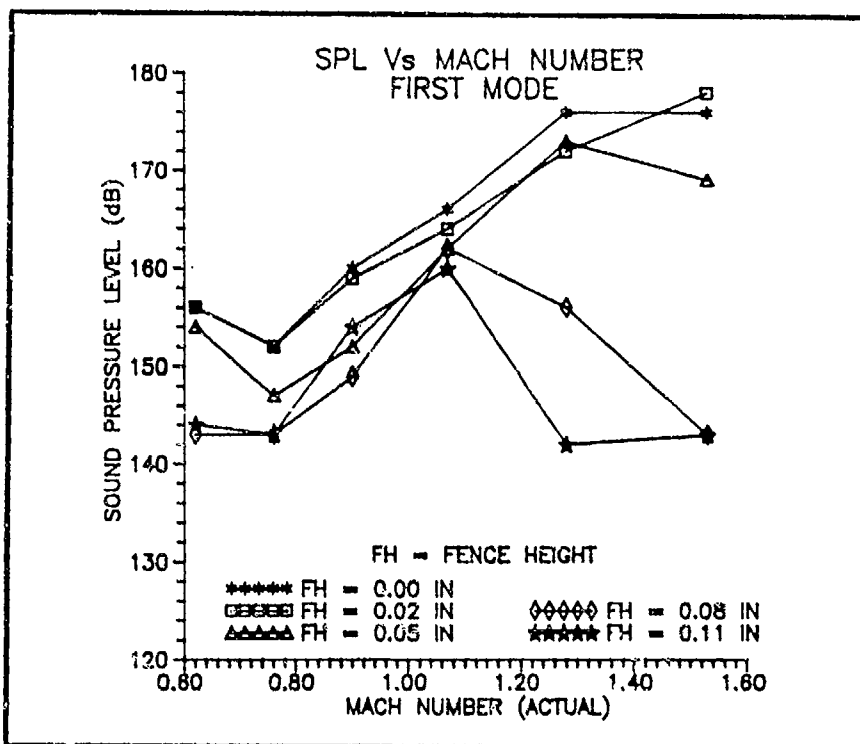
Figure 5-9.   First Mode SPL Vs Mach Number
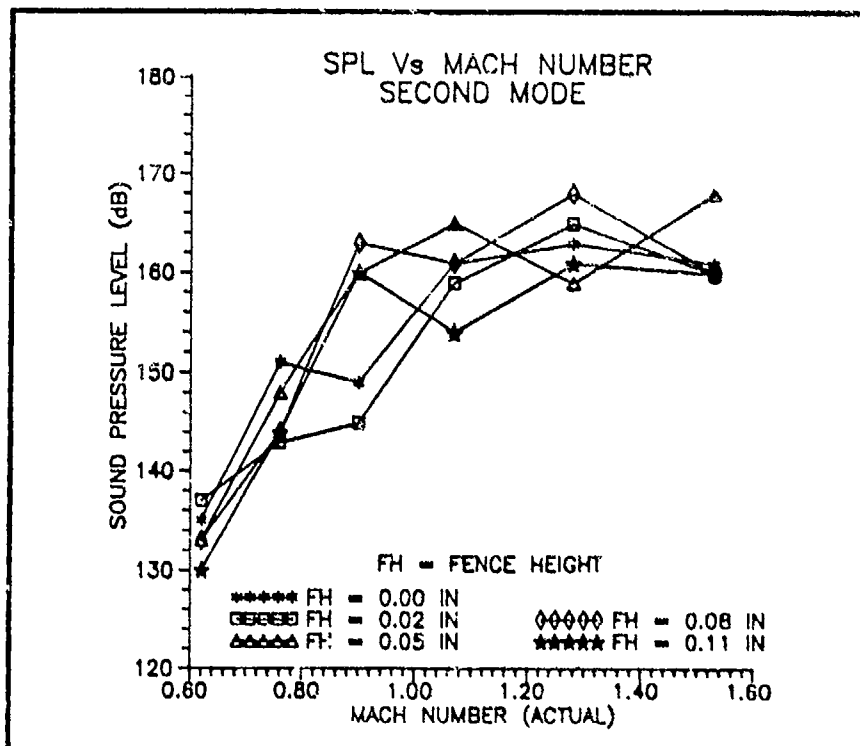   For Various Fence Heights

Figure 5-10.   Second Mode SPL Vs Mach Number
               For Various Fence Heights

5/64, 1/64, 0, 7/64, and 3/64 inch in that order). Because
of the relatively small spacing of data points, this could
be due, at least in part, to normal variation in the data.

The data obtained with static fence heights of zero and
7/64 inch compare well with the results obtained by
Malnquist (12:44-47) for the first and second modes. In
addition, the SPL amplitudes and overall trends for the
baseline cavity (L/D = 2) for M = 0.62 to 1.53 is consistent
with those obtained by Heller and Bliss (8:105-106).

Steady Flow Injection

The method used to pulse secondary flow injection
resulted in substantial pulse amplitude decrease at high
frequencies. As the pulsating amplitude decreased due to a
frequency increase, the average pressure at the flow
injection nozzle entrance increased resulting in near steady
flow injection conditions. To evaluate the suppression
effectiveness of steady flow injection, runs were conducted
with two flow injection nozzles (45 degree and parallel to
the external flow) at M = 1.28 for increasing secondary flow
supply pressure. In addition, SPL data was also taken with
steady parallel flow injection and no external flow to
determine the pressure oscillations in the cavity solely due
to flow injection.

45 Degree Flow Injection. This suppression technique
was more effective overall than the parallel flow injection
method. For the 45 degree flow injection angle, shown in

Figure 5-11, a 10 db decrease (176 to 166 dB) in SPL for the first mode occurred over a range of mass flow rate per unit cavity widths from 0.0 to 1.0 lbm/sec/ft. However, from 1.0 to 1.25 lbm/sec/ft flow injection rate the SPL increased by 2 dB (156 to 168 dB). For the second mode, also shown in Figure 5-11, the trend was nearly the same with a 9 dB decrease (163 to 154 dB) in SPL from 0.0 to 0.9 lbm/sec/ft flow injection rate. Above 0.9 lbm/sec/ft injection rate the SPL increased 4 dB (154 to 158 dB) at nearly a constant rate to 1.25 lbm/sec/ft flow injection.

Parallel Flow Injection. This suppression technique was the least effective of all the methods evaluated. As shown in Figure 5-12, the first mode was suppressed only 5 dB (174 to 169 dB) over a range of flow injection rates, per unit width, from 0.0 to 1.45 lbm/sec/ft. The second mode SPL increased 4 dB (162 to 166 dB) with 0.35 lbm/sec/ft injection rate, then decreased 8 dB (166 to 158 dB) from 0.35 to 0.75 lbm/sec/ft injection rate, and remained relatively constant from 0.75 to 1.45 lbm/sec/ft injection rate.

Parallel Flow Injection, No External Flow. The purpose of this evaluation was to determine the SPL in the cavity as a result of the flow injection. Unexpectedly, the flow injection alone was able to create disturbances in the cavity as great and similar to that due to the external flow. Figure 5-13 contains a graph of SPL versus
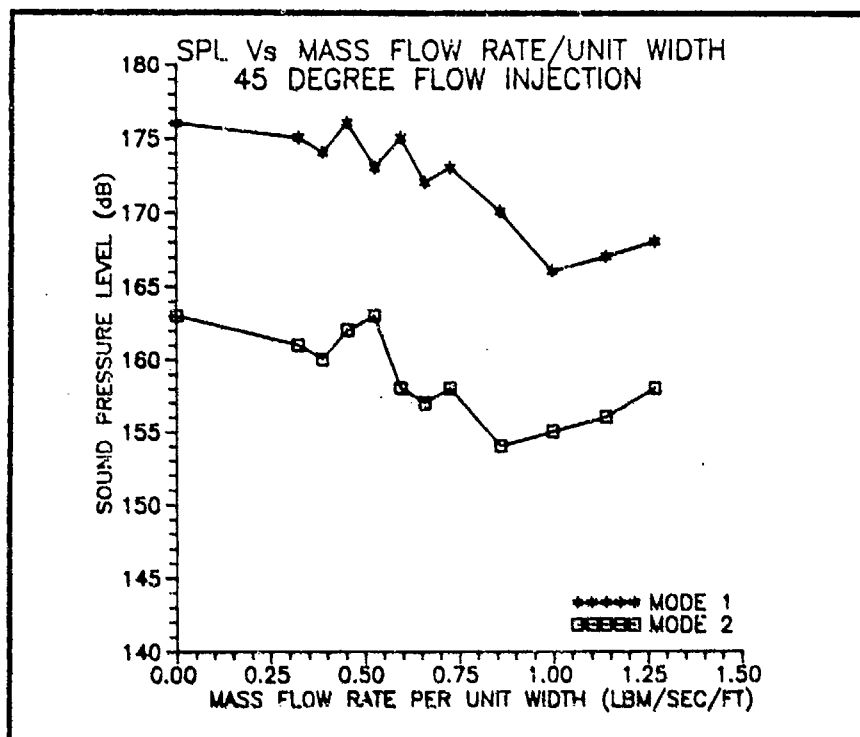
Figure 5-11.   SPL Vs Mass Flow Rate Per Unit Cavity Width
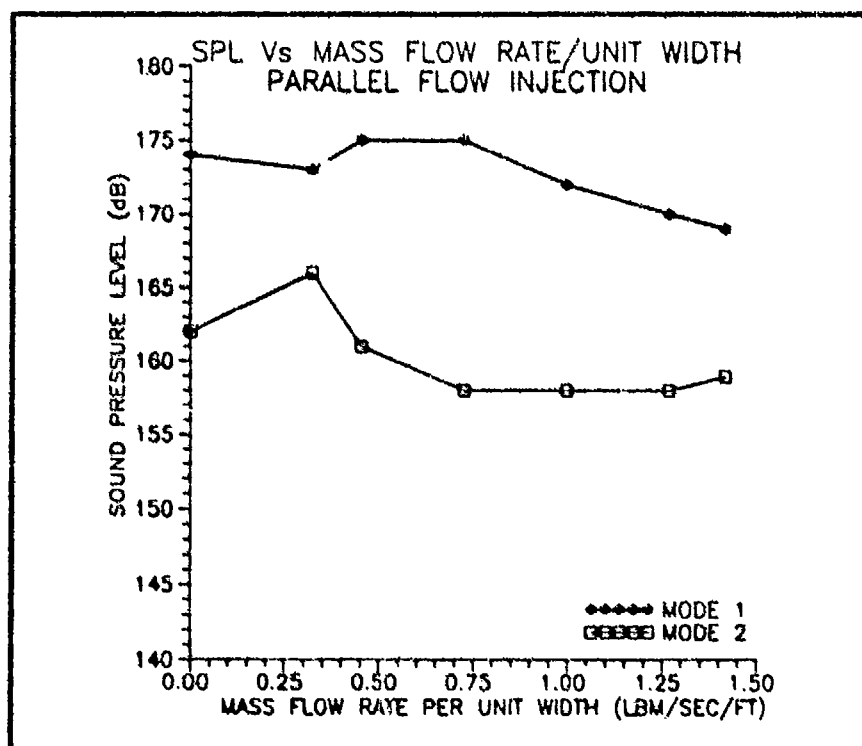For 45 Degree Flow Injection Angle

Figure 5-12.   SPL Vs Mass Flow Rate Per Unit Cavity Width
For Parallel Flow Injection Angle

oscillation frequency in the cavity due to a 1.27 lbm/sec/ft
flow injection rate with no external flow. For a
comparison, Figure 5-14 contains a graph of the SPL versus
oscillation frequency for M = 1.28 external flow condition
and no secondary flow injection. In addition, a schlieren
photograph of the resulting flow is provided in Figure 5-15.

To illustrate the effect of flow injection rate on
cavity response, Figure 5-16 contains a plot of the SPL
amplitude for the first two modes versus flow injection rate
with no external flow. As shown, there is a substantial
increase in the SPL with an increase in flow injection rate.
This could explain why flow injection parallel to the
external flow did not significantly suppress large amplitude
cavity pressure oscillations.

Pulsed Flow Injection

This suppression technique incorporated pulsed
secondary flow injection at an angle 45 degrees and parallel
to the free-stream flow at the cavity leading edge.
However, due to design limitations, the amplitude of the
pulse dropped significantly with increasing pulse frequency
while the average pressure offset at the injection nozzle
entrance increased. Thus a high frequency pulse responded
like a reduced pressure steady flow injection. Consequently
only one Mach number (M = 1.28) was used to evaluate this
suppression technique.

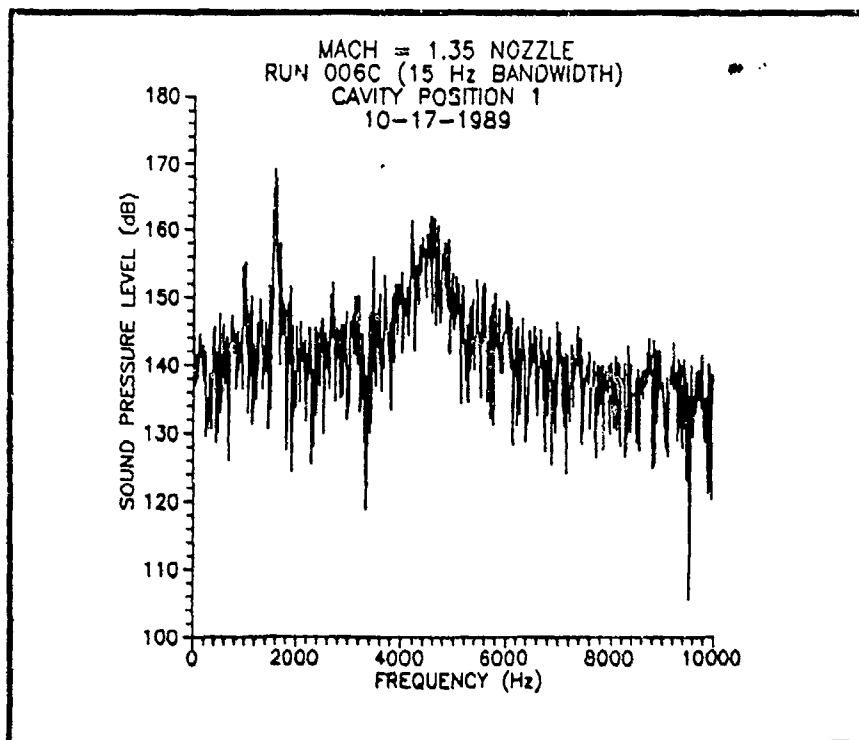Figure 5-13.   SPL Vs Frequency Spectrum Plot With Parallel
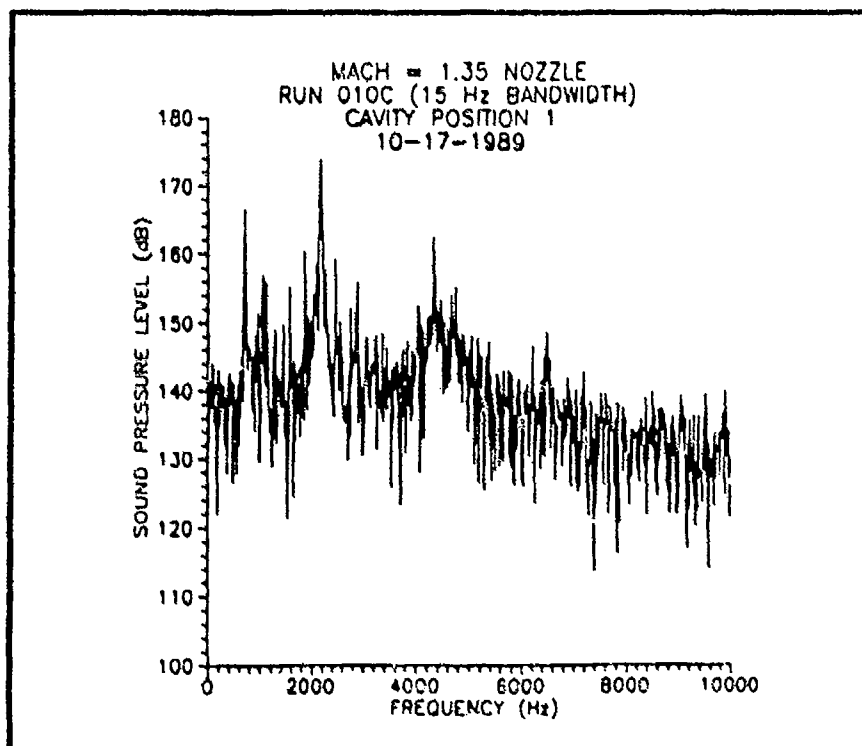   Flow Injection and No External Flow

Figure 5-14.   SPL Vs Frequency Spectrum Plot With M = 1.28
                External Flow and No Flow Injection

Figure 5-15. Photograph of Parallel Flow Injection
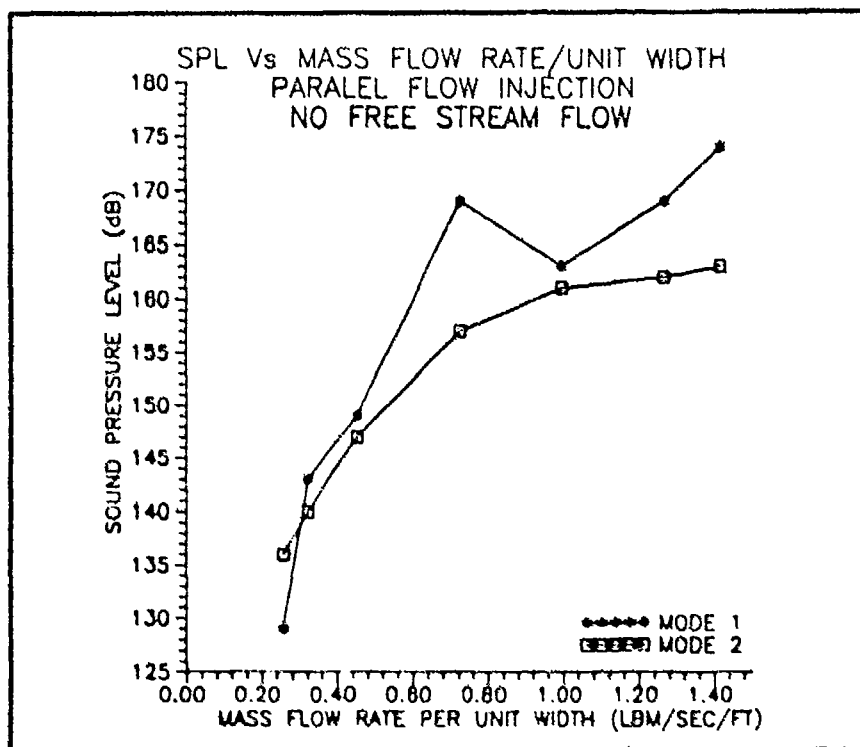and No External Flow

Figure 5-16. SPL Vs Mass Flow Rate Per Unit Cavity Width
For Parallel Flow Injection, No External Flow

45 Degree Flow Injection. This suppression technique demonstrated only moderate effectiveness. As shown in Figure 5-17, the first mode SPL decreased 9 dB (177 to 168 dB) by pulsing a 50 psig supply pressure at 10 Hz. From 10 to 50 Hz the SPL slowly increased (4 dB) and then leveled off from 50 to 80 Hz. The second mode, Figure 5-18, also decreased 9 dB (164 to 155 dB) by pulsing a 50 psig supply pressure at 10 Hz, but remained constant at that level for higher frequencies.

Parallel Flow Injection. Flow injection pulses parallel to the free-stream direction (50 psig valve supply pressure) was less effective than the corresponding 45 degree flow injection pulses. As shown in Figure 5-19, the first mode remained relatively constant with increasing pulse frequency. The second mode decreased 7 dB (164 to 157 dB) with a 10 Hz pulse, but then increased 5 dB (157 to 162 dB) from 10 to 40 Hz. From 40 to 60 Hz it decreased 4 dB (162 to 158 dB).
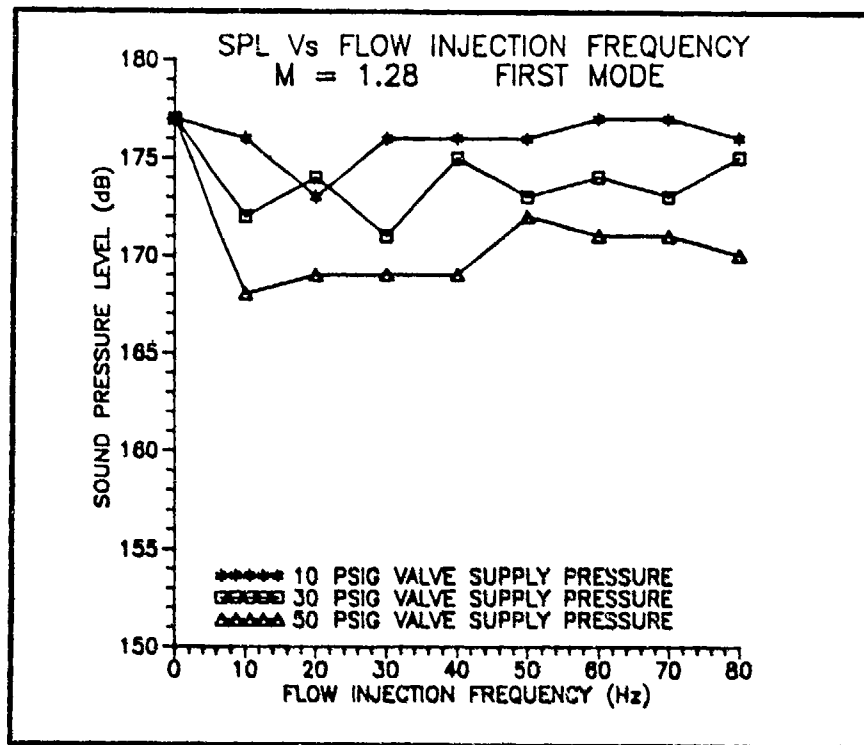
Figure 5-17.   First Mode SPL Vs 45 Degree Flow Injection
              Frequency For Varying Valve Supply Pressure
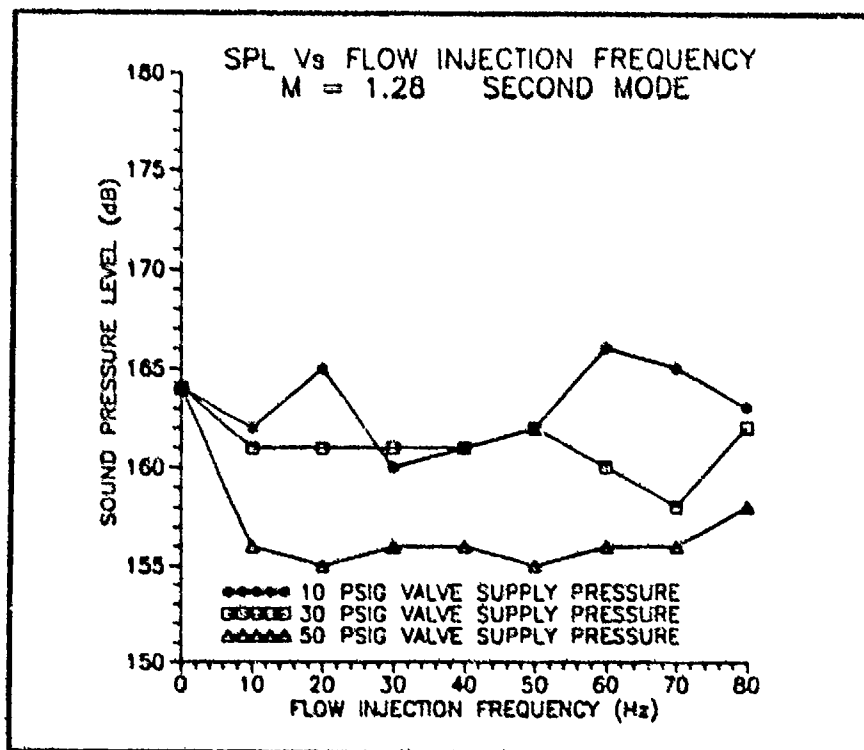

Figure 5-18.   Second Mode SPL Vs 45 Degree Flow Injection
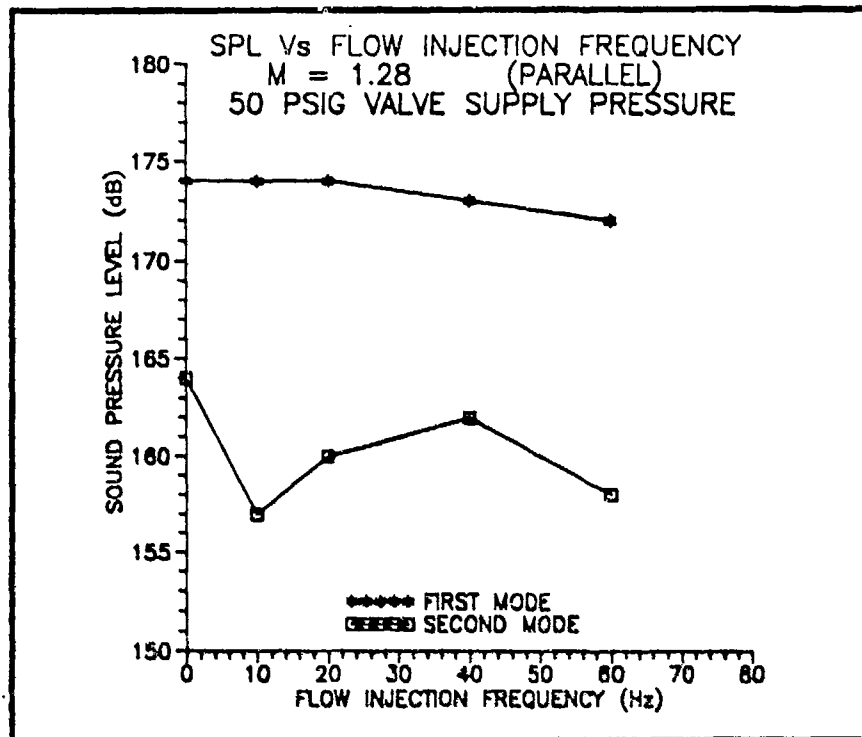   Frequency For Varying Valve Supply Pressure

Figure 5-19.   SPL Vs Parallel Flow Injection Frequency
For 50 psig Valve Supply Pressure

5-23

VI. Conclusions and Recommendations

Conclusions

The purpose of this experiment was to determine the effectiveness of suppressing pressure oscillations in a cavity through manipulation of the shear layer. The cavity tested was a small-scale, two-dimensional cavity with a length to depth ratio of two.

The pulsating fence was effective in suppressing pressure oscillations, but only at two of the six Mach numbers tested (0.90 and 1.53). The pulse frequencies evaluated ranged from 20 to 120 Hz. Higher frequencies were not tested due to a design limitation of the pulsing mechanism. For the frequencies tested, the level of suppression provided by a pulsating fence was less than that attainable with a static fence of the same height. However, the fence was able to invoke disturbances in the cavity as great as those caused by external flow resonance. Thus higher pulse frequencies with a smaller amplitude may be effective in suppressing cavity pressure oscillations.

The static fence was the most effective suppression technique evaluated. However, it was only significantly effective in suppressing the first mode for fence heights greater than 75 percent of the boundary layer thickness, and only at two of the six Mach numbers tested (M = 1.28 and 1.53). The second mode was relatively unaffected by the

fence at all heights tested (zero to 200 percent of the boundary layer thickness) and all Mach numbers except M = 0.90 where the SPL was significantly increased for increasing fence height.

The pulsating secondary flow injection suppression technique was only minimally effective in suppressing cavity pressure oscillations for both injection angles evaluated (parallel and 45 degrees to the external flow). However, the amplitude of the pulse decreased for increasing pulse frequency resulting in near steady, reduced pressure flow injection. Therefore low frequencies (10 to 80 Hz) were somewhat qualitatively evaluated. In any case, pulsating the flow at an angle 45 degrees to the external flow suppressed cavity pressure oscillations better than injection parallel to the flow. This was probably due to the shear layer becoming more turbulent as a result of the 45 degree flow injection angle and thus invoked lower amplitude pressure oscillations in the cavity (2:5).

Steady flow injection at 45 degrees to the external flow was more effective than steady parallel flow injection for the same mass flow rate. Although the magnitude of the suppression from steady flow injection was slightly greater than that from pulsating flow, it was still significantly less than the levels achievable with a static fence.

Steady parallel flow injection at the cavity leading edge, with no external flow, can invoke pressure oscilla-

tions in the cavity of the same order of magnitude and similar spectrum shape as observed for external flow only. Thus it was concluded that parallel flow injection alone can cause cavity resonance.

The test section assembly used in this evaluation worked well overall. However, due to the small cavity length, the resonant frequencies were relatively high with respect to the frequencies achievable with the mechanical pulsing mechanisms used. Consequently, dynamic testing (pulsating fence and flow injection) at or near the resonant frequencies was unachievable.

Recommendations

In the early stages of this investigation, the scope of this investigation, although ambitious, seemed doable. The parameters used to determine the scope were; frequency, amplitude, mass flow rate, Mach number, injection angle, and L/D. Most of these were evaluated, at least partially, but because of the large number of runs required, some were not. In addition, as data were taken and processed, many interesting phenomena occurred requiring additional and sometimes different runs and configurations. Some of these phenomena were partially evaluated and others unfortunately were not. Consequently many recommendations for further investigation can be made.

Probably the most important recommendation as a result of this experiment is the evaluation of the suppression

methods (pulsating fence and pulsating flow injection) at higher frequencies relative to the cavity resonant frequencies. For the type of fence mechanism used in this experiment, higher frequencies may be unattainable due to large cyclic loadings. Thus a new approach to manipulate the shear layer might have to be used. Two recommended methods to consider include a vibrating ribbon or high frequency vibrator.

Since the pulsating fence invoked its own large amplitude pressure oscillations in the cavity, recommend further investigation on the effect due to fence deflection amplitude. A related parameter that should also be evaluated is the location of the pulsating fence with respect to the cavity leading edge. Perhaps moving the fence mechanism further upstream of the cavity, where the boundary layer is much smaller, might allow significantly lower fence deflection amplitudes and thus reduce the cyclic loading on the fence mechanism allowing higher frequencies to be evaluated.

Achieving higher frequency flow injection pulses with the current design is probably not feasible. Recommend a new design be used that puts the pulsing mechanism at the injection nozzle exit. This should alleviate most of the problem of amplitude decrease due to frequency increase. Consequently, much higher amplitudes could be evaluated.

Recommend different flow injection angles be evaluated,

6-4

especially perpendicular to the flow. Also, evaluate the
position of the injection pulse relative to the cavity. As
with the fence, perhaps moving the injection pulse upstream
of the cavity would require significantly lower pulse
amplitudes and mass flow rates for effective pressure
oscillation suppression.

Since time permitted testing for only one cavity length
to depth ratio ($L/D = 2$), recommend different values ($L/D > 2$) be investigated regardless of the suppression technique
used. Also, larger length to depth ratios will reduce the
cavity resonant frequencies thus enabling active-type
suppression techniques to be evaluated at lower frequencies.

Appendix A: <u>Pulsating and Static Fence Data</u>

<u>Description of Contents</u>

This appendix contains the Sound Pressure Level (SPL) versus frequency data obtained from the pulsating and static fence evaluations. Although not a complete set of all the data obtained, it does contain all the data (cavity position one only) used to generate the graphs presented in the body of the thesis as well as some selected schlieren photographs considered representative of the flow conditions tested. Due to the large quantity of data only plots for cavity position one are included. Cavity position one was selected because the SPL amplitudes for this position were consistently between those for cavity position 2, which was usually the lowest, and cavity position 3, which was usually the highest. In addition, the spectrum shape for cavity positions 1 and 3 were very similar and thus considered representative of the cavity.
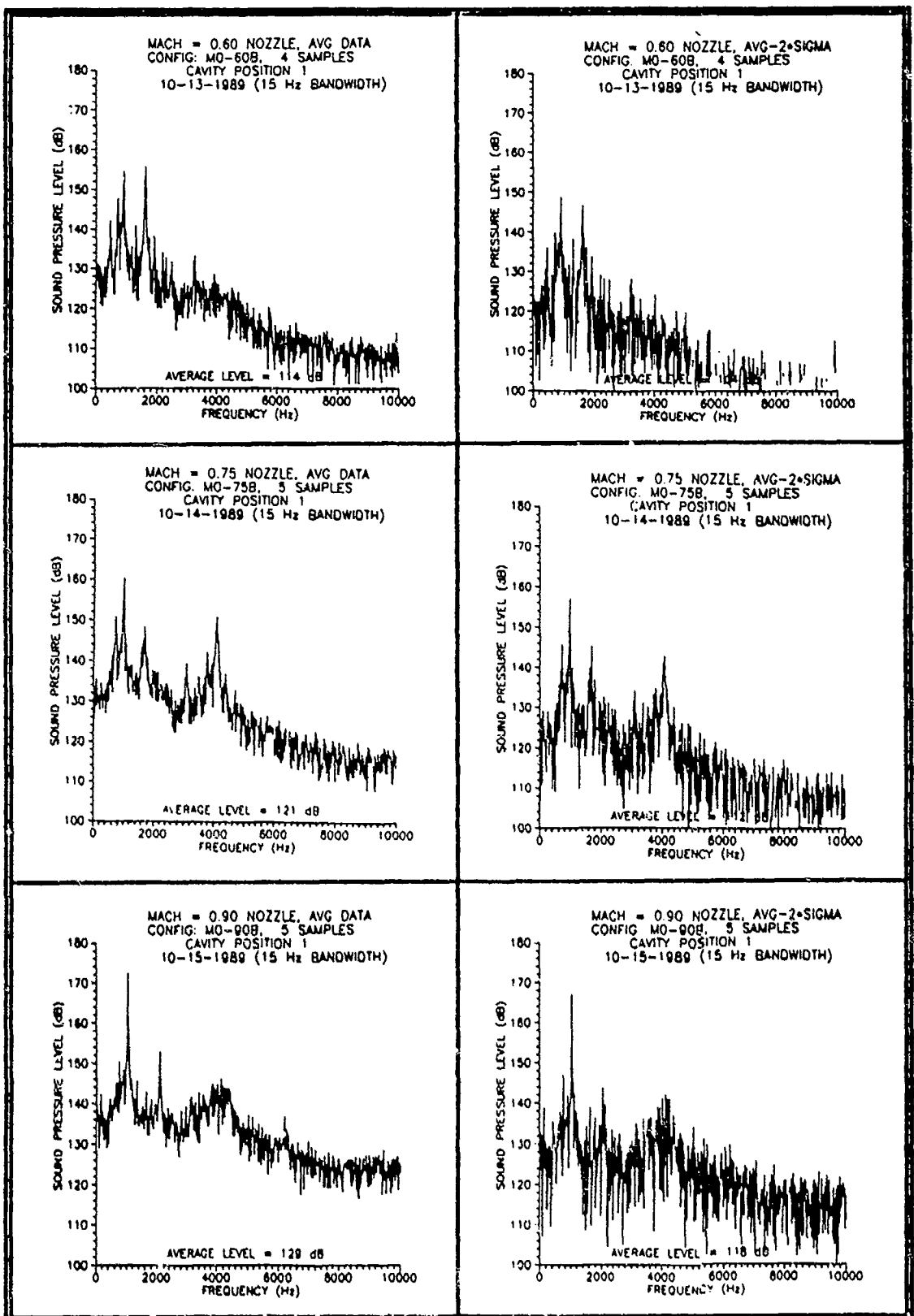
Figure A-1.   Baseline Data Sets: Average Data and
Average - 2 σ Data Respectively, For
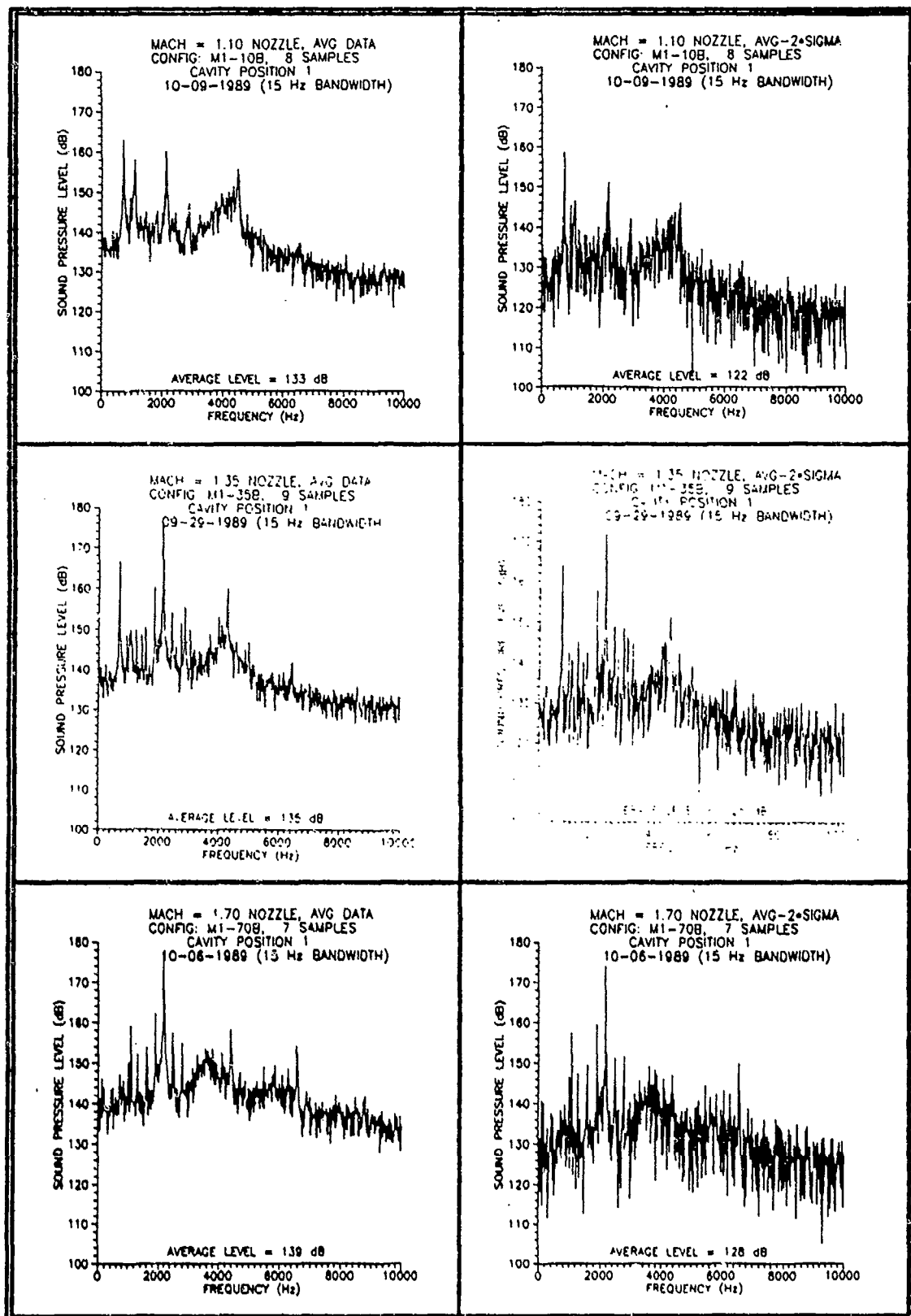M = 0.62 (Top), 0.76 (Mid), 0.90 (Bot)

Figure A-2.   Baseline Data Sets: Average Data and
               Average - 2 σ Data Respectively, For
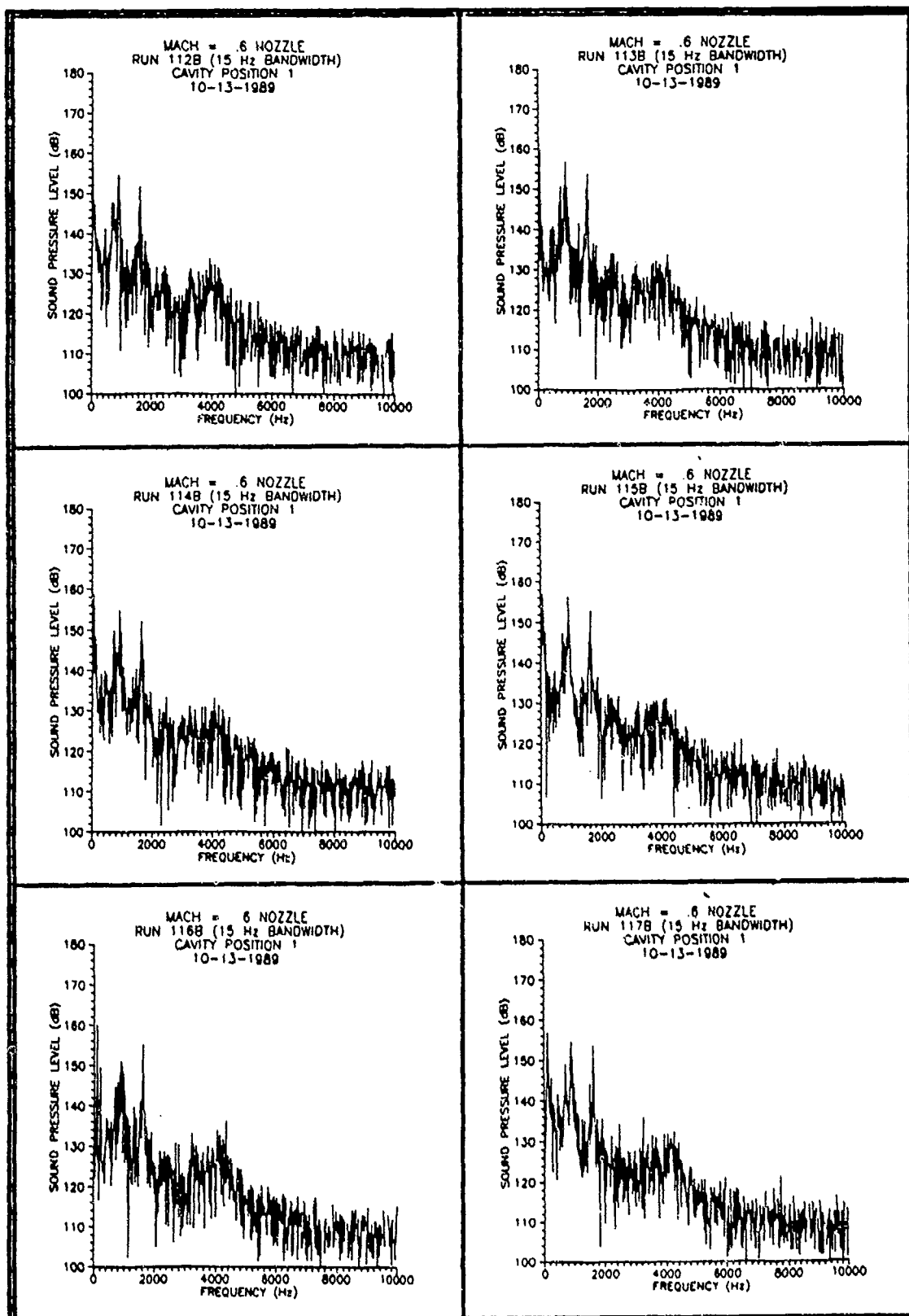   M = 1.07 (Top), 1.28 (Mid), 1.53 (Bot)

Figure A-3. Pulsating Fence SPL Vs Frequency Data,
M = 0.62 20 and 30 Hz (Top),
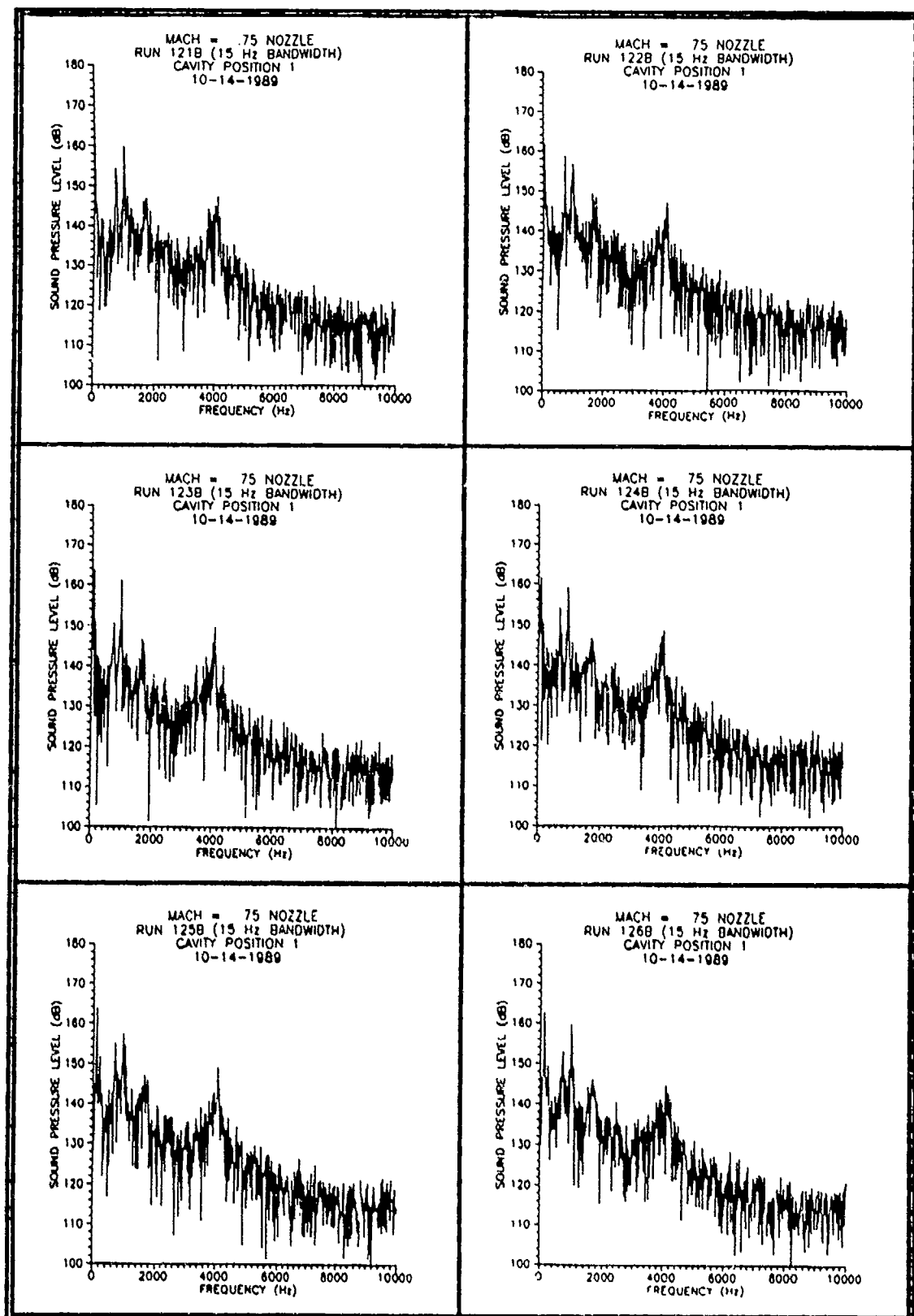40 and 60 Hz (Mid), 80 and 100 Hz (Bot)

Figure A-4.   Pulsating Fence SPL Vs Frequency Data,
M = 0.76   20 and 30 Hz (Top),
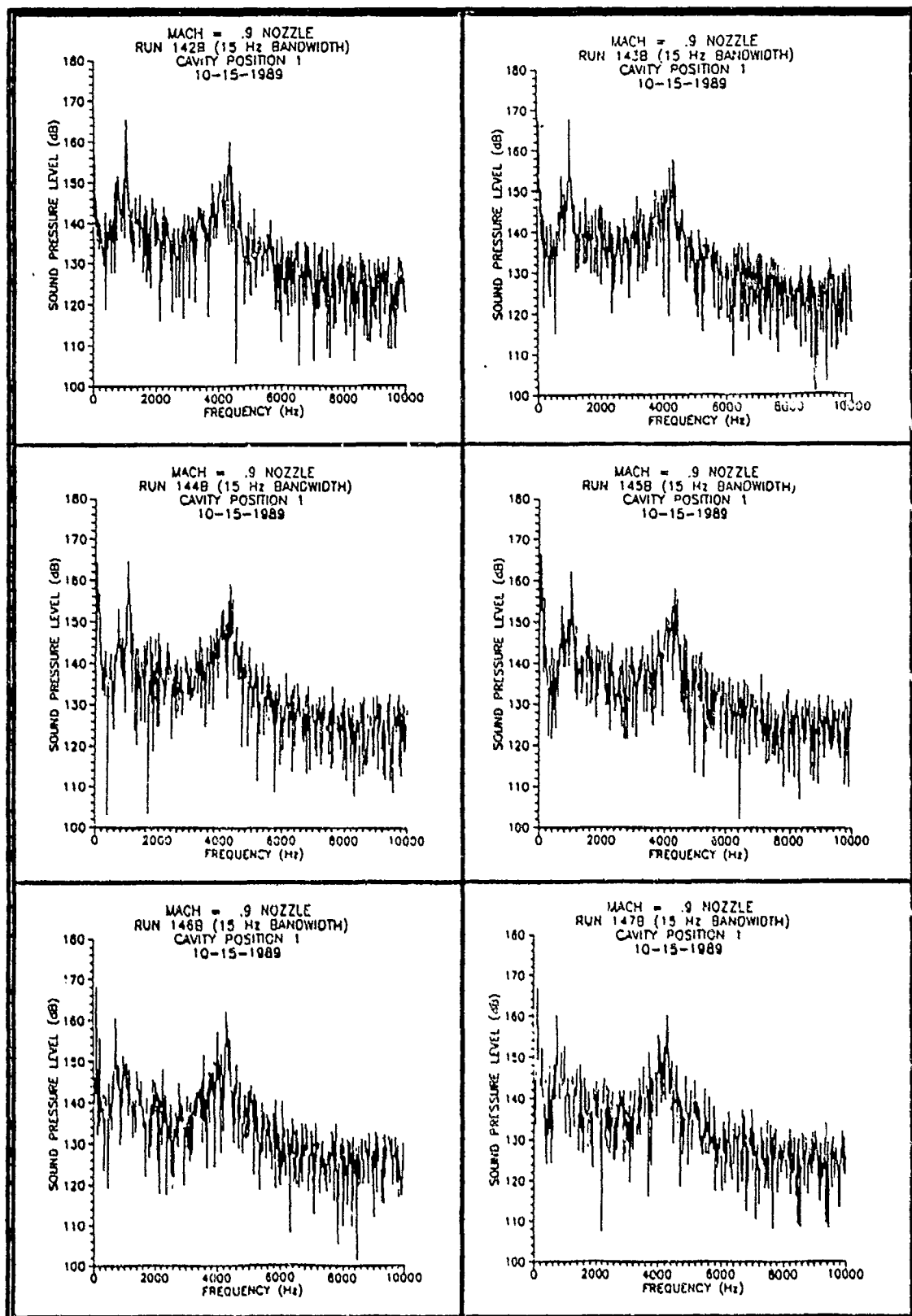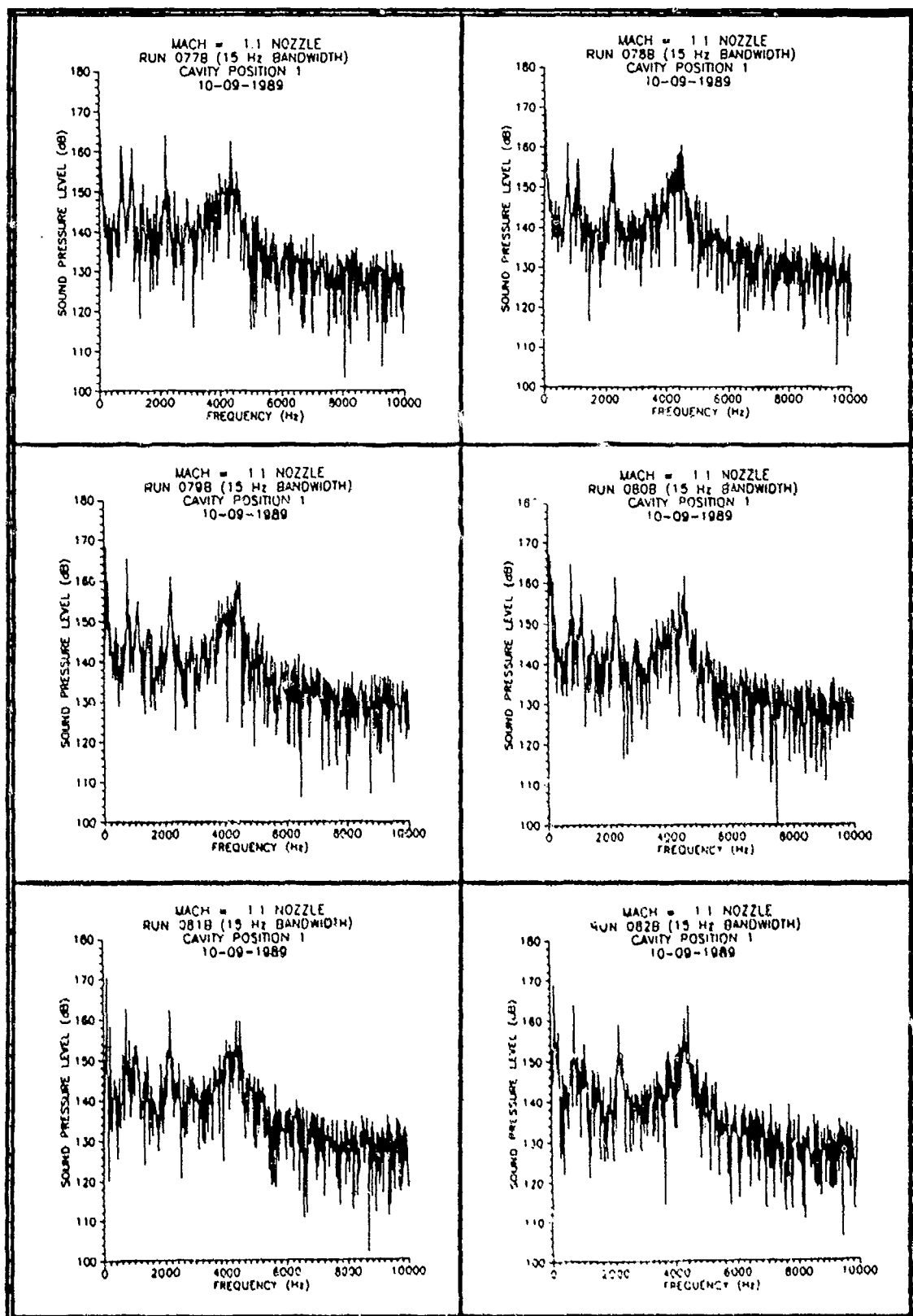40 and 60 Hz (Mid), 80 and 100 Hz (Bot)

A-5

Figure A-5. Pulsating Fence SPL Vs Frequency Data,
M = 0.90 20 and 30 Hz (Top),
40 and 60 Hz (Mid), 80 and 100 Hz (Bot)

Figure A-6.   Pulsating Fence SPL Vs Frequency Data,
           M = 1.07   20 and 30 Hz (Top),
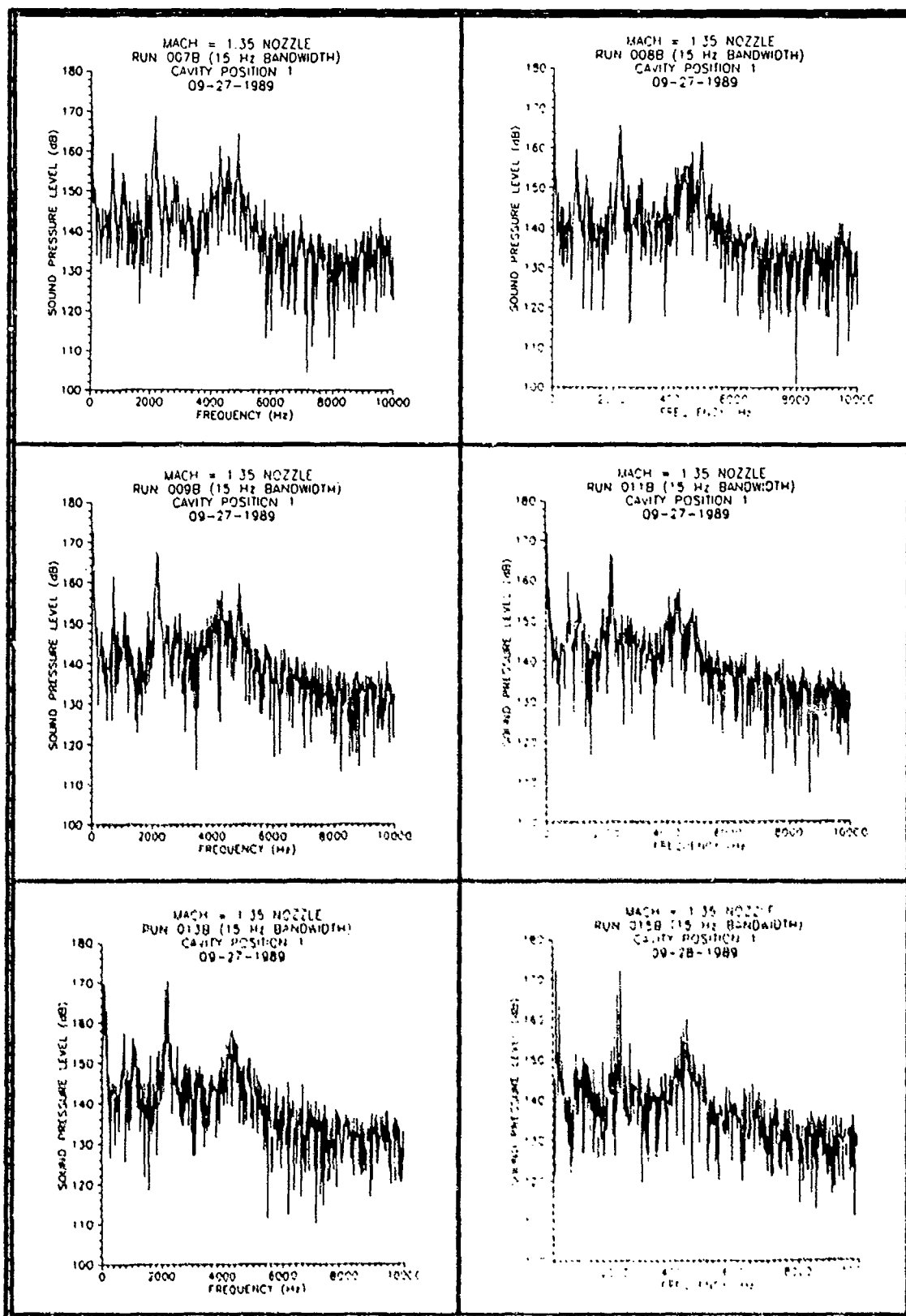   40 and 60 Hz (Mid), 80 and 100 Hz (Bot)

A-7

Figure A-7.   Pulsating Fence SPL Vs Frequency Data,
            M = 1.28   20 and 30 Hz (Top),
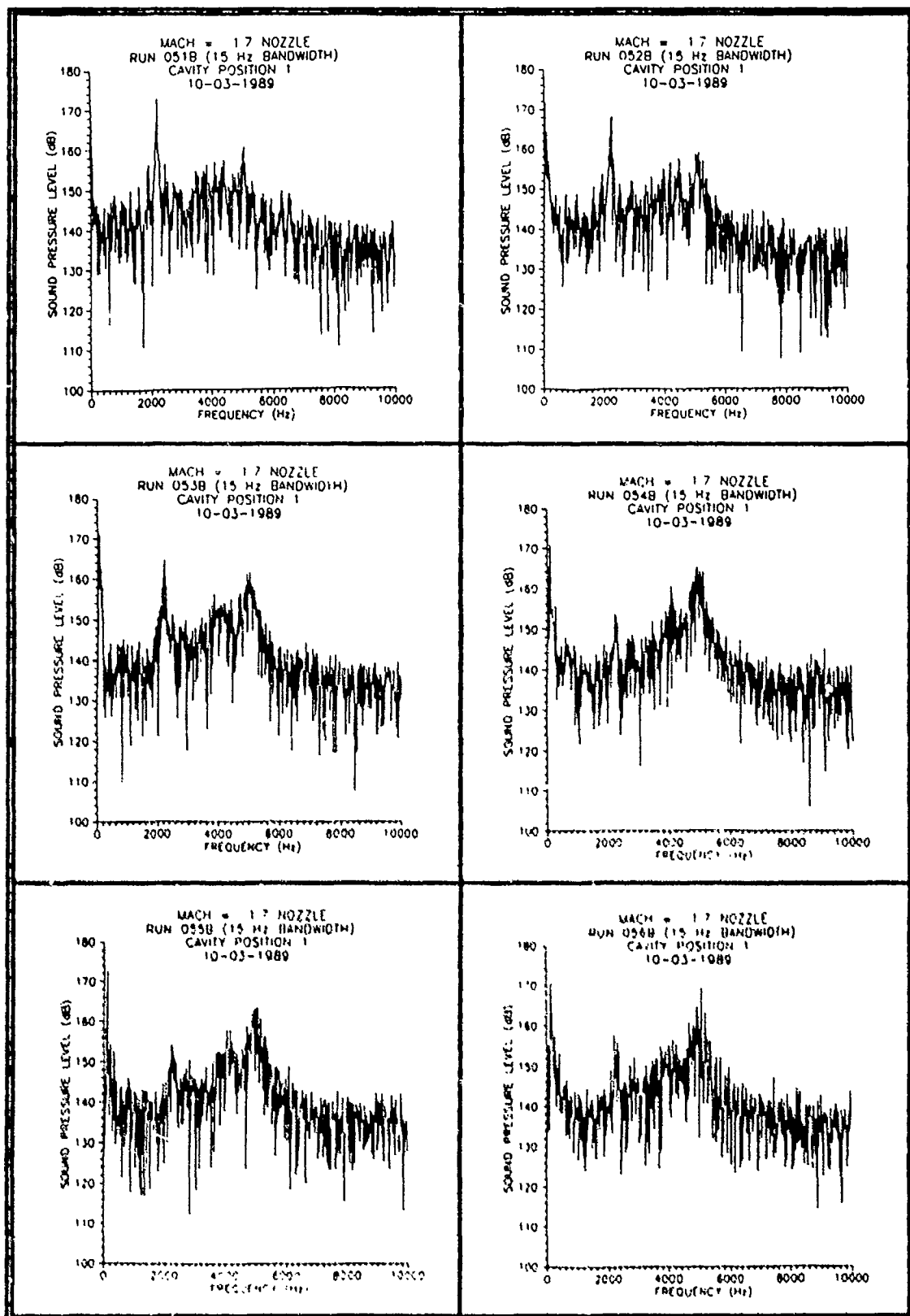   40 and 60 Hz (Mid), 80 and 100 Hz (Bot)

Figure A-8.   Pulsating Fence SPL Vs Frequency Data,
M = 1.53   20 and 30 Hz (Top),
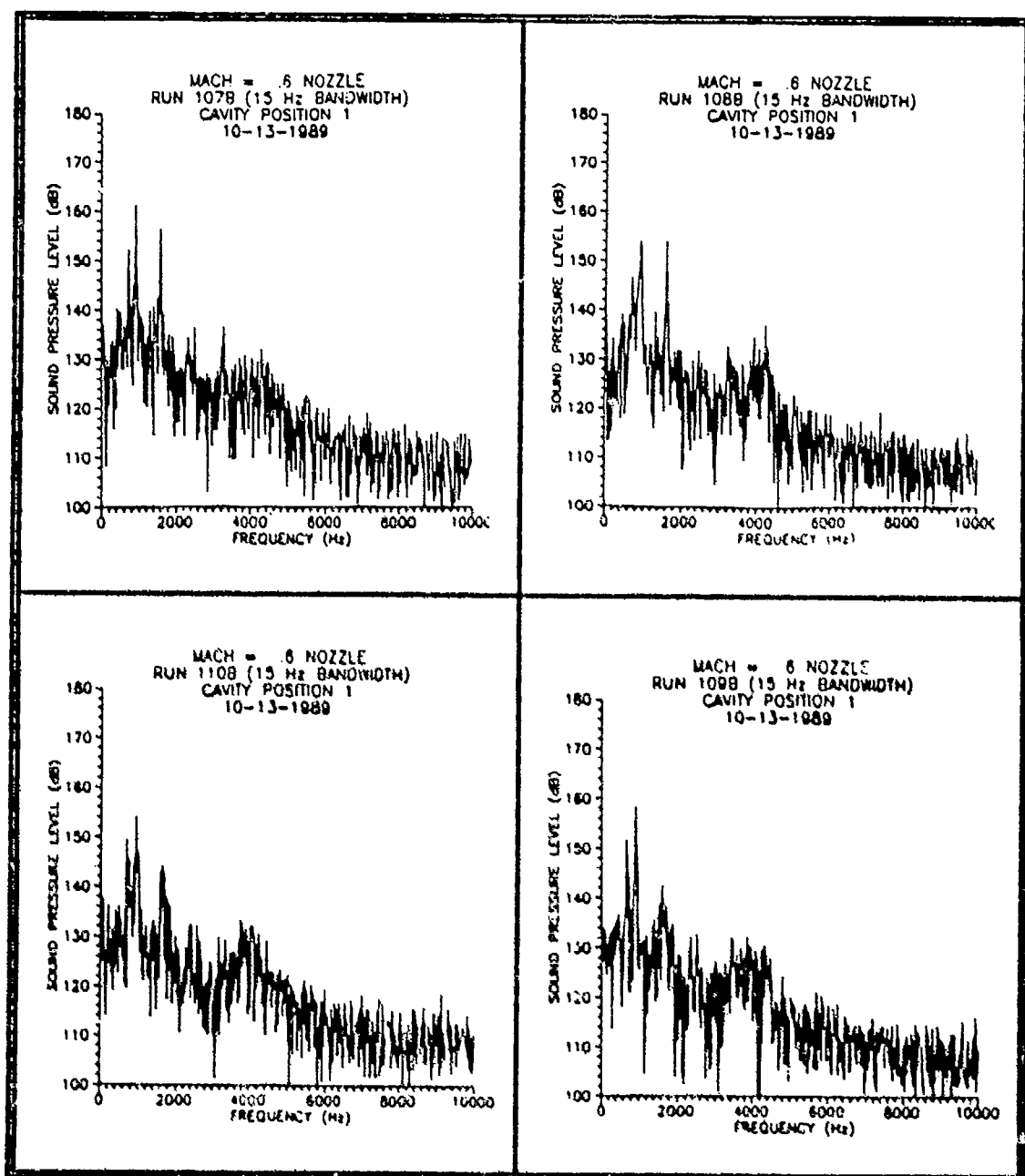40 and 60 Hz (Mid), 80 and 100 Hz (Bot)

Figure A-9. Static Fence SPL Vs Frequency Data, M = 0.62
Fence Height = 1/64 and 3/64 Inch (Top)
Fence Height = 5/64 and 7/64 Inch (Bot)

Figure A-10.   Schlieren Photograph, M = 0.62
Baseline, No Fence

Figure A-11.   Schlieren Photograph, M = 0.62
Fence Height = 5/64 Inch

A-11

Figure A-12.   Static Fence SPL Vs Frequency Data, M = 0.76
                Fence Height = 1/64 and 3/64 Inch (Top)
                Fence Height = 5/64 and 7/64 Inch (Bot)

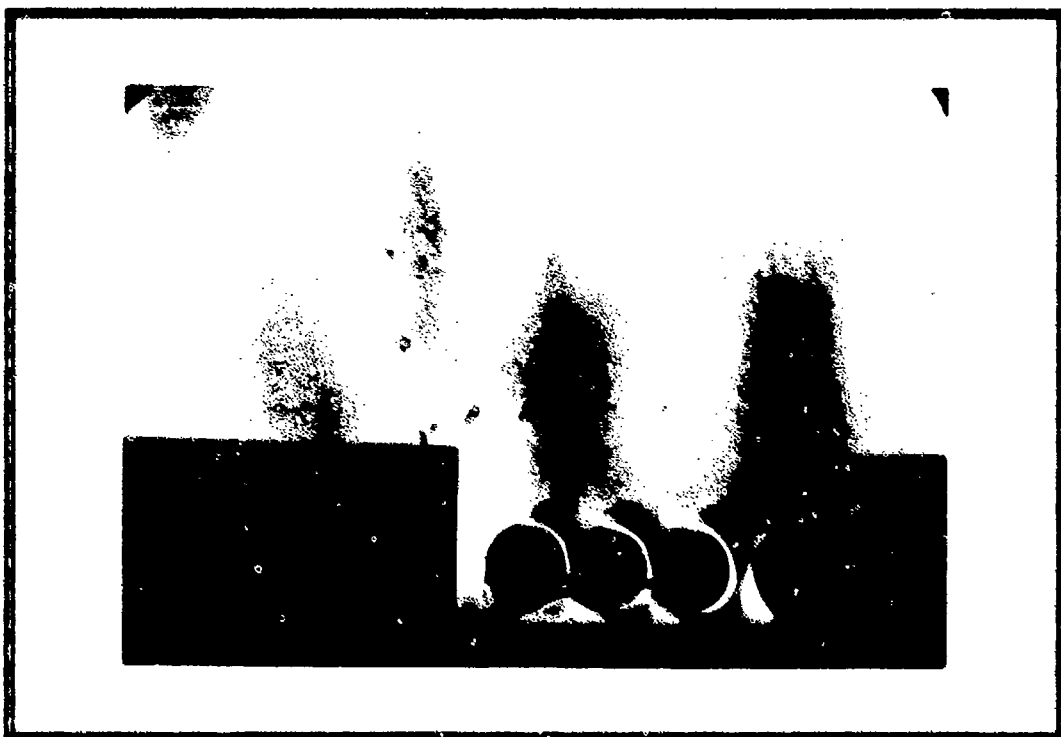Figure A-13. Schlieren Photograph, M = 0.76
Baseline, No Fence

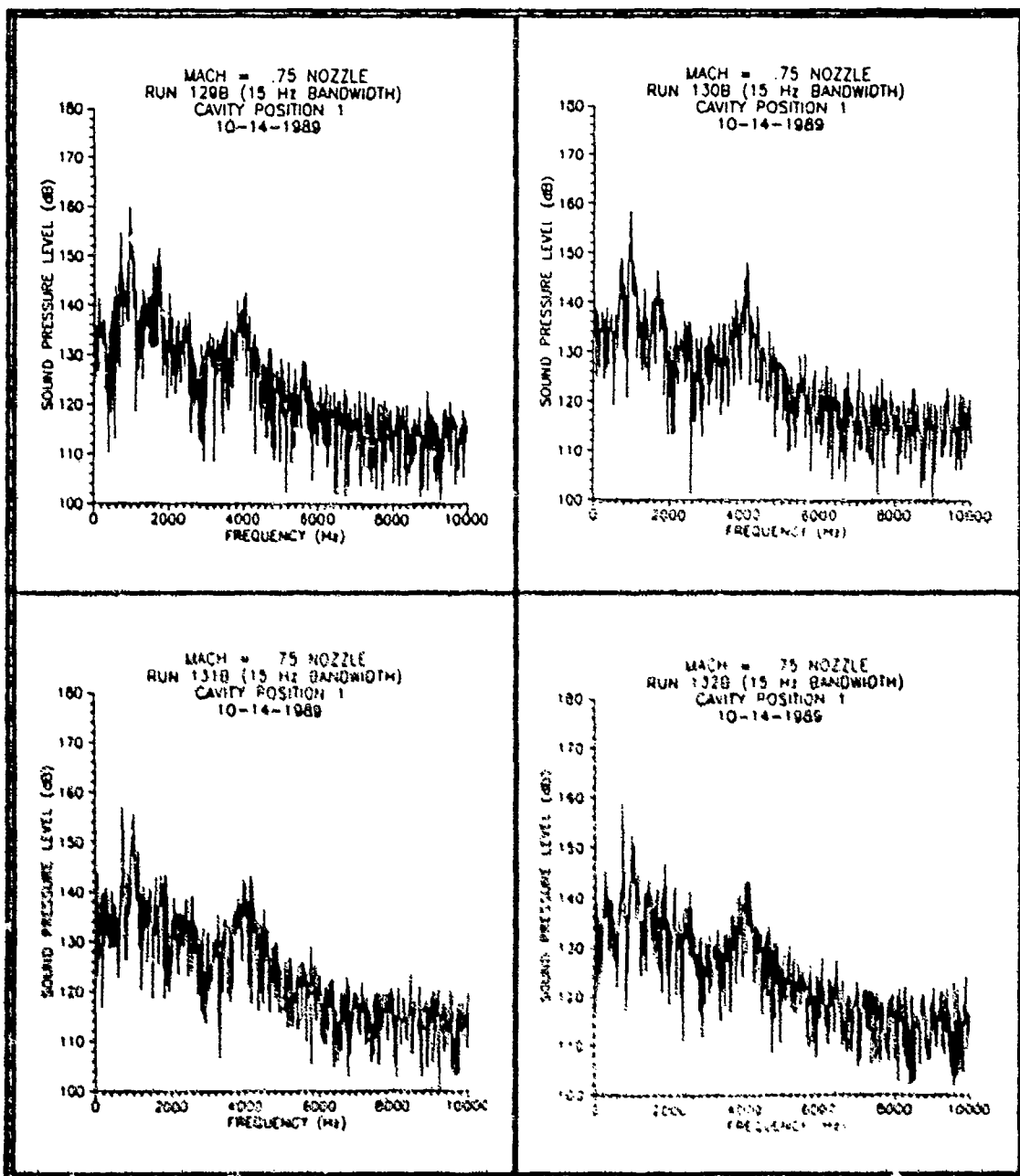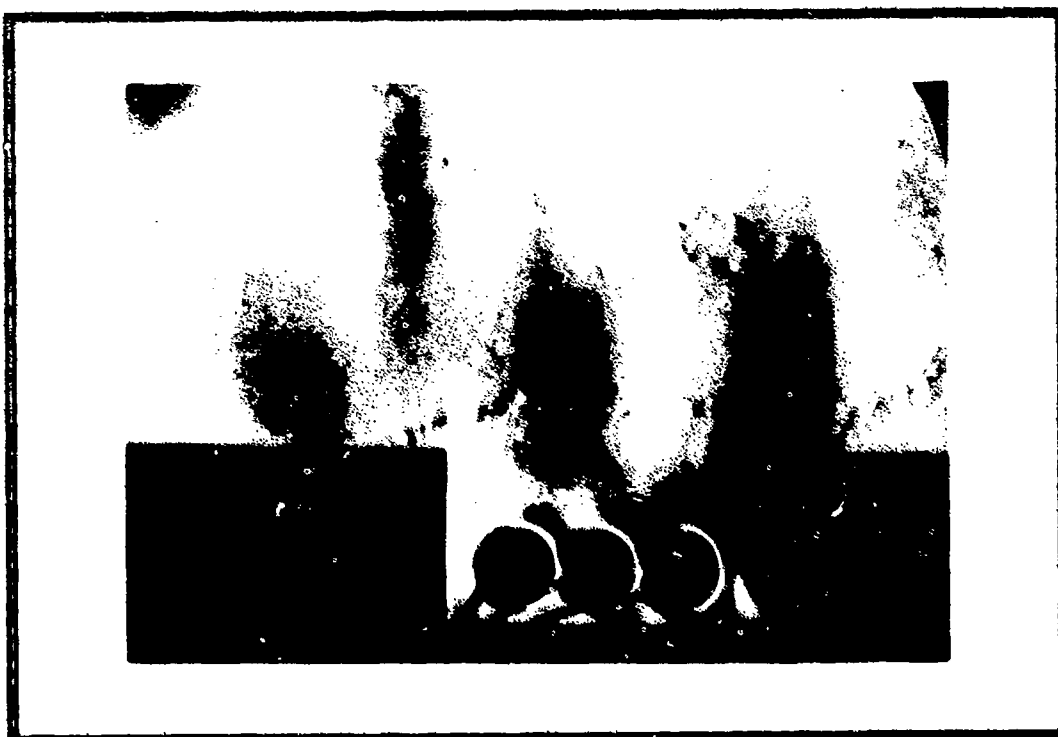Figure A-14. Schlieren Photograph, M = 0.76
Fence Height = 5/64 Inch

A-13

Figure A-15. Static Fence SPL Vs Frequency Data, M = 0.90
Fence Height = 1/64 and 3/64 Inch (Top)
Fence Height = 5/64 and 7/64 Inch (Bot)

Figure A-16.   Schlieren Photograph, M = 0.90
Baseline, No Fence

Figure A-17.   Schlieren Photograph, M = 0.90
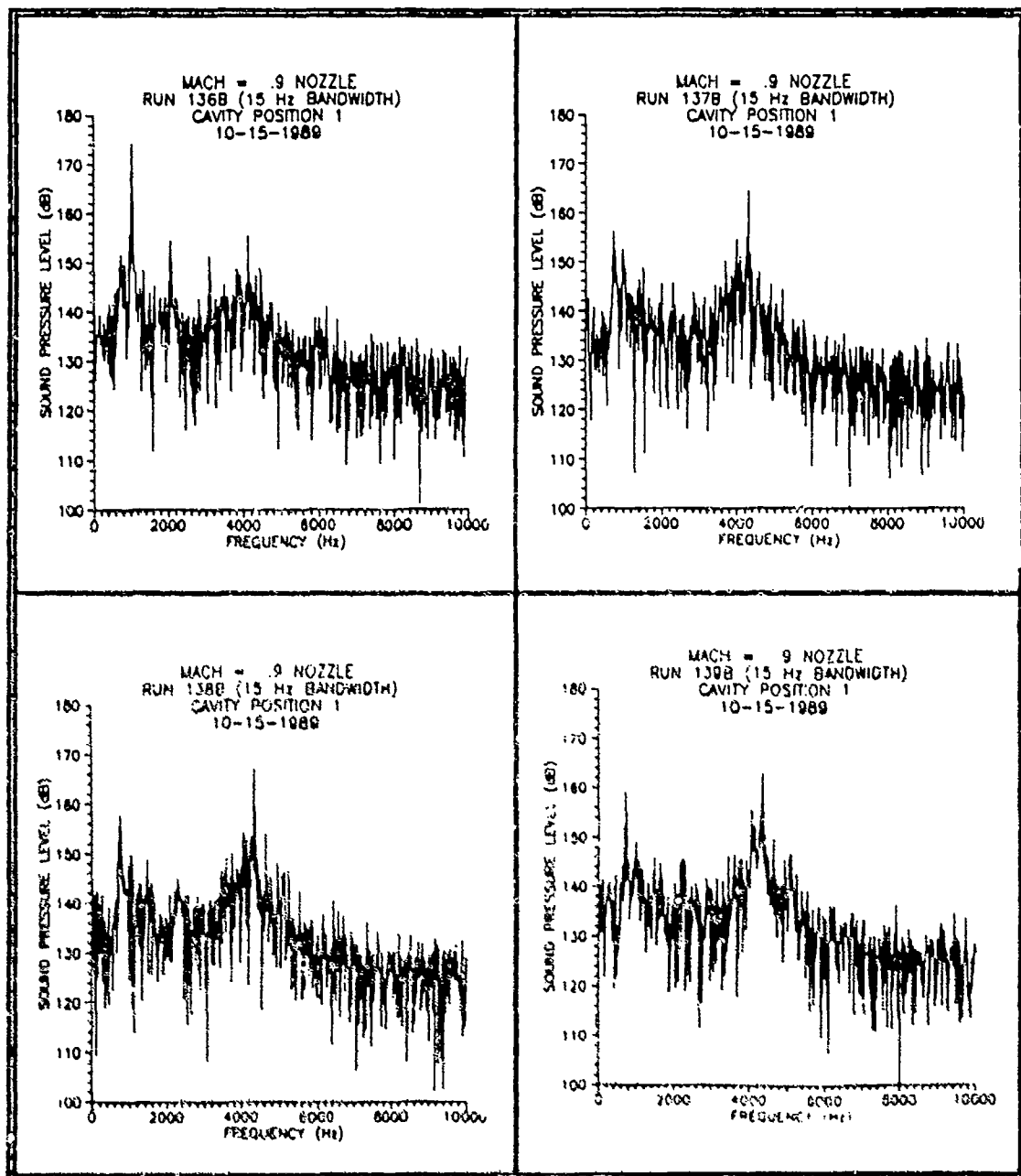Fence Height = 5/64 Inch

Figure A-18.   Static Fence SPL Vs Frequency Data, M = 1.07
                Fence Height = 1/64 and 3/64 Inch (Top)
                Fence Height = 5/64 and 7/64 Inch (Bot)

Figure A-19. Schlieren Photograph, M = 1.07
Baseline, No Fence

Figure A-20. Schlieren Photograph, M = 1.07
Fence Height = 5/64 Inch

A-17

Figure A-21.   Static Fence SPL Vs Frequency Data, M = 1.28
                Fence Height = 1/64 and 3/64 Inch (Top)
                Fence Height = 5/64 and 7/64 Inch (Bot)

Figure A-22.   Schlieren Photograph, M = 1.28
Baseline, No Fence

Figure A-23.   Schlieren Photograph, M = 1.28
Fence Height = 5/64 Inch
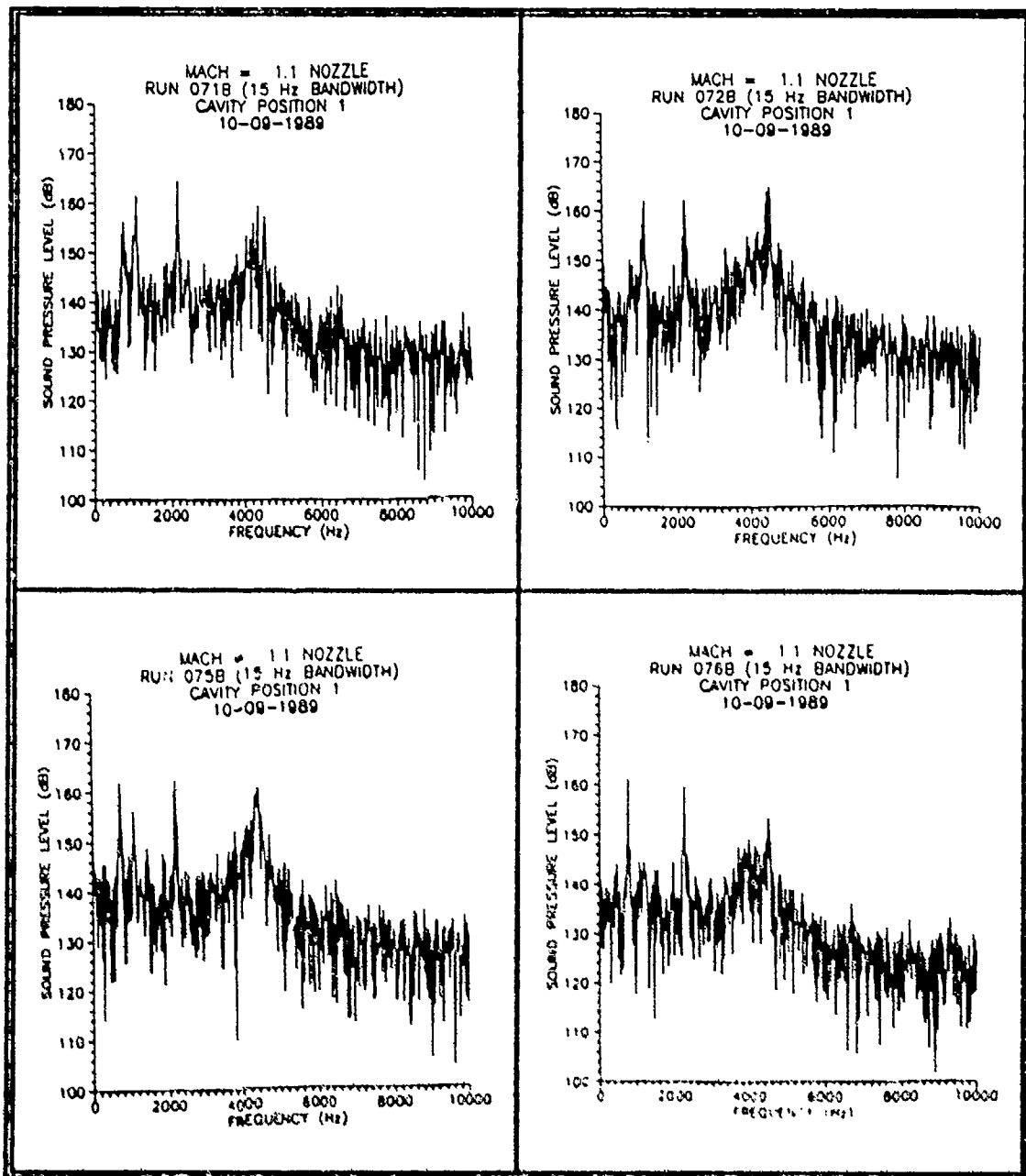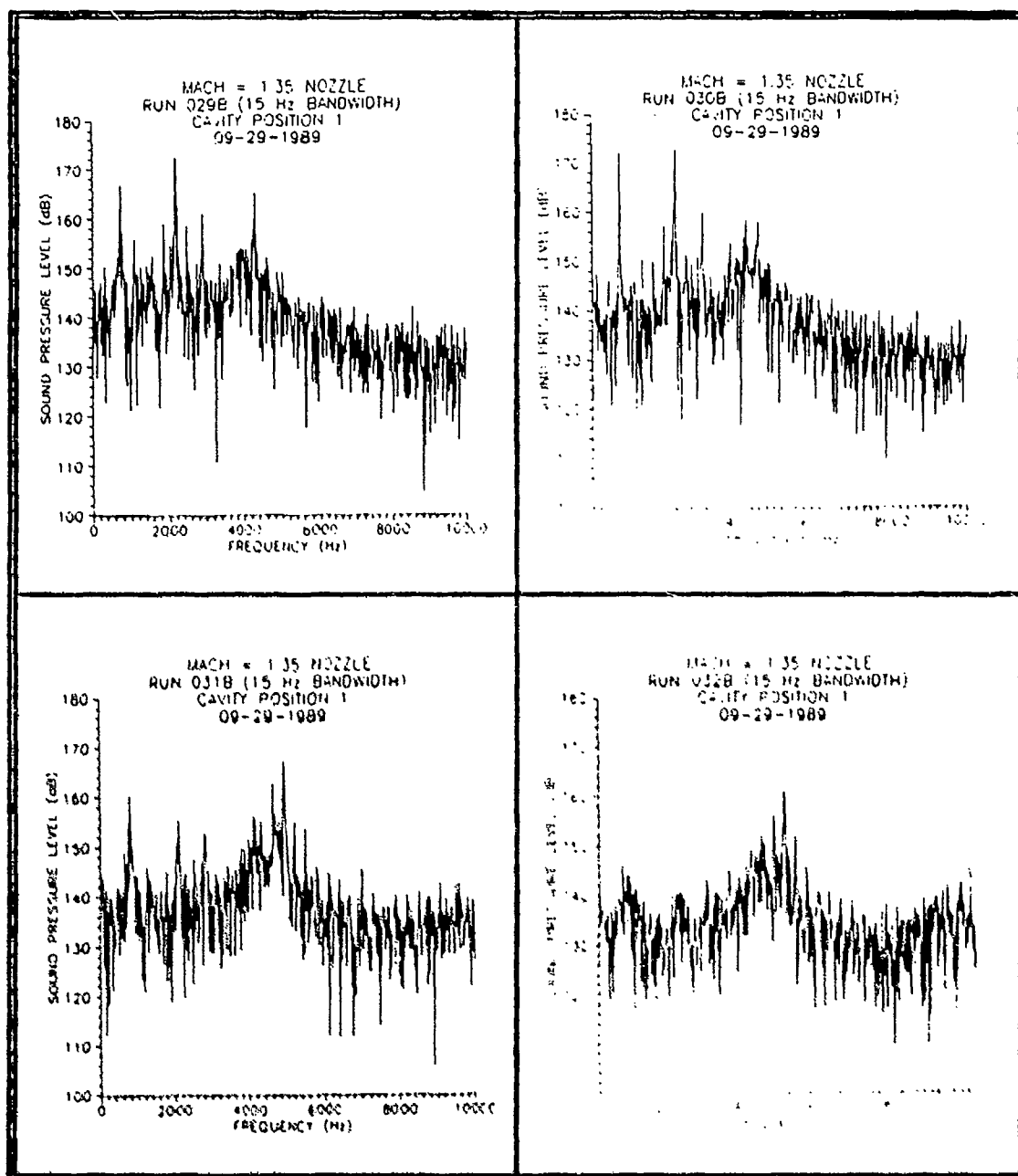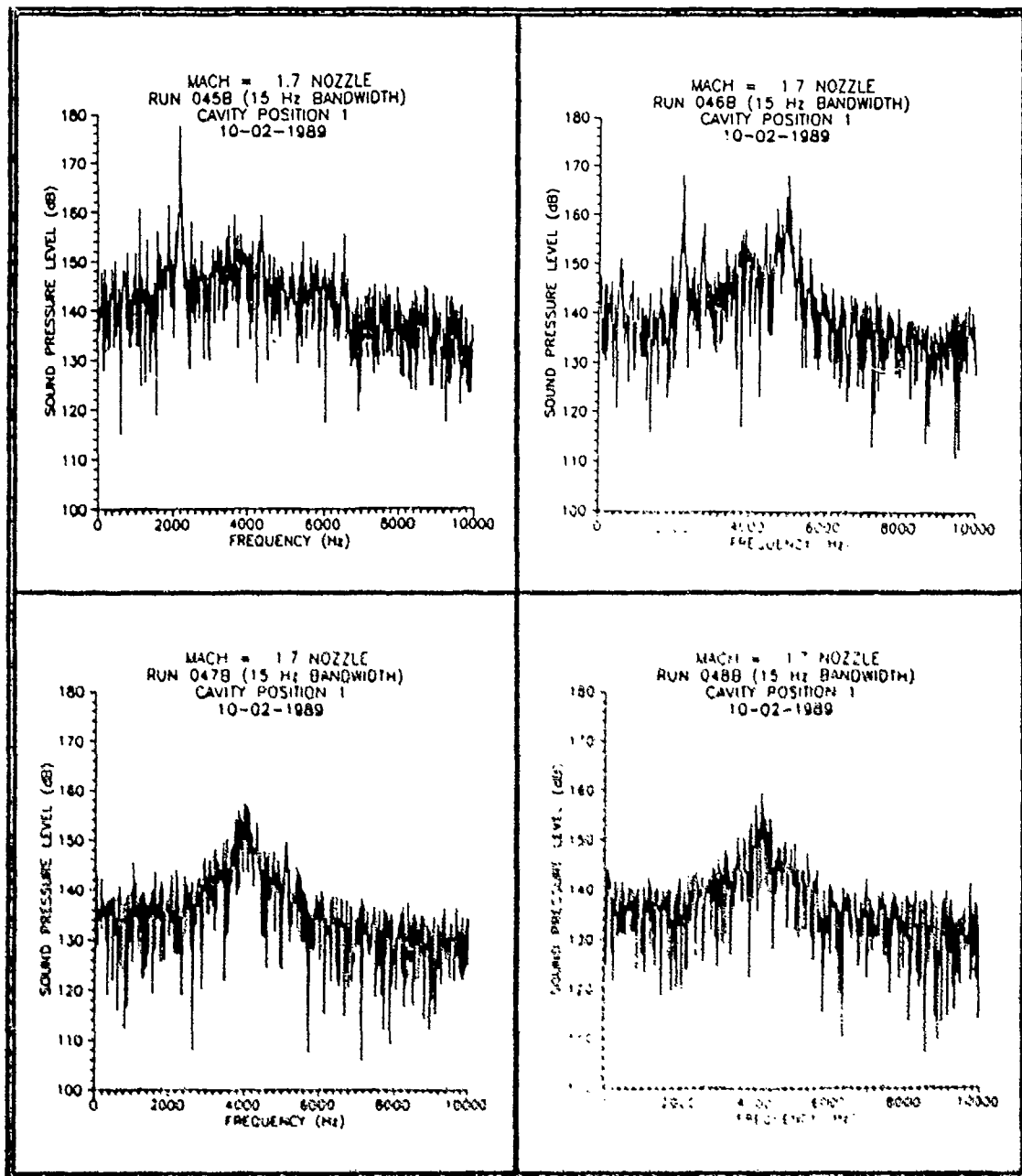
Figure A-24. Static Fence SPL Vs Frequency Data, M = 1.53
Fence Height = 1/64 and 3/64 Inch (Top)
Fence Height = 5/64 and 7/64 Inch (Bot)

Figure A-25. Schlieren Photograph, M = 1.53
Baseline, No Fence

Figure A-26. Schlieren Photograph, M = 1.53
Fence Height = 5/64 Inch

A-21

Appendix B: 45 Degree Flow Injection Data

Description of Contents

This appendix contains the Sound Pressure Level (SPL) versus frequency data obtained from the pulsating and steady flow injection evaluations. Although not a complete set of all the data obtained, it does contain all the data (cavity position one only) used to generate the graphs presented in the body of the thesis as well as some selected schlieren photographs considered representative of the flow conditions tested. Due to the large quantity of data collected only plots for cavity position one are included. Cavity position one was selected because the amplitudes for this position were consistently between those for cavity position 2, which was usually the lowest, and cavity position 3, which was usually the highest. In addition, the spectrum shape for cavity positions 1 and 3 were very similar and thus considered representative of the cavity.

Figure B-1. Baseline Data Set: Average Data and Average - 2 σ Data For M = 1.28

Figure B-2. Schlieren Photograph, M = 1.28 Baseline, No Flow Injection

Figure B-3.   SPL Vs Frequency Data For Pulsating 45 Degree
Flow Inject, 50 psig Valve Supply Pressure,
10 & 20 Hz (Top), 40 & 60 Hz (Mid), 80 & 100

Figure B-4.   SPL Vs Frequency Data For Steady 45 Degree
                Flow Inject, Mass flow rates/width lbm/sec/ft
                0.32 & 0.45, 0.60 & 0.73, 1.00 & 1.27

Figure B-5.   Schlieren Photograph, M = 1.28
              45 Degree Flow Injection (40 Hz)

Figure B-6.   Schlieren Photograph, M = 1.28
              Steady Flow Injection (0.86 lbm/sec/ft)

Appendix C: Parallel Flow Injection Data

Description of Contents

This appendix contains the Sound Pressure Level (SPL) versus frequency data obtained from the pulsating and steady parallel flow injection evaluations. Although not a complete set of all the data obtained, it does contain all the data (cavity position one only) used to generate the graphs presented in the body of the thesis as well as some selected schlieren photographs considered representative of the flow conditions tested. Due to the large quantity of data collected only plots for cavity position one are included. Cavity position one was selected because the amplitudes for this position were consistently between those for cavity position 2, which was usually the lowest, and cavity position 3, which was usually the highest. In addition, the spectrum shape for cavity positions 1 and 3 were very similar and thus considered representative of the cavity.

Figure C-1.   Baseline Data Set: Average Data and
Average - 2 σ Data For M = 1.28

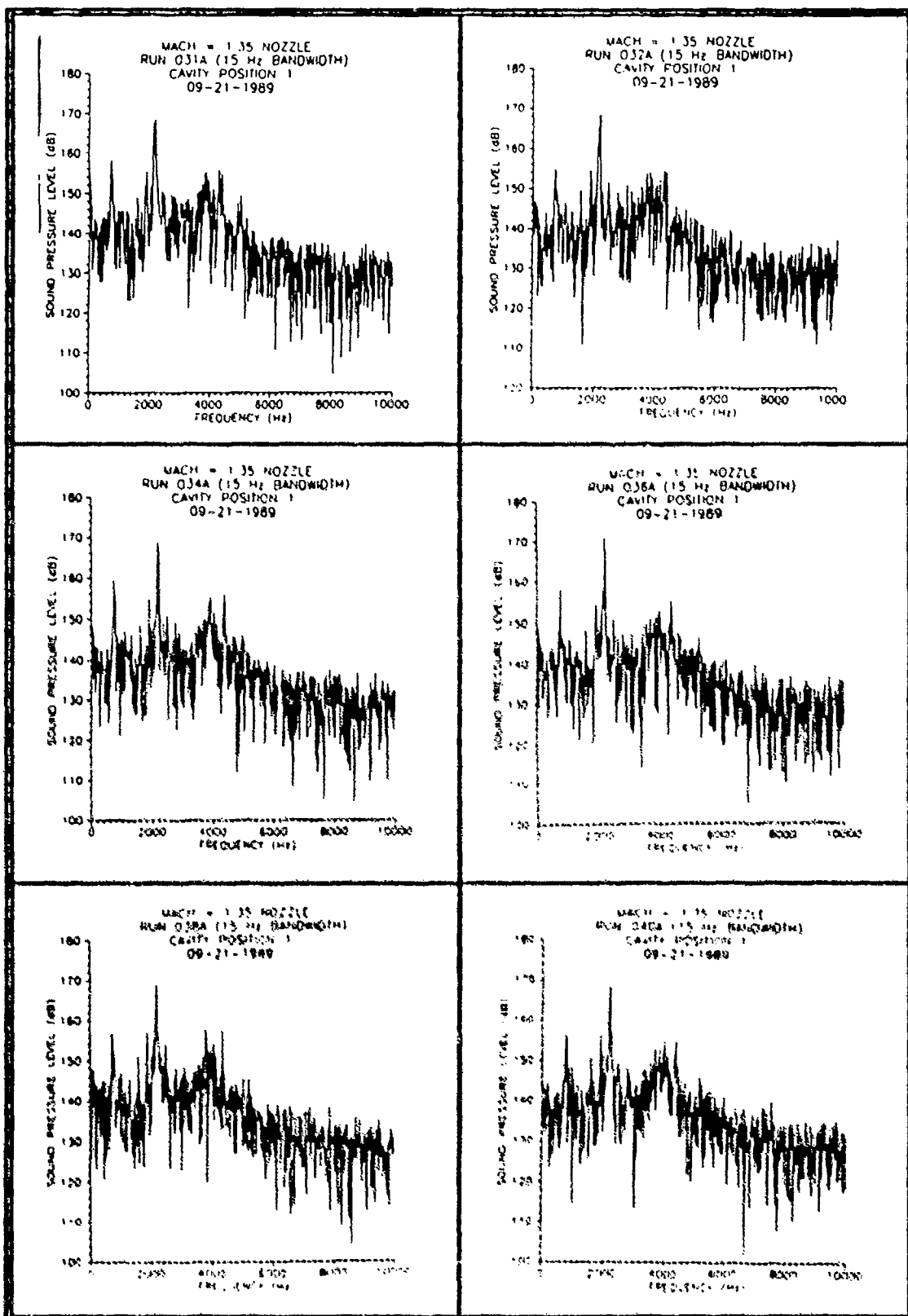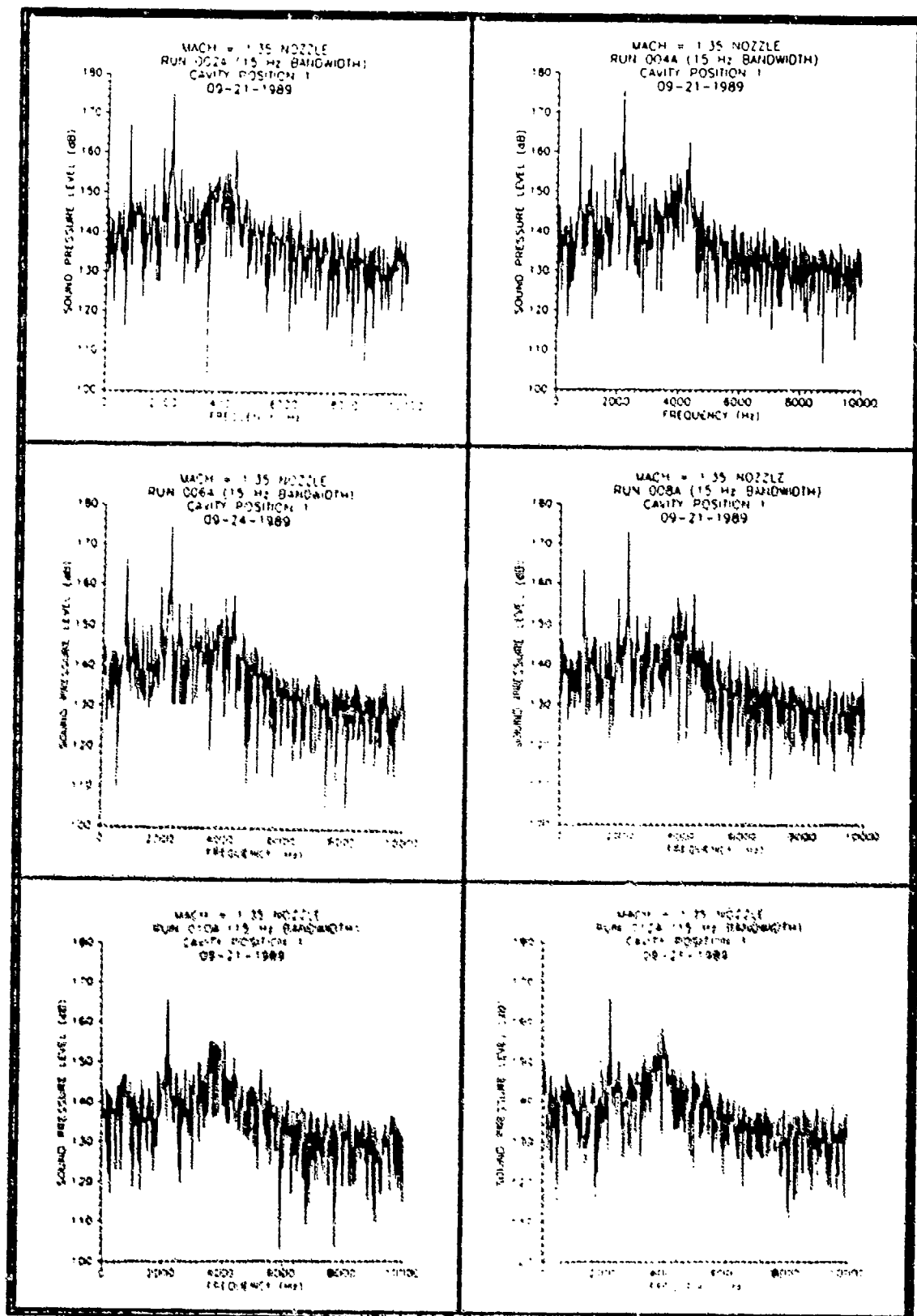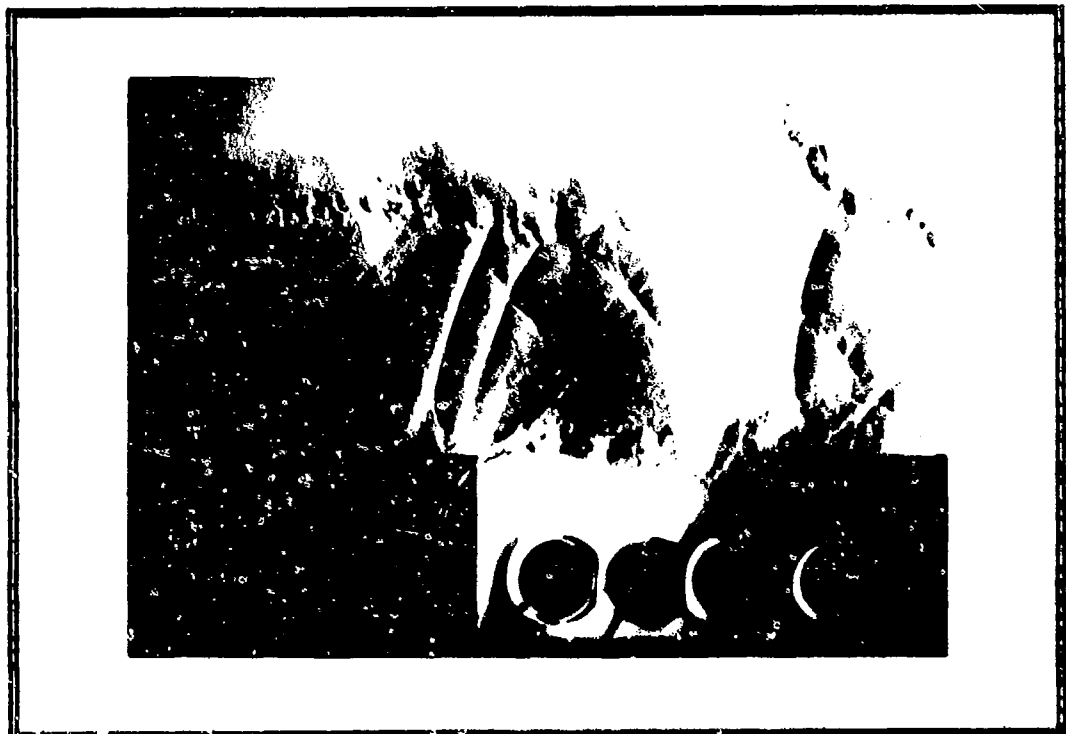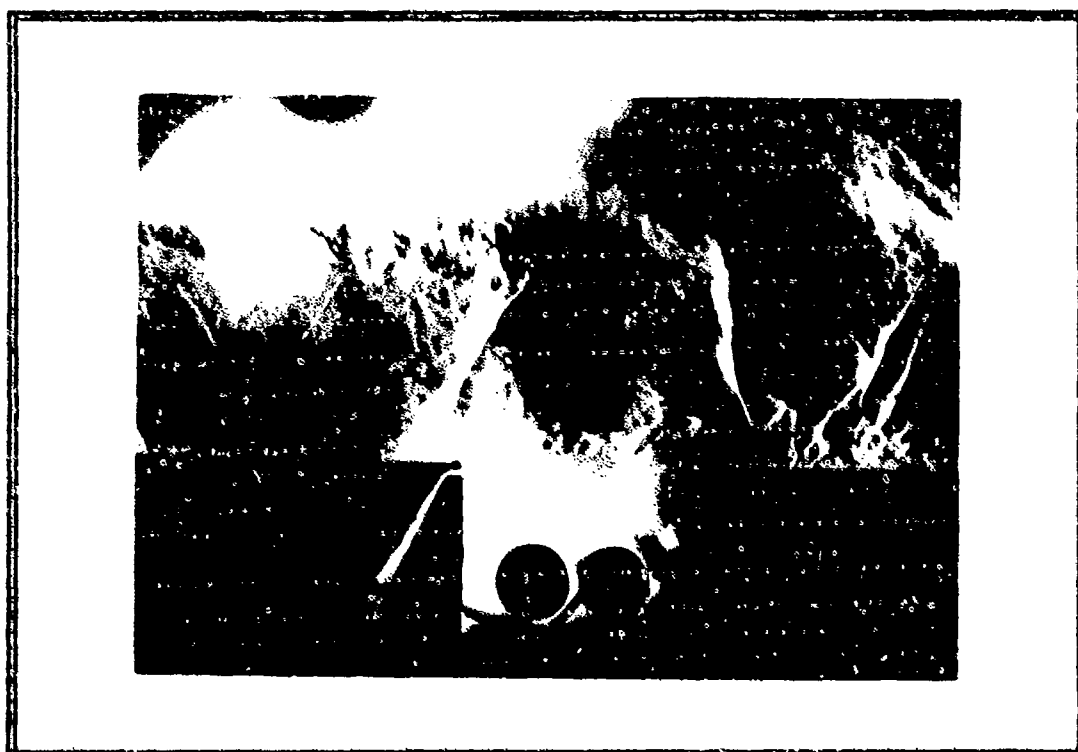Figure C-2.   Schlieren Photograph, M = 1.28
Baseline, No Flow Injection
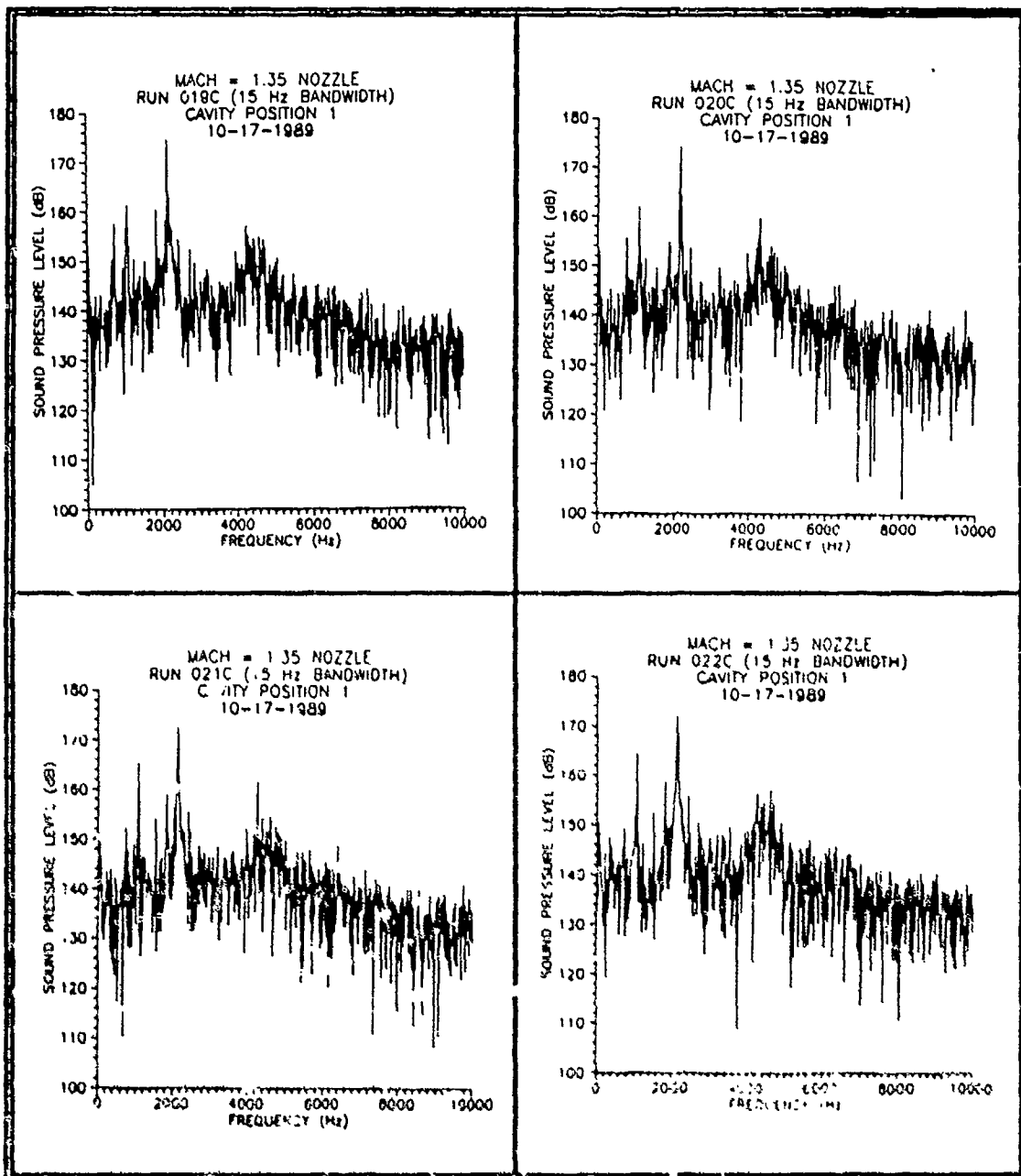
Figure C-3.   SPL Vs Frequency Data For Pulsating Parallel
               Flow Inject, 50 psig Valve Supply Pressure,
               10 & 20 Hz (Top), 40 & 60 Hz (Bot)
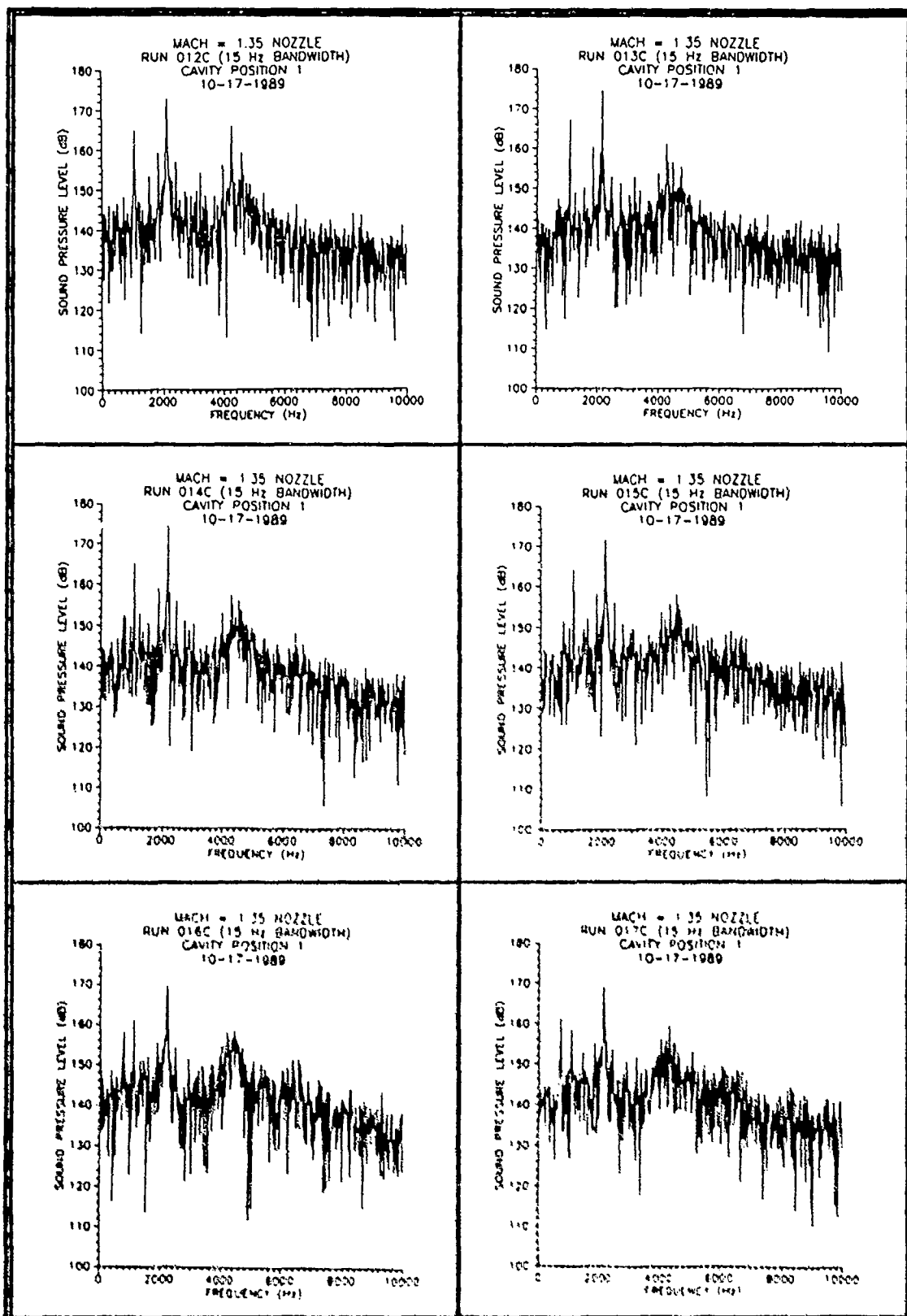
Figure C-4.   SPL Vs Frequency Data For Steady Parallel
              Flow Inject, Mass flow rates/width lbm/sec/ft
              0.32 & 0.45, 0.73 & 1.00, 1.27 & 1.42
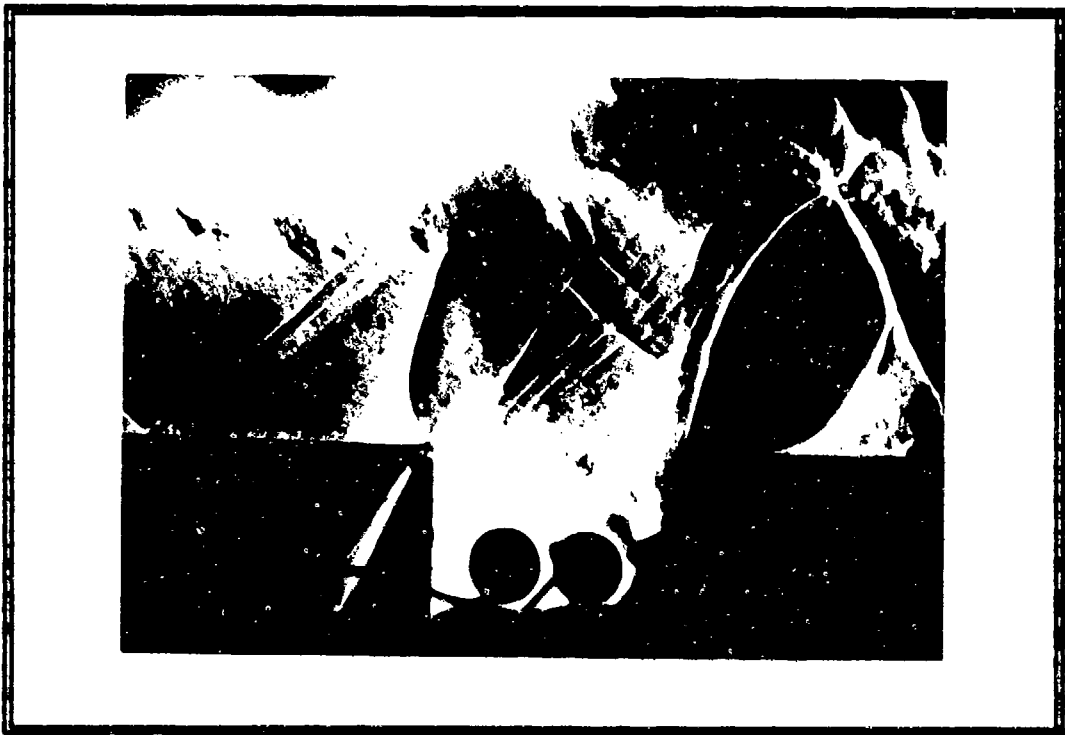
Figure C-5.   Schlieren Photograph, M = 1.28
              Parallel Flow Injection (40 Hz)
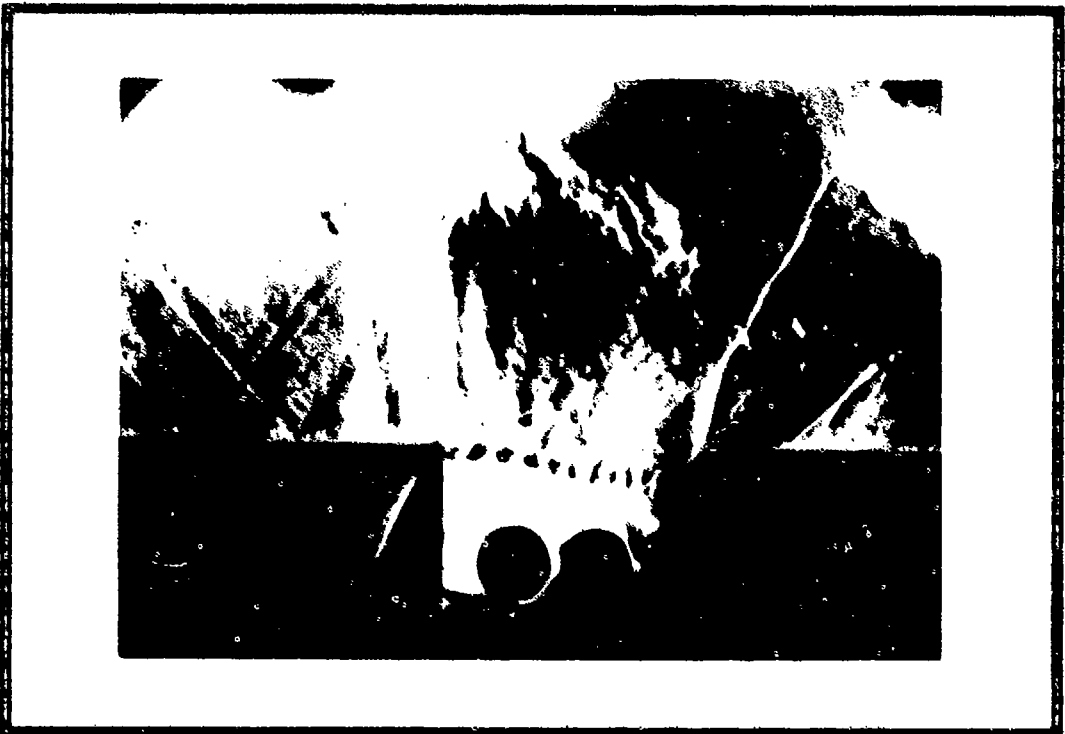
Figure C-6.   Schlieren Photograph, M = 1.28
              Steady Flow Injection (0.86 lbm/sec/ft)

Bibliography

1. Heller, H. H., G. Holmes, and E. E. Covert. <u>Flow Induced Pressure Oscillations in Shallow Cavities</u>. Technical Report, AFFDL-TR-70-104. Air Force Flight Dynamics Laboratory, Wright-Patterson Air Force Base, Ohio, 1970.

2. Karamcheti, K. "Acoustic Radiation from Two-Dimensional Rectangular Cutouts in Aerodynamic Surfaces," <u>National Advisory Committee for Aeronautics Technical Note (NACA TN) 3487</u>: August 1955.

3. Komerath, N. M., K. K. Ahuja, and F. W. Chambers. "Prediction and Measurement of Flows Over Cavities - A Survey," <u>Proceedings of the AIAA 25th Aerospace Sciences Meeting</u>. Paper No. 87-0166, New York, NY: American Institute of Aeronautics and Astronautics, January 1987.

4. Covert, E. E. "An Approximate Calculation of the Onset Velocity of Cavity Oscillations," <u>AIAA Journal, 8</u>: 2189-2194 (December 1970).

5. Charwat, A. F. <u>et al</u>. "An Investigation of Separated Flows - Part I: The Pressure Field," <u>Journal of Aerospace Sciences, 28</u>: 457-470 (June 1961).

6. Sarohia, V. <u>Experimental and Analytical Investigation of Oscillations in Flows Over Cavities</u>. PhD thesis. California Institute of Technology, Pasadena, CA, 1975.

7. Heller, H. H., and D. B. Bliss. "The Physical Mechanism of Flow-Induced Pressure Fluctuations in Cavities and Concepts for their Suppression," <u>AIAA 2nd Aero-Acoustic Conference</u>. Paper No. 75-491, New York, NY: American Institute of Aeronautics and Astronautics, March 1975.

8. Heller, H. H., and D. B. Bliss. <u>Aerodynamically Induced Pressure Oscillations in Cavities - Physical Mechanisms and Suppression Concepts</u>. Technical Report, AFFDL-TR-74-133. Air Force Flight Dynamics Laboratory, Wright-Patterson AFB OH, 1975.

9. Carr, Capt Dennis L. <u>An Experimental Investigation of Open Cavity Pressure Oscillations</u>. MS Thesis AFIT/GAE/AE/74S-1. School of Engineering, Air Force Institute of Technology (AU), Wright-Patterson AFB OH, September 1974.

10. Rossiter, J. E. <u>Wind Tunnel Experiments on the Flow Over Rectangular Cavities at Subsonic and Transonic Speeds</u>. ARC R&M 3438. Royal Aircraft Establishment, 1966.

11. Marquardt, Capt Michael F. <u>An Experimental Investigation of Pressure Oscillations in Two-Dimensional Open Cavities</u>. MS Thesis AFIT/GAE/AE/75D-14. School of Engineering, Air Force Institute of Technology (AU), Wright-Patterson AFB OH, December 1975

12. Mainquist, 1st Lt Randall S. <u>An Experimental Investigation into the Suppression of Flow-Induced Pressure Oscillations in Two-Dimensional Open Cavities</u>. MS Thesis AFIT/GAE/AA/78M-8. School of Engineering, Air Force Institute of Technology (AU), Wright-Patterson AFB OH, March 1978.

13. Bean, Howard S. <u>Fluid Meters</u> (Sixth Edition). New York: The American Society of Mechanical Engineers, United Engineering Center, 1971.

14. Press, William H. and et al. <u>Numerical Recipes</u>. New York: Cambridge University Press, 1986.

15. Schlichting, Herman. <u>Boundary Layer Theory</u> (Fourth Edition). New York: McGraw-Hill Book Company, 1960

Vita

   Captain Robert Sarno was born 27 November 1962 in Chicago, Illinois. He graduated from Forest View High School, Arlington Heights, Illinois, in 1980 and attended Embry-Riddle Aeronautical University, Daytona Beach, Florida, from which he received a Bachelor of Scienc in Aeronautical Engineering in April 1984. Upon graduation, he received a commission in the USAF through the ROTC program and was assigned to the 3246 Test Wing, Eglin AFB, Florida where he worked as a Store Certification Program Manager until entering the School of Engineering, Air Force Institute of Technology, in June of 1988.

        Permanent address: 33 Lake Point Circle
                Port Orange, Florida 32124

REPORT DOCUMENTATION PAGE		Form Approved OMB No. 0704-0188

1a. REPORT SECURITY CLASSIFICATION UNCLASSIFIED	1b. RESTRICTIVE MARKINGS NCNE		
2a. SECURITY CLASSIFICATION AUTHORITY	3. DISTRIBUTION / AVAILABILITY OF REPORT		
2b. DECLASSIFICATION / DOWNGRADING SCHEDULE	Approved for public release; distribution unlimited		

4. PERFORMING ORGANIZATION REPORT NUMBER(S) AFIT/GAE/ENY/89d-32	5. MONITORING ORGANIZATION REPORT NUMBER(S)

6a. NAME OF PERFORMING ORGANIZATION School of Engineering	6b. OFFICE SYMBOL (If applicable) AFIT/ENY	7a. NAME OF MONITORING ORGANIZATION

6c. ADDRESS (City, State, and ZIP Code) Air Force Institute of Technology Wright-Patterson AFB, OH 45433	7b. ADDRESS (City, State, and ZIP Code)

8a. NAME OF FUNDING / SPONSORING ORGANIZATION Structural Vibrations Branch	8b. OFFICE SYMBOL (If applicable) WRDC/FIBGD	9. PROCUREMENT INSTRUMENT IDENTIFICATION NUMBER

8c. ADDRESS (City, State, and ZIP Code) WRDC/FIBGD Wright-Patterson AFB, OH 45433	10. SOURCE OF FUNDING NUMBERS			
	PROGRAM ELEMENT NO.	PROJECT NO.	TASK NO	WORK UNIT ACCESSION NO.

11. TITLE (Include Security Classification)
EXPERIMENTAL INVESTIGATION TO SUPPRESS FLOW-INDUCED PRESSURE OSCILLATIONS IN OPEN CAVITIES

12. PERSONAL AUTHOR(S)
Robert L. Sarno, B.S., Capt, USAF

13a. TYPE OF REPORT MS Thesis	13b. TIME COVERED FROM _____ TO _____	14. DATE OF REPORT (Year, Month, Day) December 1989	15. PAGE COUNT 118

16. SUPPLEMENTARY NOTATION

17. COSATI CODES			18. SUBJECT TERMS (Continue on reverse if necessary and identify by block number)
FIELD	GROUP	SUB-GROUP	Cavity Oscillations Shear Layer
01	01		Pressure Oscillations Rectangular Cavity
20	01		Cavity Oscillation Suppression

19. ABSTRACT (Continue on reverse if necessary and identify by block number)

Thesis Advisor: Milton E. Franke, PhD
                          Professor of Aerospace Engineering

20. DISTRIBUTION / AVAILABILITY OF ABSTRACT ☐ UNCLASSIFIED/UNLIMITED ☒ SAME AS RPT. ☐ DTIC USERS	21. ABSTRACT SECURITY CLASSIFICATION UNCLASSIFIED	
22a. NAME OF RESPONSIBLE INDIVIDUAL Milton E. Franke, Professor	22b. TELEPHONE (Include Area Code) 513-255-2362	22c. OFFICE SYMBOL AFIT/ENY

DD Form 1473, JUN 86	Previous editions are obsolete.	SECURITY CLASSIFICATION OF THIS PAGE

UNCLASSIFIED

Abstract

Large pressure oscillations are generated by high speed tangential flow over an open cavity. The purpose of this experimental study was to determine the effectiveness of suppressing pressure oscillations by manipulating the shear layer over a two-dimensional cavity with a length-to-depth ratio of two. Two methods, a frequency controllable control surface (fence) and pulsating secondary airflow at the cavity leading edge, were used to manipulate the shear layer. The suppression effectiveness of the fence utilized in both passive and active modes (zero to 120 Hz) was evaluated at six airflow Mach numbers (0.62, 0.76, 0.90, 1.07, 1.28, 1.53). The effectiveness of pulsating secondary airflow was evaluated at one airflow Mach number (1.28) and two flow injection angles (parallel and 45 degrees to the flow) at frequencies ranging from zero to 80 Hz. The effect of steady flow injection was also evaluated at mass flow rates per unit width ranging from 0.323 to 1.27 (lbm/sec/ft).

Pressure recordings from within the cavity were made for each test. A narrow band Fourier analysis of these recordings produced plots of the sound pressure level amplitude versus frequency. Schlieren photographs of the flow were also taken for each test to observe the shear and determine the cavity Mach number.

The effectiveness of a pulsating fence in suppressing the peak mode pressure oscillations proved to be less than that achievable with the fence static. However, due to mechanical restrictions of the model design, the maximum frequency was limited to only 120 Hz, an order of magnitude below cavity resonant frequencies.

The pulsed secondary flow injection technique was most effective when pulsed at a 45 degree angle to the external flow, but less effective than that achievable with steady 45 degree flow injection. However, the pulsed secondary flow suppression method was not effectively evaluated since substantial decrease in pulse amplitude occurred with small frequency increases. Recommend additional testing be accomplished to evaluate the effectiveness of both these methods at higher frequencies.